An investigation into mesenchymal stromal cells' behaviour in 3D environment of PNIPAM-based hydrogel

Dmitrijs Limonovs

PhD

University of York

Biology

September 2014

Abstract

Mesenchymal stromal cells (MSCs) are multipotent cells, known for the ability to differentiate into cells of bone, fat and cartilage. MSCs are commonly sourced from the bone marrow environment, where these cells reside in a 3-dimensional (3D) environment and are exposed to components of the extracellular matrix (ECM), other cells types, biochemical and mechanical stimuli. Conventional monolayer culture cannot replicate the complexity of the *in vivo* bone marrow environment. Therefore, a more representative MSC culture environment is required.

The aim of this project was to develop a highly tunable synthetic hydrogel, on the basis of poly(N-isopropylacrylamide) (PNIPAM), to allow temperature-driven encapsulation and subsequent study of MSC behaviour in three dimensional (3D) environment. The highly branched (HB) architecture of PNIPAM polymer was obtained by means of living radical polymerisation. Further polymer functionalisation with tri-arginine peptide sequence (RRR) has stabilised hydrogel structure and reduced solvent expulsion (syneresis). Rheological studies have revealed overall resistance to deformation (G*; complex modulus) of 5wt% HB PNIPAM+RRR to be equal to 542.3 Pa at 37˚C.

MSC single cell suspensions were successfully encapsulated in HB PNIPAM+RRR 3D droplet hydrogels, demonstrating rounded morphology, absence of proliferation and stable cell viability. Differentiation potential studies of the cell-loaded hydrogels, cultured in osteogenic or adipogenic media, demonstrated osteo-conductive, osteo-inductive and adipo-inhibitive responses.

In summary, HB PNIPAM+RRR is a novel chemical entity with a thermo-responsive nature, which forms a porous and hydrated scaffold with osteo-inductive properties for MSC encapsulation at physiologically relevant temperature. HB PNIPAM is a highly functional and amenable hydrogel platform for assessment of MSC behaviour and guidance of differentiation in 3D environment.

List of contents

List of figures

List of tables

Acknowledgements

I would like to thank my supervisors, Paul Genever and Stephen Rimmer, for their support throughout my time in the lab and during the write-up period.

I also would like to thank everyone who helped me by sharing their knowledge, time and patience. I am thankful for having an opportunity to work alongside science-passionate people in both Genever and Rimmer labs.

A special thank you is dedicated to my parents, Anna-Maria and my close friends for their support and encouragement.

Declaration

All the work presented herein is performed by the author, with the exception of Figure 7. The output data for Figure 7 assembly was collected by Simon Thorpe from the mass spectrometry service at the University of Sheffield.

This thesis has not been previously submitted for an award at the University of York or any other university.

1 Introduction

Global population, especially in Europe, is aging rapidly. At present, every sixth person in the UK is 65 or over, and by 2050 every fourth will be of this age (Cracknell 2010).

These demographic changes were termed “Silver tsunami” in the field of medicine and economics, as the consequences of global aging are expected to have a lasting effect on all aspects of human life (Economist.com 2010; Balducci et al. 2010). From the medical perspective, an increase in the elderly population will also escalate problems with treating age-relating diseases (Balducci et al. 2010; Woolf & Pfleger 2003).

Increase in age-related diseases is connected to organ function loss (Dugdale 2013; Stolzing et al. 2008), and when taken in account with existing lack of organs for transplantation, creates an unprecedented demand for organ regeneration and repair solutions (Organdonation.nhs.uk 2014).

The field of tissue engineering and regenerative medicine has been addressing the needs of organ regeneration for the last two decades (Langer & Vacanti 1993). Especially in the last 10 years a tendency towards using the autologous cell-centred approach has become one of the principal ideas in tissue engineering. Atala and his colleagues were the pioneers of the “transplantation without a donor” concept, where patient’s bladder tissue was restored with use of autologous cells (Shay 2001; Oberpenning et al. 1999). The shift in the organ repair paradigm was also stimulated in large part by findings of the tissue and organ forming cells: embryonic stem cells (ESC) and mesenchymal stromal/stem cells (MSC)(Thomson et al. 1998; Caplan 1991; Pittenger et al. 1999). These totipotent and multipotent cells, ESC and MSC respectively, became a focal point of numerous studies, medical solutions and even industries.

At this introductory stage it is important to clarify MSC nomenclature. In the literature, MSC, as an abbreviation, is used interchangeably to describe mesenchymal stem and stromal cells. Use of the term ‘stem cell’ implies specific

functional characteristics, which this cell must demonstrate, i.e. capacity for long-term self-renewal, in addition to ability for differentiation into several cell types *in vivo* (Horwitz et al. 2005). Hence, to describe surface adherent cells, displaying differentiation potential and a specific set of markers, multi-lineage differentiation potential and self-renewal has to be clearly demonstrated *in vivo*. No up-to-date studies have verified this property *in vivo* (Bianco et al. 2013). In addition, due to the lack of 100% specific and unique marker of mesenchymal stem cells, current methods of isolation produce heterogeneous population, where only a fraction of cells display multipotency (Boxall & Jones 2012; Pittenger et al. 1999). Therefore, to provide more scientifically accurate description of surface-adherent cells with differentiation potential, International Society for Cellular Therapy (ISCT) has proposed the term 'multipotent mesenchymal stromal cells' to indicate unique properties of the cells and avoid connection to homogeneity and upper-mentioned characteristics of a stem cell (Horwitz et al. 2005; Dominici et al. 2006). Furthermore, such separation in nomenclature helps to distinguish *in vitro* cultured cells from their *in vivo* precursors. Therefore, throughout this thesis the 'MSC' abbreviation will represent multipotent mesenchymal stromal cells.

Research on ESCs is of a great importance, as it provides fundamental understanding of the organism development processes (Koehler et al. 2013) and is used in disease models (Yazdani et al. 2012). At the same time, clinical translation of these cells is limited due to high probability of teratoma development after implantation (Fong et al. 2010), requirement for specialised growth conditions and ethical roadblocks (Findikli et al. 2006).

In contrast, MSCs are currently dominating the clinical trial arena (Clinicaltrials.gov 2014). Attractiveness of MSCs for use in clinical applications is explained by a host of beneficial properties, which are exhibited by these cells. MSCs are characterised by their ability to undergo symmetrical and asymmetrical division (Matsumoto et al. 2011). As a result of symmetrical division, two identical cells are produced. Conversely, asymmetrical division gives rise to a duplicate cell of itself and a daughter cell, which will undergo tissue specific differentiation.

Differentiation potential of the MSCs is currently paving the way for cell therapies and tissue regeneration solutions (Grayson et al. 2010; Bhumiratana et al. 2014; Frith et al. 2010). MSCs are recognised for their ability to differentiate into cells of bone, cartilage and adipose tissue (Pittenger et al. 1999). However, these multipotent cells have been also found to differentiate into other cells of mesenchymal origin, such as tenocytes and myocytes (Wakitani et al. 1995; Caplan 1991). In addition, reports are showing capacity of MSCs to differentiate into neurons, cells of non-mesenchymal lineage (Zhao et al. 2002; Black & Woodbury 2001). However, clinical applicability of non-mesenchyme sourced cells, is questionable due to findings of MSC-derived neuron-like cells not being able to demonstrate key function of a neuron – generation of the action potential (Augello & De Bari 2010; Hofstetter et al. 2002).

Alongside with differentiation, MSCs have demonstrated immuno-regulating properties: immune response modulation (Aggarwal & Pittenger 2005) and supportive interaction with hematopoietic stem cells (HSC) within one of the specialised stem cell environments – the bone marrow niche (Méndez-Ferrer et al. 2010). Moreover, Caplan group claims that the most important function of MSCs under injury settings is secretion of the bioactive molecules, including growth factors, chemokines and cytokines (Meirelles et al. 2009). Lastly, MSCs are inherently free from the risk of teratoma formation after implantation, in contrast to ESCs, what demonstrates an added benefit of using multipotent MSCs in cyto-therapeutic applications (Fong et al. 2010).

In order to harness full regenerative potential of MSCs, it is crucial to conduct pre-clinical experiments in physiologically relevant conditions. Current MSC research is stagnated by rudimentary culture method, monolayer culture, where cell innate *in vivo* growth requirements are poorly accounted for. Popularity of this culture method is explained by the fact that for most of the last century, cell biology research was conducted in two-dimensional monolayer cultures (Ryan 2008; Carrel 1923). However, as a result of development in the tissue engineering field, shift in the cell culture convention is taking place: natural scaffolds, like collagen, silk, chitosan and alginate, are widely used in 3D cell culture (Thiele et al. 2014; Mobini & Solati-Hashjin 2013).

Bioactivity and biocompatibility is an inherited property of the natural hydrogels, as majority of these gels are extracellular matrix-derived, and therefore, may contain components of hyaluronic acid, hydroxyapatite (HA), glycosaminoglycans (GAG) and others (Gutowska et al. 2008). Moreover, bioactivity of these materials is stemming from numerous endogenous factors, that can direct cell proliferation and differentiation in various cell types (Muzzarelli et al. 1988; Colorado et al. 2000; Anselme 2000; Mobini & Solati-Hashjin 2013). At the same time, lack of control over architecture and complexity of the gel creates a substantial drawback for the whole natural scaffold class. Specifically, due to chemical complexity of the natural hydrogel it is very challenging to rule out exactly which signals are provoking cellular response (Cushing & Anseth 2007). In addition, other factors that limit application of the natural hydrogels are: batch-to-batch variability, causing an uncontrolled effect on cell proliferation, migration and differentiation; problematic tuning of the mechanical properties; risk of contamination, contracted from the original tissue (Tibbitt & Anseth 2009).

On the other hand, fully synthetic materials, like polyacrylamide (PAA) and polyethylene glycol (PEG), are also frequently used for 3D culture and provide control over the architecture (Salinas & Anseth 2008; Fischer et al. 2012). However, in their original formulation these hydrogels lack chemical moieties that the cells may respond to, what makes these materials biologically inert. In order to create a truly physiologically-representative scaffold, a highly functional (i.e. chemically amenable) and synthetic material with controlled architecture is needed.

Therefore, the research work, conducted in this study, was directed towards generation of the 3D environment, based on a thermo-responsive hydrogel poly(N-isopropylacrylamide) (PNIPAM), which would support MSC viability and allow analysis of the cellular behaviour within the physiologically relevant conditions.

Prior to presenting the research finding of this project, it is vital to demonstrate literature-derived context of this project. Firstly, the description of MSC origin and properties will be provided (section 2.1 – 2.7), followed by introduction of the tissue engineering concept (section 2.8). Secondly, fundamental importance of the 3D *in vivo* mimicking environment will be illustrated on the basis of hydrogel scaffolds

(section 2.10). Finally, the route to choosing PNIPAM hydrogel as a 3D scaffolding environment and unique properties of this material will be covered (sections 2.11 - 2.14).

2 Literature review

2.1 MSC discovery and initial characterisation

The initial concept of the multipotent stem cell was proposed by A. Maximow in 1909, where he stipulated that all blood cells are derived from the same parental cell (Maximow 2009; Maximow 1909). One century later, an extensive understanding of the hematopoietic and mesenchymal stem cells location, structure and function is accumulated (Charbord 2010). However, the stem cell field has not become less disputable over time.

MSCs were found to reside in various tissues around the body, including bone marrow, cord blood, dental pulp, tendon, cartilage, muscle tissue and gut (Lindner et al. 2010). However, bone marrow and adipose-derived mesenchymal cells are currently cells of choice for musculoskeletal cell therapy clinical trials (Labusca et al. 2013; Clinicaltrials.gov 2014).

The concept of a mesenchymal stem cell was initially experimentally demonstrated by Friedenstein and his group in 1970s. They were the first to note that the bone marrow contains a population of plastic surface-adherent cells; when seeded individually, these were able to form colonies of fibroblasts (Friedenstein 1976). Friedenstein and colleagues have successfully demonstrated differentiation capacity of these colony-forming and surface-adherent cells by implantation of the diffusion chambers into mice (Friedenstein et al. 1966; Friedenstein 1976). Implanted cells were observed to form tissues of bone, cartilage and fibrous tissues *in vivo* (Friedenstein et al. 1987). Due to inclination of these cells to form primarily bone tissue, Friedenstein referred to these cells as "determined osteogenic progenitors" (Friedenstein 1976; Boxall & Jones 2012). Subsequently, the progress in the field was reviewed by Caplan, who has focused on multipotentiality of these cells and coined the term "mesenchymal stem cell" (Caplan 1991).

Thereafter, seminal study of Pittenger and colleagues identified first definitive markers of MSCs and provided reproducible *in vitro* assays for MSC differentiation towards bone, fat and cartilage progenitor lineages (Pittenger et al. 1999).

2.2 Developmental view on MSC origin

To gain a better understanding of the functions, such as self-renewal and multi-lineage differentiation, and therapeutic properties exhibited by MSCs, it is vital to clarify the origin of these cells.

Schematic representation of the key stages in human embryogenesis and post-natal development is depicted in Figure 1. After fusion of the sperm cell and the egg gametes, followed by the pluripotent diploid zygote formation, the process of cells division initiates. This process results in the blastocyst formation. Inner cell mass, contained in the blastocyst, can be extracted and used for embryonic stem cell generation *in vitro* (Thomson et al. 1998). Embryonic stem cells in culture conditions are pluripotent and undergo self-renewal without differentiation, and with appropriate stimuli, are capable to differentiate into cell lineages of endodermal, mesodermal and ectodermal germ layers (Thomson et al. 1998; Reubinoff et al. 2000).

During the next key stage of embryogenesis *in utero*, gastrulation, clear germ layer specialisation takes place. At this stage, each germ layers gives rise to the germ-specific tissues. However, there are exceptions to the germ-specific differentiation. For example, ectoderm layer is classically recognised for the ability to form cells of epidermis, spinal cord and neurons. However, during neurulation (the process of neural tube formation) neural crest is formed, close to neural tube (Figure 1). Neural crest is represented by multipotent migratory cells, which are involved in development of tissues of mesodermal (i.e. smooth muscle cells, adipocytes, chondrocytes, osteoblasts and osteoclasts) and ectodermal origin (melanocytes, Schwann cells and neurons) (Hauser et al. 2012; Widera et al. 2009; Isern et al. 2014).

After gastrulation and extensive differentiation, fetal tissues are formed, which develop into systems of organs. Multipotent somatic, or adult, stem cells can be found in numerous fetal and post-natal tissues (Hass et al. 2011; Robel et al. 2011; Gronthos et al. 2000). These somatic cells exhibit self-renewal, and with appropriate

signals, multi-lineage differentiation is observed, what together confirms "stemness" of the cells (Blanpain et al. 2004; Sung et al. 2010).

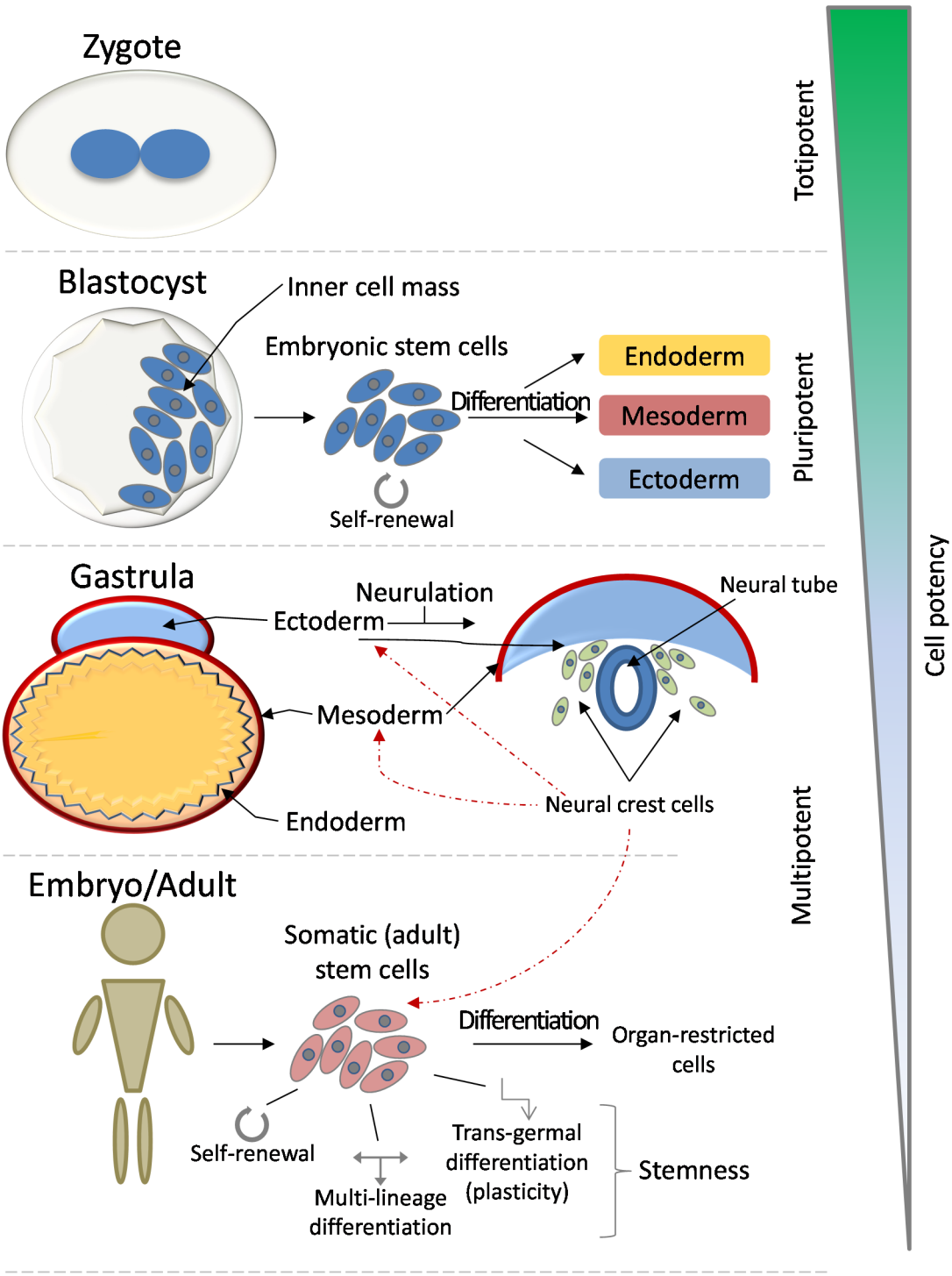

Figure 1: Different types of stem cells are developed during embryogenesis and post-natal development. Stem cell potency and availability is reduced as the specialist tissues are formed. Pluripotent embryonic stem cells can self-renew and are able to become cells of any germ layer, giving rise to any organ in the body. Multipotent somatic stem cells are present virtually in every developed organ and are able to remain quiescent, to self-renew and to differentiate into germ layer-specific cells or undergo trans-germal differentiation.

In an established view, somatic stem cells are capable of differentiating into cell lineage of an organ, from which they were derived (Pittenger et al. 1999; Gronthos et al. 2000). However, a growing collection of studies is suggesting that some somatic stem cells have a trans-germal differentiation potential, also known as plasticity (Wislet-Gendebien et al. 2005; Planat-Benard et al. 2004; Wagers & Weissman 2004). This view still remains controversial, as extent of the stem cell plasticity is not studied in full (Leychkis et al. 2009).

Partial understanding of the MSC phenotype and functions can be drawn from the describing adjective – mesenchymal. The terms mesenchyme is of a Greek origin and it represents a composite of two words: "middle" (mesos), referring to mesoderm germ layer, and "infusion" (enkhuma), referring to high migratory capacity of a cell (Mosby 2009).

Mesenchymal cell migration is most pronounced during the early embryonic development, where these cells cross between the endodermal and ectodermal layers. In addition, migratory and space-filling function of the mesenchymal cells is instrumental for wound repair processes in the adult tissues. (Caplan 1991)

Whereas, mesenchyme as a tissue, can be described as an embryonic connective tissue meshwork of a mesodermal origin. Mesenchyme is harbouring unspecialised cells with a potential to give rise to connective and skeletal tissues, as well as to circulatory/hematopoietic and lymphatic systems. However, some (e.g. craniofacial skeleton; smooth muscle, dermis and adipose tissue of skin in the head and neck region) of the mesenchymal tissues can be also derived from the ectoderm germ layer through neural crest cell migration (Gilbert 2000; Olsen et al. 2000).

2.3 MSC functions and unique identity

MSCs are universally known for their ability to self-renew and to demonstrate commitment to towards osteogenesis, chondrogenesis, adipogenesis, myogenesis, tendeno/ligamentogenesis and formation of the marrow stroma (Pittenger et al. 1999; Young et al. 1998).

Alongside with the ability of the MSCs to undergo differentiation and play key role in tissue repair and homeostasis, these cells are also recognised for providing supportive environment (expression and presentation of growth factors; secretion of the ECM proteins) for other cells in the shared organ (Caplan & Dennis 2006), such as hematopoietic stem cells (HSCs) in the bone marrow (Majumdar et al. 1998). In recent years more attention was drawn to trophic factor production by the mesenchymal stem cells, as means of providing stimulating environment for specialised (organ-specific) cells to drive the regeneration process (Caplan & Dennis 2006). With appropriate environmental stimuli (e.g. inflammatory cytokines, hypoxic environment, exposure to ligands of tall-like receptors (TLR)) MSCs can act as the growth factor factories, producing vascular endothelial growth factor (VEGF), insulin-like growth factor 1 (IGF-1), basic fibroblast growth factor (bFGF), hepatocyte growth factor (HGF), interleukin-6 (IL-6) and others (Wei et al. 2013; Crisostomo et al. 2008; Uccelli et al. 2006; Caplan & Dennis 2006).

In addition to direct regenerative capacity of the MSCs (DiMarino et al. 2013), reports are showing immunologic properties of these cells, which can be grouped under two terms: immunosuppression and immunoprivilege. Mesenchymal stem cells are able to suppress activity of T-, B-, dendritic and natural killer (NK) cells, as well as being immunoprivileged by avoiding lysis by cytotoxic T- and NK-cells (Uccelli et al. 2006; Hass et al. 2011; Le Blanc 2003).

Mesenchymal stem cells are also known for being motile when mobilised, most often, by inflammatory cytokines (Spaeth et al. 2008). This property is particularly important for tumour targeting. Tumour tissue is an active inflammatory cytokine producer (Dvorak 1986), and affinity of the mesenchymal stem cells to inflammatory cytokines can be therapeutically explored, as these versatile cells can also be used as carriers for tumour-killing agents (Loebinger et al. 2009; Ren et al. 2008) and nanoparticles (Roger et al. 2010).

Established immuno-modulation and injured tissue repair capacity of MSCs is being actively explored in clinical studies. MSC-based treatments which are being most investigated in the clinical studies are myocardial infarction, graft-versus-host disease, diabetes and liver cirrhosis (Wei et al. 2013).

Such diverse functionality of MSCs raises the question – where precisely these multipotent cells are located in the tissues? *In vivo* identification of MSCs is a long-standing and unresolved issue in the field. However, several concepts were proposed, which are suggesting relationship between MSCs, pericytes (Meirelles et al. 2009) or adventitial reticular cells (ARC) (Jones & McGonagle 2008). Pericytes are similar to MSCs *in vitro*, in terms of differentiation potential and surface marker expression (Crisan et al. 2008; Covas et al. 2008). Pericytes, also known as periendothelial cells, are located on the outer (abluminal) side of the blood vessels. Some research groups are equating the bone marrow pericytes with ARC, by taking in consideration their location and functional characteristics (Meirelles et al. 2009; Bianco et al. 2001). Assumed association between ARC, pericytes and MSCs is based on the linkage of these cells and the vasculature density (da Silva Meirelles et al. 2009). However, in avascular tissues, such as articular cartilage, a subset of MSCs was found (Barbero et al. 2003), suggesting that MSCs, ARC and pericytes may have common properties and functions, but ultimately these cells most probably are representing different subsets of multipotent adult stem cells, which perform unique role in tissue repair. This idea is further supported by analysis of the differentiation potential and gene expression between MSCs and pericytes. Work of Meirelles and colleagues demonstrates that the gene expression in the fetal MSCs and fetal pericytes is different, suggesting that these discrepancies are formed during the prenatal development (Meirelles et al. 2009).

In addition, a recent study, done by Isern et al., has demonstrated presence of two distinct populations of MSCs in the bone marrow, which originated from different sources and are demonstrating dissimilar properties. First population, mesoderm-derived nestin$^-$ MSCs, is involved in fetal skeleton development, but the MSC activity is lost after birth. Where second population is nestin-positive, with preserved mesenchymal stem cell activity, and is of neural crest origin. Instead of developing skeletal tissues, nestin$^+$ cells are involved in HSC niche formation. (Isern et al. 2014) It can be concluded that the bone marrow is comprised of the mesenchymal stem cell populations with non-overlapping functions, which play unique roles in tissue development and homeostasis.

2.4 Definition of "stemness" in MSCs

Maintenance of "stemness" of the stem cells in the adult organism is essential for injury response, tissue homeostasis and regeneration (Kuhn & Tuan 2010). Additionally, in order for any cell to be considered a stem cell, it needs to demonstrate two parameters: 1) extensive proliferation with retention of the mulitpotency; 2) multilineage differentiation (Caplan 1991). The concept of "stemness" can be analysed from following positions: "stemness" as a pattern of gene expression, which is shared by all stem cells (Pyle et al. 2004; Wagner et al. 2005); or "stemness" as a description of exogenous and endogenous factors, which are playing key roles in maintaining stem cells in their undifferentiated and post-multipotent states. Both approaches allow to identify "stemness" markers. However, in order to obtain genuine "stemness" markers, the initial population of stem cells should be homogenous (Wagner et al. 2006).

In order to trace changes in "stemness", Song and colleagues has compared gene expression between undifferentiated MSCs, tri-lineage differentiated MSCs (cells formed osteoblasts, chondrocytes and adipocytes) and de-differentiated MSCs. 11 shared genes of "stemness" were highly expressed in both non-differentiated and de-differentiated cells. Expression of the same genes was found to be significantly lowered during MSC differentiation into adipocytes, chondrocytes and osteoblasts (Song et al. 2006). To ensure that the identified "stemness" gene is not a housekeeping gene and it will produce a functional protein, which will effect "stemness" of the cell, products of the gene translation are required. From the list of "stemness" genes, identified by Song et al., which may serve as markers of MSCs or regulatory factors of differentiation, were selected. By analysing gene transcripts, cytokine interleukin-6 (IL-6) was found to be important for MSC maintenance, as it stimulated proliferation, inhibited serum starvation-induced apoptosis, suppressed adipogenic and chondrogenic differentiation (Pricola et al. 2009). In addition to IL-6, ECM molecule, α4-laminin, is secreted by the MSCs and is commonly found in the bone marrow; α4-laminin stimulates cell proliferation, at the same time inhibiting conventional tri-lineage differentiation into adipocytes, chondrocytes and osteoblasts (Kuhn & Tuan 2010).

Assessment of "stemness" can be also performed on stem cells from different sources and stages of development. Sung et al. has compared "stemness" of the cells from placentas, at different stages of development, and MSCs from the adult bone marrow, according to these parameters of "stemness": mesoderm differentiation, expression of the pluripotency markers (including telomerase activity), immuno-phenotypic expression and proliferation capacity. All of the analysed cells shared similar mesodermal differentiation potential, where other parameters did not match. (Sung et al. 2010)

Finally, surface marker expression is a common method for "stemness" and *in vivo/vitro* phenotype identification in populations of MSCs (Lv et al. 2014).

2.5 MSC-specific surface markers

In order to identify MSCs from a highly heterogeneous population within the cell aspirate, flow cytometry is routinely employed. A unifying surface marker for MSC identification has not yet been agreed on. As a result, a combination of surface markers are used as indicators for putative MSC properties (Frith et al. 2010; Prins et al. 2014).

Typical cell surface molecules, also termed "clusters of differentiation", used for initial MSC identification are CD105, CD73 and CD90 (mentioned markers should be present on 95% or more of the cell fraction). These surface markers were standardised by the ISCT position statement (Dominici et al. 2006). The ISCT has also suggested that MSCs should not express (or have less than 2%) following markers: HLA-DR, CD45, CD34, CD79a or CD19, CD14 or CD11b. These negative markers are primarily required to exclude possibility of contaminations with hematopoietic cells.

MSCs in culture display stable and positively-strong expression of CD73, CD90 and CD105 (Pittenger et al. 1999; Jones et al. 2010). The CD73 marker represents ecto-5'-nucleltidase and is involved in production of an active adenosine and may also function as cell adhesions molecule. The CD90 marker, also known as Thy-1, is involved in cell-matrix and cell-cell interactions. And the CD105 marker, also

known as endoglin, is involved in mediation of cellular response to TGF-β superfamily ligands. (Lin et al. 2013) However, these markers are not exclusive to MSCs (Lin et al. 2013; Boxall & Jones 2012). Skin fibroblasts do also express CD73 and CD105 (Ishii et al. 2005; Jones et al. 2004). Similarly, CD73 and CD105 markers are expressed by umbilical vein endothelial cells (Narravula et al. 2000; Chan et al. 2004), suggesting that adherent cell selection by CD73 and CD105, without CD90, is not sufficient for MSC identification.

Fundamental issue with relying on CD73, CD90 and CD105 as markers of MSCs became apparent, when Digirolamo and colleagues have demonstrated reduction in MSC's capacity to form colonies with increase in cell passage number (Digirolamo et al. 1999), when CD73, CD90 and CD105 were stably expressed in MSCs, regardless of the passage. This fact suggests that CD73, CD90 and CD105 are being applicable for basic MSC characterisation *in vitro*, but not for potent cell identification.

In search for highly specific markers of MSCs, CD106 (vascular cell adhesion molecule 1 (VCAM-1)) and Stro-1 markers have shown high selectivity for CFU-F-rich cell fraction (Gronthos et al. 2003). In addition, expression of these markers is dependent on the time in passaging (Halfon et al. 2011; Jung et al. 2011; Jones et al. 2010). Furthermore, recent finding of Liu et al. demonstrated CD106 as a marker of the potent (naïve) MSC in monolayer culture, as the marker expression was much lower after differentiation of the cells towards bone, fat and cartilage (Liu et al. 2008).

Observing expression of the passage dependant and independent markers for MSC characterisation, Boxall et al. has proposed a categorising approach for the MSC marker panel design (Boxall & Jones 2012). Surface markers, which are continuously expressed at the same level during MSC culture and are donor-independent, can be referred to as the 1st tier markers (e.g. CD73, CD90 and CD105) to identify "generic" MSCs. Whereas, markers which show expression-dependence on passage, donor, as well as attachment properties, seeding density and other variables, can be attributed to the 2nd tier (e.g. CD106 (Liu et al. 2008)).

Knowledge of the markers that would allow MSC identification is essential for fundamental research and clinical application. However, a constant strive to find unique marker(s) of MSCs also leads to finding new markers which are able to suggest differentiation potential of MSCs. It is a well-accepted view that the gene and miRNA expression, and subsequently alterations in phenotype and differentiation potential, are acquired by MSCs with increase in passage number (Wagner et al. 2008). In addition, with increase in passage number MSCs were observed to have a predisposition to differentiate into cells of osteogenic lineages, and reduced differentiation potential towards adipogenic and chondrogenic lineages, when compared to early passage cells (Muraglia et al. 2000). Furthermore, CD73 and CD105 markers are expressed on initially *in vitro*-expanded and later sub-cloned MSCs (Pittenger et al. 1999). However, after differentiation towards osteogenic, adipogenic and chondrogenic lineages, only approximately 30% of the cells were actually multipotent (Pittenger et al. 1999; Boxall & Jones 2012). This observation suggests that markers, such as CD106 (Jones et al. 2010; Jung et al. 2011; Liu et al. 2008), whose expression is reduced with progression of differentiation, can be instrumental in selection of the truly multipotent MSCs.

Despite the concerted effort the *in vivo* identity of MSCs is not yet established, as it is for HSCs (Wognum et al. 2004). The list of candidate-markers for MSCs is continuously being extended (Lv et al. 2014). With increase in numbers of candidate markers, a new issue becomes apparent – co-expression of the same markers by different cell types (reviewed by Boxall et al.). Majority of common MSC surface markers are shared by endothelial lineage cells. However, CD90 and CD271 are not expressed by endothelial cells, but are present on the MSCs. (Boxall & Jones 2012)

The $CD271^+$ (low-affinity nerve growth receptor) surface marker was found as an effective MSC discriminator by Quirici and colleagues (Quirici et al. 2002). To increase the purity of the fraction, the removal of hematopoietic cells, which carry CD45 receptor, is often required. CD45 gaiting is also performed to avoid selection for false-positive MSCs, as hematopoietic progenitor cells of erythroid lineage express CD271 `at low levels (Tormin et al. 2011; Cuthbert et al. 2012). Several studies have identified $CD271^+$ as one of the key markers for achieving high MSC purity (Cuthbert et al. 2012; Jones et al. 2010; Poloni et al. 2009).

Alongside with $CD271^+$ marker, MSCA-1 (mesenchymal stem cells antigen-1) was also found to be a highly selective marker for MSC isolation and specific differentiation potential (Bühring et al. 2009). Battula et al. has used positive MSCA-1^+, together with negative $CD56^-$ (neural cell adhesion molecule (NCAM)) markers to show 90-fold enrichment in CFU-F, with strong cellular propensity to differentiate into adipocytes. Whereas, cell fraction positive for MSCA-1^+ and $CD56^+$, yielded 180-fold enrichment in CFU-F, and differentiation progression of the cells towards chondrocytes and pancreatic-like islets (Battula et al. 2009).

Another surface marker, which can be an excellent identifier of multipotent MSCs *in vivo* is Leptin (fat-specific hormone) Receptor, also known as CD295. In the study of Zhou et al. 0.3% of the mice bone marrow cells were $CD295^+$, where these cells formed 94% of CFU-F colonies. $CD295^+$ were also able to from bone, cartilage and adipocytes in monolayer culture and after *in vivo* transplantation. Through fate-mapping $CD295^+$ cells were found to be a major source of bone and adipocytes in the bone marrow. In addition, Zhou et al. has observed $CD295^+$ to be quiescent under normal physiological conditions, but being active and bone-forming after an injury (*in vivo*). (Zhou et al. 2014)

Alternatively to surface markers, MSC identity can also be elucidated by analysing intracellular proteins, such as Nestin (Isern et al. 2013) – an intermediate filament protein, or gene transcripts could be used to identify MSC with further verification of *in vivo* functions through expression in knock-out animal models (Boxall & Jones 2012).

A single and unique marker for BM MSC, which would guaranty 100% purity of the subset, has not yet been found. However, it is already possible to pre-select MSCs with desired properties through marker analysis for clinical application (Cuthbert et al. 2015; Battula et al. 2009; Zhou et al. 2014). Recommendations, provided by the ISCT back in 2006, was a key step towards standardising the MSC field (Dominici et al. 2006). However, the search for unique markers of MSCs from different locations should continue, as BM MSCs are expressing MSCA-1, but placenta-derived MSCs don't (Battula et al. 2007). The future milestone for the field is to identify an *in vivo* BM MSC phenotype, potentially leading to new therapy applications.

2.6 Differentiation in MSCs: identification and regulation

It is vital to develop a rigorous systematic approach to identifying MSCs. However, it is equally important to be able to precisely characterise differentiation potency of the MSCs at various stages of development, as differentiation capacity is the key characteristic of MSCs.

Differentiation is the process of cell transition from a less-specialised to a more-specialised cell, what is reflected in phenotype and function of the cell. As it was described above, surface markers and gene expression can be used to reveal "stemness" and MSC identity. Identical methods can be used to trace differentiation fate of MSCs and characterise their progenitors.

Ability of the MSCs to demonstrate osteogenesis, adipogenesis and chondrogenesis – is a fundamental requirement for identifying this cell type *in vitro*. Differentiation is an elaborate process with multiple stages, which is orchestrated by cascades of biochemical and mechanical signals (Engler et al. 2006; Augello & De Bari 2010). Progression of the differentiation can be monitored through expression of specific markers. Numerous factors are affecting differentiation progression, but several master regulators, which act as differentiation markers, will be highlighted (Table 1). For MSC osteogenesis and adipogenesis such regulators are Runt-related transcription factor 2 (Runx2) and peroxisome proliferator-activated receptor-γ (PPARγ), respectively. Both of these transcription factors are cytokine mediators (James 2013; Marie 2008).

Apart from being a key regulator of adipogenesis, PPARγ has also an anti-osteogenic effect (Akune et al. 2004). PPARγ is considered to be a master regulator of adipogenesis, as it is a single known transcription factor, which is able to recover adipocyte generation when PPARγ is knocked out. In addition, majority of the pro-adipogenic cell signalling pathways are connected with PPARγ. (Tzameli et al. 2004; Siersbæk et al. 2010)

It is important to note, that in case of osteogenesis and adipogenesis an inverse relationship is observed – progression of osteogenesis prevents development of adipogenesis (James 2013).

Osteogenic differentiation is activated and regulated by Runx2 (Marie 2008). Importance of Runx2 *in vivo* was demonstrated by Otto et al., when Runx2-deficient mutant mice would die short after birth, and would demonstrate absence of osteoblasts and bone tissue (Otto et al. 1997).

Kulterer et al. has conducted gene expression profiling of expanded human bone marrow MSCs and differentiated osteoblasts (MSC-derived), where through microarray analysis crystalline-αB (CRYAB) was identified as a candidate marker for osteogenesis in MSCs (Kulterer et al. 2007). After observing several fold increase in CRYAB protein expression in MSCs, differentiating towards osteogenic lineage, Graneli et al. has confirmed CRYAB protein to be a specific marker for osteogenesis in MSCs (Granéli et al. 2014).

In the same study Graneli et al. has looked at adipogenesis in MSCs as well. Two surface markers, CD10 (neprilysin) and CD92 (choline transporter-like protein 1), were identified as markers of adipogenesis differentiation *in vitro*. However, the same markers were also shared by differentiated osteoblasts. (Granéli et al. 2014) Considering osteogenesis-adipogenesis inverse relationship, differentiation marker sharing is rare, however, it can be observed at signalling pathway level: bone morphogenic protein (BMP) and insulin growth factor (IGF) signalling have adipocytic and osteogenic stimulating properties (James 2013).

Endochondral type of bone formation clearly demonstrates relationship between osteogenesis and chondrogenesis on a morphological level (Olsen et al. 2000). These processes are also related on signalling pathway level, where fibroblast growth factor (FGF) signalling, orchestrates osteogenesis in cortical and trabecular bones, as well as chondrogenesis in the growth plate (Liu et al. 2002). FGF signalling pathway is not an exclusive signalling pathway in the development process of bone and cartilage. The Wnt signalling pathway is also observed in both differentiation lineages (Hartmann & Tabin 2000; Etheridge et al. 2004).

Apart from signalling pathways, chondrogenesis in MSCs is tightly regulated by SOX9 (SRY (sex determining region Y)-box 9) transcription factor during the lineage commitment stage (Cheng & Genever 2010). Where progression towards terminally-differentiated chondrocyte can be traced by the expression of aggrecan and collagen II markers (Williams et al. 2003; Banfi et al. 2000). Chondrogenic stimulation of MSCs has an inhibitory effect on osteogenesis, as SOX9 can inhibit trans-activation of RUNX2 and induce dose-dependent degradation of RUNX2 (Cheng & Genever 2010).

In summary, differentiation potential in MSCs commonly is being traced with surface marker, transcription factor and gene expression. However, considering multi-stage nature of the differentiation process (Augello & De Bari 2010), several lineage-specific markers should be monitored to enable accurate demonstration of differentiation progression. Apart from all of the differentiation markers listed above, there are available other well-recognised markers of differentiated MSCs. Most commonly used markers are presented in the Table 1.

Table 1: Key transcription factors and genes, which are expressed particularly during osteogenesis, adipogenesis or chondrogenesis, and are acting as specific markers of differentiation in MSCs.

Osteogenesis	Adipogenesis	Chondrogenesis
• *Runx2* (Otto et al. 1997; Cheng & Genever 2010) • *Osteocalcin (OCN)* (Banfi et al. 2000) • *Alkaline phosphatase (ALP)* (Whyte 1994)	• *PPARγ* (Zhang et al. 2010; Siersbæk et al. 2010) • *Lipoprotein Lipase (LPL)* (Clabaut et al. 2010) • *Leptin (LEP)* (Rodriguez et al. 2008)	• *SOX9* (Cheng & Genever 2010) • *Aggrecan* (Williams et al. 2003) • *Collagen II* (Banfi et al. 2000)

2.7 MSCs in monolayer culture

Alongside with surface marker and gene expression, MSCs are also selected on the basis of adherence to the tissue culture plastic (TCP) (Dominici et al. 2006). After attachment to the TCP surface, bone marrow MSCs (BM MSCs) are taking up fibroblast-like morphology (Figure 2).

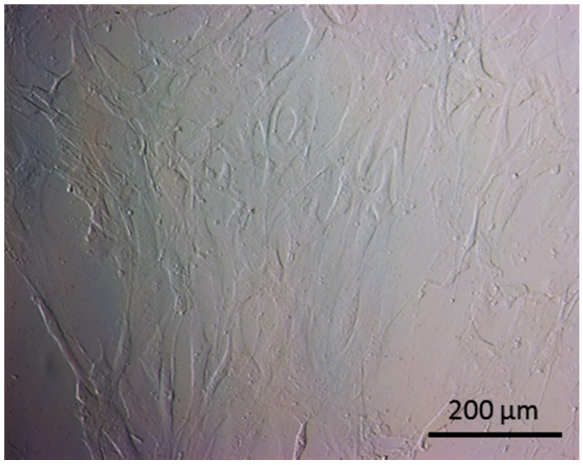

Figure 2: A brightfield micrograph of the bone marrow MSCs on 2D TCP, displaying representative fibroblast-like morphology.

Loss of a dimension, as a result of transfer from 3-dimensional (3D) architecture into 2-dimensional (2D), has a substantial effect on the native MSC phenotype. A summary view of the negative effects of the monolayer culture onto MSC native phenotype and genotype is presented in the Table 2.

Table 2: Effects of culture in 2D conditions on MSC and fibroblast natural phenotype

Effects of 2D monolayer culture on MSC and fibroblast *in vivo* phenotype and genotype	Notes	References
Loss of stemness.	Subculture of MSCs for more than 10 passages has shown to significantly reduce population doubling count, cell cycle arrest, increased senescence and reduction in MSC marker expression.	(Otte et al. 2013)
ECM production delay.	After initial adhesion to the TCP surface, MSCs are demonstrating retardation in ECM production.	(Treiser et al. 2010)
MSC-produced ECM structure alteration.	Deposited ECM in 2D is not analogous to one produced *in vivo*. *In vivo*-like ECM is needed to retain multipotency of MSCs.	(Scadden 2006)
Phenotype of the connective tissue cells is drastically affected by monolayer culture.	Fibroblasts in 2D demonstrate cell polarity, but it is absent *in vivo*.	(Cukierman et al. 2001)
Only primitive adhesion complexes are formed between the cell and the substrate in 2D culture.	In 3D ECM scaffolds mature integrin-containing focal adhesion complexes are formed in minutes, compared to 72 hours required on the 2D glass surface for ECM to be deposited.	(Cukierman et al. 2001; Chen 2010; Treiser et al. 2010)
Autocrine growth factor secretion into surrounding culture media.	During MSC culture on 3D ECM substrates, autocrine growth factors are deposited into the surrounding matrix. As a result, growth factor presentation to the cells is more physiological.	(Chen 2010)
Alterations in gene expression	MSC culture in 3D spheroids produces gene expression more representative of *ex-vivo*, than in 2D culture.	(Frith et al. 2010)

Unsuitability of 2D culture methods for analysis of the physiological response by the cells was voiced several decades ago (Bissell et al. 1982), however the importance of the third dimension was fully recognised in 1997. In a landmark study, Bissell's group has demonstrated that inhibition of the β1-integrin surface receptor in breast cells, within a 3D cancer model, leads to functional and morphological reversion to a non-cancerous phenotype of the same cells (Abbott 2003; Weaver et al. 1997).

2.8 Tissue engineering - concept introduction

With growth in understanding of potency, cellular growth and differentiation requirement, together with increasing availability of biomaterials, a discipline of tissue engineering was formed (Langer & Vacanti 1993). The vision of the tissue engineering concept is often represented by reciprocal interplay of three central factors: cells, scaffolds and stimulating signals (Figure 3).

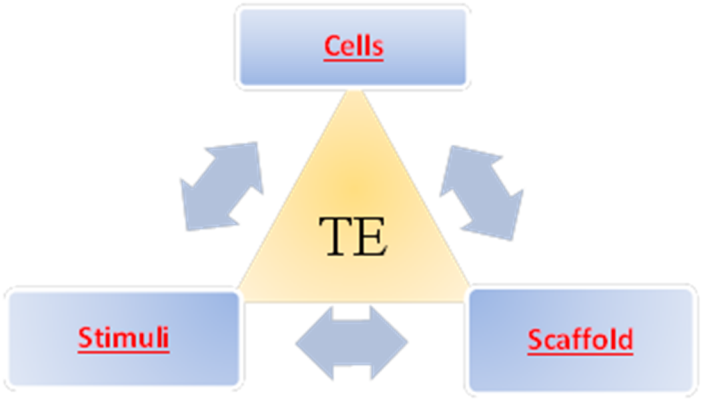

Figure 3: Conceptual view of the tissue engineering (TE) paradigm, also known as the tissue engineering triangle, represented by a reciprocal interplay between cells, scaffolds and stimuli.

Each of the key tissue engineering factors represents a list of parameters, which should be considered during the design stage of the tissue engineering solution.

MSCs are an integral part of the tissue engineering paradigm and in many aspects these cells are unique, due to their regenerative and immuno-regulating capacity. In order to produce a successful tissue engineering solution, cellular components are often supported by a mechanical "skeleton", most frequently represented by a scaffolding structure. In its core principle, scaffolding material is designed to provide a supporting 3D architecture for the cells, in order to mimic physiologically-relevant

conditions. Central part of the scaffold design process should include understanding of the target tissue architecture and internal processes, to ensure *in vivo*-like cell behaviour within final scaffold structure. To achieve the objective of matching scaffold properties with target tissue requirements, numerous scaffolding materials were designed over the last two decades (Thiele et al. 2014).

Tissue engineering and cell biology studies are inseparable, where cell culture is a fundamental aspect in both areas. At the same time, the cell culture process involves exposure of the cells to a non-natural environment. Currently, none of the available scaffolding materials can replicate cell-matrix interactions, found *in vivo*, and entire complexity of natural tissues. (Thiele et al. 2014)

Moreover, due to high variability in scaffold architecture, mechanical properties, porosity and other cell growth-related factors, the selection process should be based on the physiological requirements of the natural tissue of interest.

Concurrently, scaffold selection process can be generalised by grading the fundamental factors of the scaffold by their relative importance for viable scaffold design. Figure 4 represents core parameters that should be considered as guidelines in most of the scaffold design processes, with cell viability and scaffold toxicity being of paramount importance for successful scaffold design and function.

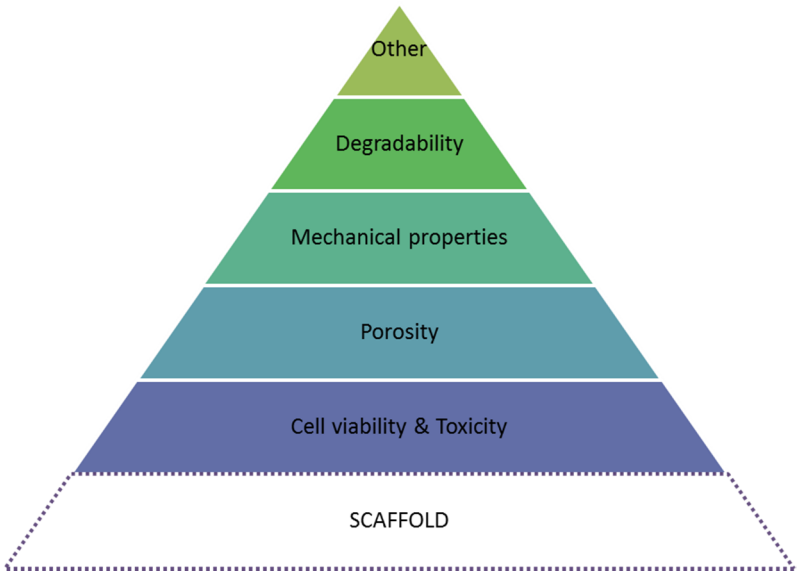

Figure 4: Central parameters in scaffold design process

2.9 MSCs in 3D environment

Mesenchymal stromal cells (MSCs) are commonly sourced from the bone marrow environment, where these cells reside in 3D and are exposed to components of the extracellular matrix (ECM), other cells types and biochemical and mechanical stimuli (Charbord 2010). Biochemical and mechanical gradients, coupled with a cascade of signals from adjacent different types of cells and ease of access to the capillary system, makes bone marrow a unique "niche" environment that facilitates MSC proliferation, preservation in non-differentiated state and cell release from the niche when required (Kolf et al. 2007; Scadden 2006).

MSC exit from the bone marrow niche is assumed to be triggered by circulating signals produced by the immune system that signals possible trauma, as well as hormonal system that helps to maintain homeostasis of the system (i.e. scheduled maintenance) (Jones & McGonagle 2008; Kim et al. 2012). It is also believed that the mechanical stimulation is an effective impetus for MSC release from bone marrow (Jones & McGonagle 2008). These finely-tuned mechanisms of tissue repair demonstrate importance of interconnected integrity of homeostatic processes *in-vivo*, which operate in a 3D context.

In attempts to trigger and manipulate innate tissue repair mechanisms of the organism or alter the development of harmful processes in the body, various drugs are being administered, most frequently intravenously or directly to the affected tissue (Hay et al. 2014; Oh et al. 2009). Along with conventional drug administration, drug-releasing scaffolds are also implanted, providing chemical and bio-mechanical stimulation at the site of implantation (Roux & Ladavière 2013). Success of any drug, addressing any process in the body, along with interaction between scaffold and the surrounding milieu, initially has to be verified in the preliminary *in vitro* tests, followed by the animal testing, culminating by testing in humans.

2.9.1 Approaches to obtaining clinically-relevant information: 2D vs 3D

The gold standard and the ultimate assessment of safety and efficacy for any therapy is clinical testing in humans. This final stage of preclinical testing is very costly and

time consuming. In order to obtain clinically relevant insight in to therapy's suitability a robust testing framework is used.

Fundamentally, all clinically-targeted research frameworks are built on the "ground-up" principle, where initial therapy testing stages are based on using system with least number of uncontrolled variables, rapid turn-around in data collection and analysis, lowest possible cost and lowest complexity of implementation. Traditionally such systems were based on 2 dimension (2D) monolayers. However, in the recent years constantly growing collection of finding suggests that overly-simplified *in vitro* models perform poorly in predicting response in animal and clinical studies (Martin et al. 2008; Härmä et al. 2010; Hirschhaeuser et al. 2010). In addition, only 10.4% of the drugs that have passed the phase 1 trial tests will reach the FDA approval (Hay et al. 2014).

Testing of novel clinical compounds on 2D monolayers became possible after invention of culture flasks in 1923 (Carrel 1923). This simplistic system gained popularity owing to relative ease of cell expansion and low operational costs. Almost 100 years later it is widely known that cells may lose their original phenotype and gene expression alterations can be acquired due to long term culture in monolayers (Røsland et al. 2009; Bara et al. 2014; Pampaloni et al. 2007; Baker & Chen 2012). The presence of a 3D structural support is often essential for non-aberrant gene expression and cell functioning, as exemplified by mammary epithelial cells (Bissell et al. 1982; Bissell et al. 2002). The importance of a 3D organisation has also been identified in MSCs (Martino et al. 2009; Jongpaiboonkit et al. 2009) and their differentiated progeny (Darling & Athanasiou 2006), where MSC expansion and long-term culture in monolayers will lead to retardation in proliferation, loss of the multi-lineage differentiation capacity and a 36-fold reduction in bone forming efficiency *in vivo* (Banfi et al. 2000).

Rapid progress in the fields of gene sequencing and high throughput systems during the last decade has provided new sophisticated research tools (Cheng et al. 2008; Huang et al. 2008), simultaneously allowing new questions to be posed regarding cell behaviour in environment that more closely resembles the complex interactions of the *in vivo* milieu.

2.10 Natural and synthetic scaffolds, commonly used in tissue engineering

In attempt to model *in vivo* environment of a cell as closely as possible, and to provide tissue engineering solutions for cell therapies, numerous natural and synthetic scaffolds were designed, characterised and adopted for the need of the fundament research and biomedical applications.

Table 3 represents a summary view of the key hydrogel materials used for cell encapsulation, analysis and therapy delivery. In addition, a description of each hydrogel's gelation method, characteristic properties, cell support and encapsulation capacity is provided.

Table 3: Natural and synthetic hydrogels, commonly used in biomedical applications

Hydrogel	Class	Gelation method (Phase transition)	Key properties	Cell support ability
Fibrin	Natural	Thrombin-driven association of the fibrinogen into a fibrillar network.	• Contains binding sites (RGD and AGDV) (Janmey et al. 2009) • Elastic modulus ≤ 0.1 kPa (Thiele et al. 2014) • Strain-stiffening (Janmey et al. 1983)	• 3D fibrin beads used to study angiogenesis by endothelial cells (Nehls & Drenckhahn 1995; Nakatsu et al. 2007) • Myoblasts in fibrin glue were injected into infarcted heart tissue, and demonstrated increased transplant survival and decreased infarct size after 5 weeks. (Christman et al. 2004)
Collagen	Natural	Three polypeptide chains interweave into a helical structure which forms collagen fibre. Peptide bonds at the end of each helix crosslink with adjacent fibres.	• Is a major component of the ECM. • Responsible for bone tissue flexibility and soft tissue elasticity (Mano et al. 2004) • Carries a potential of the antigenic and immunogenic response during in vivo use. (Lynn et al. 2004)	• Fabrication of the 3D stable matrices, which support cell seeding and spreading (Gillette et al. 2008) • Keratinocytes were successfully cultured in spongy collagen scaffolds in static conditions. Whereas dynamic perfusion settings demonstrated higher cell proliferation in the identical constructs (Navarro et al. 2001).
Gelatin	Natural	It is a mixture of peptides derived from collagen by hydrolysis. Gelation occurs at 30˚C. Is in need of crosslinking as it lacks thermal stability. (Thiele et al. 2014)	• Can be degraded by a broad range of proteases. (Palmer 1993) • Has reduced potential of an antigenic response, than collagen. (Rose et al. 2014)	• Endothelial cell sheet delivery (Lai 2010) • 3D CAD scaffold supports porcine MSC's adhesion and proliferation (Ovsianikov et al. 2011)

Matrigel	Natural	It is a mixture of the basement membrane proteins, isolated from a mouse sarcoma. Rapid protein polymerisation takes place between 22˚ and 35˚C. (Corning 2013)	• Composition after isolation: ca. 60% laminin, 30% collagen IV, and 8% entactin. (Corning 2013) • It also contains perlecan and various growth factors (i.e. TGF-β and IGF-1). (Corning 2013)	• Promotes tumour cell growth in vivo (Fridman et al. 1990) • Promotes self-renewal and pluripotency in stem cells in 2D cultures (McElroy & Reijo Pera 2008) • Endothelial differentiation of MSCs in 3D setting (Portalska et al. 2012)
Hyaluronic acid (hyaluronan)	Natural	Hyaluronan is structurally-simplest glycosaminoglycan (Kogan et al. 2007). However, to forma hydrogel it requires a chemical modification (often crosslinking) (Burdick & Prestwich 2011).	• It is an immunoneutral and non-sulphated ECM component with important role in tissue homeostasis and repair. (Burdick & Prestwich 2011) • It can be degraded in vivo by hyaluronidase (Leach et al. 2003)	• Fibroblast, hepatocyte, MSC and endothelial cell expansion in 3D with following cell recovery via gel dissolution. (Zhang et al. 2008) • Hyaluronic acid – tyramine conjugates can undergo crosslinking in vivo. Resultant injectable scaffold supported caprine MSCs in 3D and modulated matrix biosynthesis and cartilage tissue histogenesis. (Toh et al. 2012)
Alginate	Natural	Non-modified alginate gels through inter-molecular electrostatic interactions. (Thiele et al. 2014)	• Alginate is inherently does not support cell adhesion, is non-fouling and not cleavable by natural enzymes (Lee & Mooney 2012) • Low immuno-response showed by the alginate implants (Zimmermann et al. 1992)	• Alginate gels, chemically conjugated with RGD peptide sequences, support myoblast adhesion and proliferation in 2D. (Rowley et al. 1999) • Alginate was photo-patterned into a 3D microfluidic system for co-culture of preosteoblasts and endothelial cells. (Chueh et al. 2010)
Chitosan	Natural	Through adjustment of pH, spontaneous gelation is triggered via balancing out of	• Chitosan, derived from natural chitin, shares some monomer units with hyaluronic acid and it closely simulates	• Chitosan-encapsulated primary rat hepatocytes demonstrated rounded morphology and production of albumin.

		the hydrogen bonding, hydrophobic and interchain electrostatic interactions. (Thiele et al. 2014)	glycosaminoglycans in the ECM of the tissue. • Non-modiefied chitosan is fully soluble below pH 5 and it is insoluble (forms a gel) above pH 7 due to cationic nature and semi-crystalline properties of a high charge density. (Yoon & Fisher 2009)	(Li et al. 2003) • Rat osteoblasts were cultured in chitosan sponges for 56 days, where cell proliferation and subsequent osteogenic differentiation was observed. (Seol et al. 2004)
Agarose	Natural	Agarose chains interact through hydrogen bonding to form a double helix. (Yoon & Fisher 2009)	• Presence of the hydroxyl groups on the backbone of the agarose induces polarity in the structure. Hence, agarose is water soluble at high temperatures and it forms a gel at lower temperatures. (Yoon & Fisher 2009) • Strength and permeability of the gel is dictated by the concentration.	• MSCs, encapsulated in agarose capsules, have demonstrated increased survival. (Karoubi et al. 2009) • ECM is readily formed by disc cells within 3D agarose gels. (Gruber et al. 2006)
Hydrogel	Class	Gelation method (Phase transition)	Key properties	Cell support ability
PNIPAM	Synthetic	At the LCST point, enthalpic contribution of hydrogen-bonded water molecules is dominated by the entropic gain within the whole system (Alarcon et al. 2005). As a result, polymer-water separation takes place with, and at the sufficient polymer concentration a colloidal gel structure is formed.	• PNIPAM is thermo-responsive and reversible hydrogel. With further functionalisation and co-polymerisation other phase transition triggers can be introduced (i.e. pH, ultrasound, salt concentration, magnetic and electric fields) (Ebara et al. 2014; Ilic-Stojanovic et al. 2011) • Molecular weight and polarity of the chain ends greatly affects temperature of the phase transition (LCST point) (Rimmer et al. 2007)	• PNIPAM hydrogel, co-polymerised with acrylic acid, has supported bovine articular chondrocytes *in vitro* for at least 28 days. Formation of a cartilage-like tissue was also observed. (Stile et al. 1999) • Modification of the PNIPAM hydrogel with cell-adhesive peptide (GRGDS) produced a thermo-responsive substrate for adhesion, proliferation and subsequent detachment (without trypsinisation) of the human dermal

				endothelial cells on demand. (Hopkins et al. 2009)
PAA	Synthetic	Poly(acrylic acid) (PAA) requires crosslinking in order to form a hydrogel. The ionic network structure of PAA is strongly affected by the pH, the monomer concentration and the ionic strength during the polymerisation. (Elliott et al. 2004)	• PAA hydrogel network is able to absorb many times its' weight in water, making this polymer a super-absorbent. Such swelling capacity is attributed to presence of the carboxylic acid groups on the chain ends. (Elliott et al. 2004)	• Polymer films were graft-polymerised with PAA, forming covalently bound brushes. Smooth muscle cells have successfully adhered and proliferated on such substrate. (Bisson et al. 2002) • Acrylic acid-functionalised scaffold supported human hepatocyte adhesion. (Hayward et al. 2013)
PEG	Synthetic	Pure poly(ethylene glycol) (PEG) requires functionalization or a crosslinker for gel formation. However, when PEG is functionalised vinyl sulfone and conjugated with cysteine-containing peptides, gelation occurs at physiological temperatures and near-physiological pH (Lutolf, Raeber, et al. 2003).	• PEG is inherently biocompatible, but it does not promote cell adhesion. (Thiele et al. 2014) • PEG hydrogel is often used as an inert structural substrate with inherent hydrophilicity and resistance to protein adsorption. (Raeber et al. 2005) • At high molecular weights PEG is an extremely hydrophilic polymer. (Place et al. 2009)	• Non-functionalised PEG gels are able to encapsulate MSCs, however, encapsulated cells undergo apoptosis due to a lack of cell-matrix binding sites. (Thiele et al. 2014) • Functionalised PEG gel has supported primary human dermal fibroblasts spreading on the surface of the gel with further migration within the gel, creating a 3D interconnected cellular meshwork after 3 weeks. (Lutolf, Raeber, et al. 2003)
PVA	Synthetic	Poly(vinyl alcohol) (PVA) gels are commonly formed by physical crosslinking (via repeated freezing-thawing	• Non-modified PVA is hydrophilic and water-soluble, but non-degradable (Place et al. 2009). • Non-functionalised PVA gels are	• Functionalised PVA was used to encapsulate murine neuroblastoma cells, demonstrating cell viability after crosslinking and during short culture

		methods), or chemically crosslinked with glutaraldehyde or epichlorohydrin. Additionally, PVA can form hydrogels by blending with other water-soluble polymers. (Zhu & Marchant 2011)	inherently non-adhesive (Schmedlen et al. 2002)	period. (Ossipov et al. 2007) • RGDS-functionalised PVA gels were seeded with dermal fibroblast, and demonstrated adhesion and cell survival during 2 weeks of culture. (Schmedlen et al. 2002)
PLA	Synthetic	Poly(lactic acid) (PLA) polymer is hydrophobic aliphatic polyester. In order to form a hydrogel, functionalization with hydrophilic PEG is required (Metters et al. 2000).	• With increase in the molecular weight of the PLA polymer, degradation rate in vivo decreases. Up to 50% weight loss is observed after 6 months of in vivo implantation. (Gogolewski et al. 1993)	• PLA scaffold degradation products can elicit a strong inflammatory response in vivo. (Bergsma et al. 1993) • Composite scaffold of PLA and bioglass were seeded with mesenchymal stem cells and endothelial progenitor cells to be tested in a rat calvarial critical size defect model for 3 months. Consequently, no long-term inflammatory reaction or tumour formation was observed. In addition, formation of new bone mass was also observed. (Eldesoqi et al. 2014)

2.11 Optimal mimicking environment of the bone marrow – synthetic hydrogel

In order to obtain understanding of the MSC behaviour within its' natural environment – bone marrow, it is important to employ a testing environment that would mimic key structural, mechanical and biochemical parameters of the bone marrow in a controlled fashion. Such particular requirements are met by a synthetic hydrogel scaffolds.

Firstly, the synthetic parameter allows precise control over structure's macromolecular architecture and defined functional group addition. Secondly, hydrogels, by definition, are cross-linked three-dimensional polymer chain networks, where water, the main component by weight, is the intra-chain space filler. In addition, the name, hydrogel, implies ability of the material to hold substantial amounts of water, where this dispersive component may serve as a transport medium for macro-molecule (i.e. nutrient and waste transport). Thirdly, any scaffold represents a supportive structure for the cell; and keeping in mind synthetic nature of the scaffold – structural parameters can be fine-tuned for the needs of the cell.

Synthetic hydrogels, which are commonly used as scaffolds for biomedical applications, can be exemplified by poly(ethylene glycol) (Burdick & Anseth 2002), poly(N-isopropylacrylamide) (Lapworth et al. 2011), poly(vinyl alcohol) and poly(acrylic acid) (Lee et al. 1996)).

However, in search for scaffolds with physiologically-exploitable properties, increasing number of research groups are conducting studies on hydrogels with environment-sensing properties (Ilic-Stojanovic et al. 2011). A particular subset of such materials is represented by hydrogels with thermo-sensitive and state-reversible properties. Thermo-sensitive properties, which are biologically-applicable, are exhibited by poly(methyl vinyl ether), poly(N-vinylcaprolactam) and poly(N-isopropylacrylamide), amongst many (Schmaljohann 2006). Due to high sensitivity of the polymer to environmental condition change and a resulting prompt phase transition, such hydrogels are named "smart" or "intelligent". Poly(N-isopropylacrylamide) is a prime example of a temperature responsive "smart" hydrogel (Maeda et al. 2000). Alongside with temperature, phase transitions

processes within “smart” hydrogels can be also triggered by pH, salt concentration, ultrasound, irradiation, electric and magnetic fields (Ilic-Stojanovic et al. 2011; Ebara et al. 2014). Furthermore, recent studies have shown that “smart” hydrogels, sensitive to biochemical agents (e.g. ligands, enzymes, antigens), hold a great promise for clinical application (Wang et al. 2010; Ebara et al. 2014; Gil & Hudson 2004). The list of “smart” hydrogels is constantly supplemented with novel gel systems, where several gelation stimuli are integrated into one polymer architecture (Glazer et al. 2013; Klaikherd et al. 2009).

Response to external stimuli by “smart” hydrogels is exhibited in two processes: swelling-deswelling or solution-gel transition (Gutowska et al. 1992; Maeda et al. 2000). The mode of polymer phase transition is predetermined by the nature of the polymer crosslinking - physical or chemical.

In contrary to chemically cross-linked hydrogels, where polymer chains are covalently bound, physically cross-linked hydrogels are held together by ionic, hydrophobic or hydrogen bonding interactions (Ebara et al. 2014; Song et al. 2013; Omidian & Park 2010). Due to the nature of the polymer chain interaction within the network, physically cross-linked hydrogels are of a particular interest for simulating *in vivo* tissue properties, as they precisely mimic the molecular integration of the biological systems. In biological systems, non-covalent intermolecular interactions are predominant (Lodish et al. 2000). Such interaction mechanism ensures dynamism in assembly and function of the biological systems (Ebara et al. 2014; Mohammed & Murphy 2009).

At the same time, physically cross-linked hydrogels represent following limitations, important for scaffold design: inability of controlling degradation and gelation times, pore size, mechanical strength and chemical functionalisation, independently from other parameters (Ebara et al. 2014). In contrast, chemically cross-linked hydrogels form an interconnected structure, which is formed, most commonly, via radical polymerisation or UV radiation (Ahmed 2013; Doycheva et al. 2004). Due to permanently linked network structure, chemically cross-linked hydrogels are mechanically strong, stable and exhibit relatively long degradation times (Hennink & van Nostrum 2012).

Despite the drawbacks, physically cross-linked hydrogel, like PNIPAM, demonstrates physiologically relevant properties, such as temperature or pH sensitivity, stimuli-driven reversible hydrogel assembly and *in vivo*-like non-covalent bonding. Such properties make PNIPAM a very attractive platform for simulation of the *in vivo*-like interactions between cells and the hydrogel. In addition, by employing polymer architecture with high number of amenable functional groups, for example highly branched architecture, it becomes possible to fine-tune the hydrogel properties for cell encapsulation.

2.12 PNIPAM architecture: synthesis and properties

In the process of exploration of the PNIPAM's stimuli-responsive nature and due to the drive to increase versatility of this "smart" material, polymers with distinct architectures were synthesised (Figure 5): "comb-like" graft, random (Lapworth et al. 2011) and block copolymers (Klaikherd et al. 2009), interpenetrating networks (IPN) (Gutowska et al. 1994) and branched polymers (Hopkins et al. 2009).

Every polymer architecture mentioned provides unique benefits (Table 4). For example, advantage of the copolymer architecture is the ability to combine properties of two or more polymers in one structure (Lapworth et al. 2011). Whereas, interlacing of two polymer networks, but without covalent bonding between them, results in formation of IPN with increased elasticity and improved mechanical strength (Guilherme et al. 2006). At the same time, highly branched polymers are demonstrating very different mechano-chemical properties, when compared to their linear analogy: reduction in viscosity is commonly seen with highly branched polymers, as the level of chain entanglement is reduced (Carter, Hunt, et al. 2005); introduction of the branched architecture into linear PNIPAM improves solubility of the polymer in conventional solvents (Carter et al. 2007).

Table 4: Examples of the PNIPAM-based polymer architecture types

Architecture type	PNIPAM-based polymer examples	Environment-responsive ("smart") properties
Linear polymer	Poly(N-isopropylacrylamide) (PNIPAM) (Kubota et al. 1990)	The phase transition of linear PNIPAM occurs above 31˚C, being also reversible and reproducible.
Block copolymer	PNIPAM-co- (2-hydroxyethyl methacrylate) (PNIPAM-co-HEMA) (Klaikherd et al. 2009)	Resultant polymer self-assembles into a micellar structure in aqueous environment and is able to encapsulate hydrophobic molecules. Assembly and degradation can be stimulated through thermal and pH triggers.
Linear random copolymer	Poly(NIPAM-co-styrene) (PNS) (Lapworth et al. 2011)	Reversible thermos-gelation was observed, allowing cell release. With increase in styrene content, gelation temperature decreased from 33.9 ˚C to 24.2 ˚C. In addition, with increase in styrene proportion, water retention has reduced dramatically. At the same time, culture media retention was improved.
"Comb-like" graft copolymer	PNS with poly(N-vinyl pyrrolidinone) (NVP) pendant grafts (PNS-g-NVP) (Lapworth et al. 2011)	Introduction of the NVP graft into PNS system separated temperature of gelation and solvent retention functions into different polymer sections (i.e. the backbone and the grafted chains (brushes)). Inclusion of the NVP improved culture media retention and an overall stability of the gel.
Highly-branched polymer	PNIPAM co-polymerised with 3H-imidazole-4-carbodithioic acid 4-vinylbenzyl ester. (Carter, Hunt, et al. 2005)	Increase in branching has reduced the intrinsic viscosity, when compared to linear analogues. Clouding of the branched PNIPAM was lower, compared to equivalent linear PNIPA polymers.
Interpenetrating network (IPN)	Semi-IPN of cross-linked PNIPAM and linear poly(ether(urethane-urea)) (Gutowska et al. 1994)	IPN architecture accelerated swelling and increased mechanical strength of the gel, when compared to cross-linked PNIPAM network. Swollen thermosensitive gel has demonstrated controlled release mechanism after heparin loading.

During polymerisation of the highly branched polymer many unreacted functional groups are formed. In theory, the number of these unreacted groups is equal to the number of repeating units. Therefore, the higher is the level of branching, the more functional groups are available for interaction, what affecting polymer's properties. Contrary to branched polymers, the number of functional groups in linear polymers is constant, and the effect of these groups on polymer properties diminishes with increase in molecular weight. (Jikei & Kakimoto 2001)

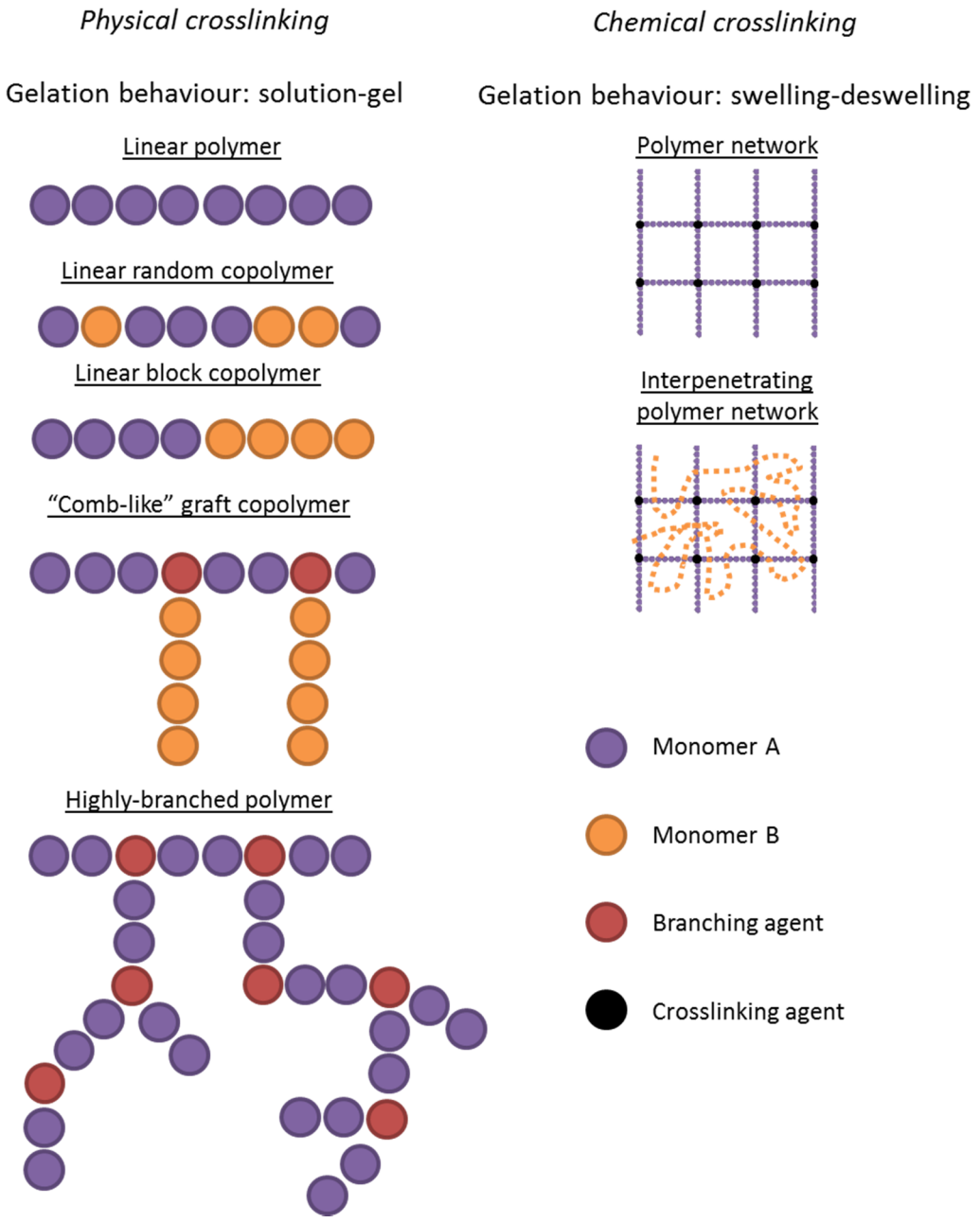

Figure 5: Main polymer chain architecture in physically and chemically cross-linked hydrogel systems.

Highly branched polymers owe their functionality to architecture of the polymerisation method used. By employing a type of a living polymerisation reaction (i.e. where chain termination ability is removed) with a free radical on the chain end, a fine control over the molecular weight and narrow molecular weight distribution can be obtained. Use of the free radical-based synthesis allows step-wise growth of the chains, so that by the end of the first polymerisation stage formed polymer chain is "capped" by a free radical. Further addition of the monomer and the initiator will propagate chain growth. In addition to control over molecular weight, functional groups of interest can be introduced in a controlled manner at every stage of polymerisation. A vastly popular living polymerisation technique that allows generation of branched polymers is reversible addition-fragmentation transfer polymerisation (RAFT), first introduced in 1998 by Chiefari and colleagues (Chiefari et al. 1998). In the RAFT system, dithioate ester, a chain transfer agent (CTA), is introduced into living polymerisation process to form a dormant-type of radical chains ends. As a result, these chain-ends are available for further polymerisation or functionalisation (Rimmer et al. 2007). A detailed description of the RAFT mechanism has been published by Moad and colleagues (Moad et al. 2005).

In case of highly branched poly(N-isopropylacrylamide) (HB PNIPAM), a material of interest in the current study, RAFT polymerisation method has produced a physically cross-linked hydrogel (Hopkins et al. 2009). After initial RAFT polymerisation, obtained highly-branched polymer structures are akin to dendrimer architecture (England & Rimmer 2010). However, instead of perfect symmetry in Brach shooting (a unique feature of dendrimer architecture), a proportion of the branches in the HB PNIPAM are not propagated, as the branching process is heavily dependent on uniform initiator decomposition and consecutive free radical formation under high temperatures (England & Rimmer 2010).

Furthermore, when the HB PNIPAM polymer is mixed with water it forms a colloidal dispersion (Hopkins et al. 2009). And when the temperature is below the lower critical solution temperature (LCST) point, all accessible hydrophilic regions become fully saturated with water molecules, what is manifested as dissolution. This dissolution process is driven by hydrogen bond formation between the solvent and

the hydrophilic sites of the polymer chains (i.e. polar and hydrophilic amide functional regions of the polymer) (Maeda et al. 2000; Tanaka et al. 2011). However, when the phase transition temperature is reached, representing solution-gel transition, these hydrogen bonds are disrupted and prevailing intrachain hydrophobic forces are driving initial coil-globule condensation and following polymer-solvent phase separation, which results in colloidal gel formation (Ding et al. 2005). The described mechanism of gelation process is indicative of the physical crosslinking of the polymer.

The LCST point and the gelation mechanism in PNIPAM has been recognised in 1967 by Scarpa and colleagues (Scarpa et al. 1967). After years of research, a conceptual view of this phase-transition process in PNIPAM can be described in thermodynamics terms as follows: at the point of LCST phase transition, enthalpic contribution of hydrogen-bonded water molecules is dominated by the entropic gain within the whole system (Alarcon et al. 2005). As a result, polymer-water separation takes place with, and at the sufficient polymer concentration a colloidal gel structure is formed.

The LCST point of linear PNIPAM is 31-32˚C - a physiologically relevant temperature (Scarpa et al. 1967; Heskins & Guillet 1968). Therefore, a system that allows generation of a 3D polymer network (Wu et al. 2014), that entraps water at physiologically-relevant temperature, is of interest and potential benefit for clinical application.

2.13 Biomedical application of the PNIPAM hydrogel

Thermo-responsive and phase transition property of NIPAM-based hydrogels has been explored by numerous research groups, with main focus on production of a "smart" drug-releasing mechanisms (Wei et al. 2006), scaffolding materials for cell encapsulation (Gan et al. 2009; Ibusuki et al. 2003) and affinity studies (Carter, Rimmer, et al. 2005).

Controlled drug release capacity of the PNIPAM systems was the initial driver for this "smart" material. By the end of 1980's, popularity of PNIPAM-based hydrogels

in the biomedical field was rapidly gaining momentum, as this material was providing novel means of controlling drug release (Schild 1992). Fine-tuning capabilities over the releasing process can be exemplified by the study of Gutowska et al., where chemically-cross-linked PNIPAM hydrogel was studied as a loading and release mechanism for heparin, an anti-coagulation factor in surface induced thrombosis (Gutowska et al. 1992). Application of this hydrogel-based system was further tested in a canine *in vivo* model, which showed significant reduction of thrombus formation (Gutowska et al. 1995).

Currently, the most promising application of the thermos-sensitive PNIPAM hydrogels – is substrate and scaffolding material design. Despite obvious benefits of the PNIPAM-based hydrogel properties for tissue engineering, several limiting factors are well known: expulsion of water at temperatures above LCST (also known as syneresis), low mechanical rigidity and opaqueness at temperatures above LCST. All of these factors hinder the applicability of the PNIPAM, where the issue of syneresis is of particular importance. In some cases overly active syneresis can lead to a complete hydrogel collapse, effecting overall mechanical strength and pore size within the gel (Gan et al. 2010).

These drawbacks are characteristic for conventional linear PNIPAM (Wu et al. 2003; Maeda et al. 2000). Practical issue of opaqueness and low mechanical rigidity are addressed by copolymerisation with mechanically strong and transparent hydrogel (Cheng et al. 2012; Ibusuki et al. 2003). In order to reduce or prevent the syneresis effect, PNIPAM polymer chains are most frequently functionalised with hydrophilic groups, like acrylic and carboxylic acids (Jha et al. 2014; Gutowska et al. 1992; Rimmer et al. 2007).

Along with affecting water retention with functional group addition, biologically active molecules can be also integrated into hydrogel architecture to direct cellular response. Perhaps, most frequently used biomolecule with NIPAM-based hydrogels is arginine–glycine–aspartic acid, also known as RGD peptide sequence (Stile & Healy 2001; Rimmer et al. 2007). RGD sequence is a recognised effector of cell saviour, both in 2D and 3D environments (Martino et al. 2009; Tibbitt & Anseth 2009; Mager et al. 2011).

With an increase in understanding of the regenerative capacity of MSCs, selective testing of the biomimetic factors, like RGD, has become commonplace with MSCs. Optimised presentation of RGD in bio-inert 3D environment has a stimulating effect on cell viability (Salinas & Anseth 2008) and differentiation (Jha et al. 2014). RGD is only one out of numerous molecules available for hydrogel functionalisation (Yokoi et al. 2005; Fonseca et al. 2011; Jongpaiboonkit et al. 2009). Another popular functionalisation molecule is a matrix metalloproteinase (MMP)-sensitive peptide sequence (Fonseca et al. 2011; Lutolf, Lauer-Fields, et al. 2003). By means of using MMP sequences, scaffold degradation is driven by cell activity, aiding adaptation of the 3D environment to the needs of the cell. Furthermore, in a recent study Jha and colleagues combined RGD functionality with MMP-sensitive architecture within PNIPAM polymer (Jha et al. 2014).

It is well understood, that function of the ECM is not only to structurally support the cells with its' architecture, but also to be a guide the development of the cells. This guiding process can be simulated by using light patterning approach, pioneered by Kloxin and colleagues (Kloxin et al. 2009). By using a multi-photon microscope and photodegradable hydrogel in the light patterning method, it has become possible to attain cellular organisation with "tissue-like" hierarchy within a scaffold 3D environment (Lutolf 2009).

2.14 Highly branched PNIPAM – focus of the research study

Thermo-responsive nature of the PNIPAM, functionalisation options, biocompatibility and versatility of application in tissue engineering is the driving force behind the interest for this "smart" hydrogel.

The central area of interest for tissue engineering filed is the understanding of the *in vivo* environment and the repair processes involved, with an ultimate intent to translate new findings into clinical applications. In order to gain this understanding, ever more research groups are employing 3D culture methods, as the conventional monolayer culture systems poorly represent *in vivo* conditions (see Table 2).

Over the last three decades, PNIPAM polymers of numerous designs were produced to obtain in-depth knowledge of the phase transition process and to explore new applications of this material. Review of the literature has highlighted the beneficial, as well as limiting, properties of PNIPAM hydrogels. It is evident, that this "smart" material holds a great promise in providing an *in vivo* mimicking environment for fundamental research and clinical application, as a non-invasive injectable scaffold.

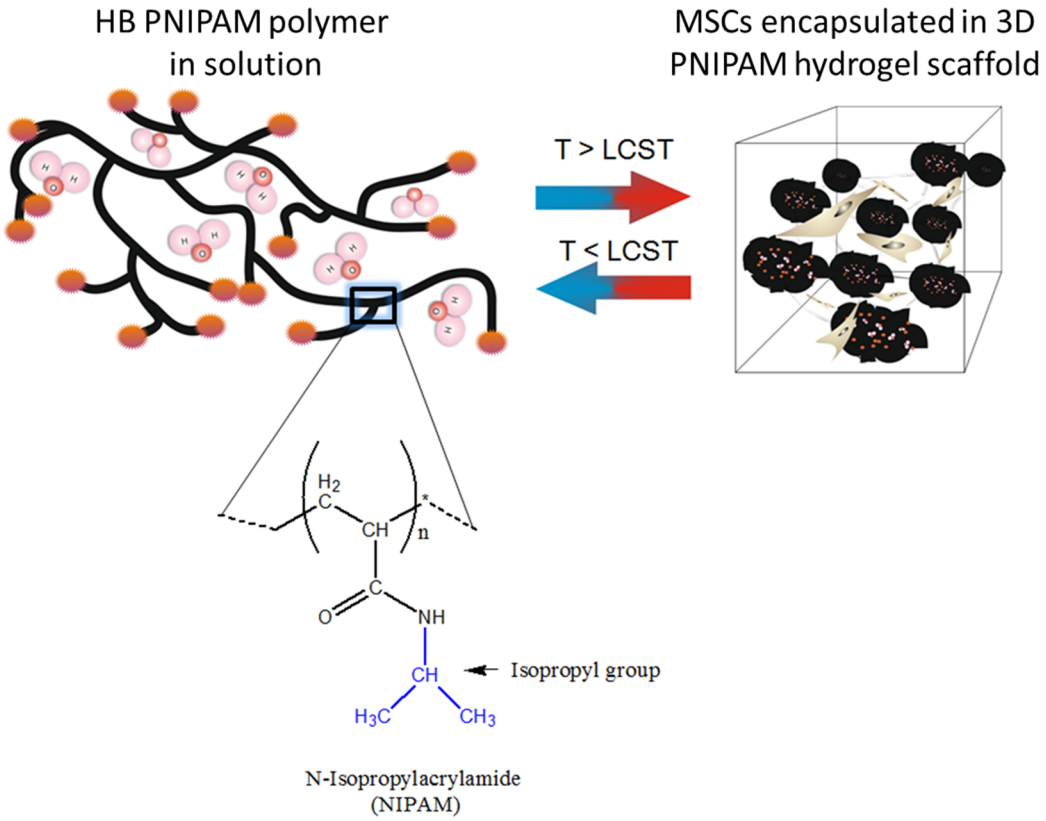

Figure 6: Conceptual view of the 3D encapsulation of MSCs by highly branched PNIPAM.

Prior to clinical translation it is vital to collect as much as possible of clinically relevant information by means of *in vitro* testing and analysis. As the literature review has demonstrated, PNIPAM hydrogels can be used for 3D cell encapsulation in attempt to generate a cell supporting environment and simulate *in vivo* conditions. Therefore, the central aim of this research is to develop a novel 3D scaffolding environment, on the basis of highly branched PNIPAM polymer, for analysis of MSC behaviour in 3D *in vivo*-like environment (Figure 6). Detailed description of the aims and objectives is presented in the next section.

2.15 Project aims and objectives

PNIPAM-based hydrogels hold a great promise for generation of the scaffolding environment for cell encapsulation. From the vast selection of the hydrogel architectures, highly branched PNIPAM hydrogel is of particular interest for cell encapsulation, due to the control over functional group presentation this polymer architecture can provide.

Previously, Hopkins and colleagues has demonstrated that highly branched PNIPAM with RGD-functionalised chain ends can be used for fibroblast and endothelial cell adhesion, monolayer culture and subsequent trypsin-free detachment upon cooling below LCST point (Hopkins et al. 2009).

Despite a considerable potential of PNIPAM in cell encapsulation, competence of the HB PNIPAM in encapsulation of MSCs has never been investigated. Therefore, the aim of this project is to develop a HB PNIPAM-based synthetic hydrogel scaffold, and employ this scaffold as a platform for assessment of MSC behaviour and guidance of differentiation in 3D environment.

Project-specific objectives are:

1. To synthesise a stable thermo-responsive PNIPAM hydrogel with highly branched architecture.
2. To characterise chemical and mechanical properties of the HB PNIPAM hydrogel
3. To optimise HB PNIPAM for encapsulation and long term culture of MSCs
4. To investigate viability, proliferation and differentiation capacity of MSCs within HB PNIPAM 3D environment.
5. To assess role of HB PNIPAM properties in fate determination by the MSCs.

The result of this research work will be a synthesis method and a characterisation data of a highly-branched PNIPAM, optimised for long-term culture of MSCs within 3D environment. This study will also yield biocompatibility data for a novel hydrogel environment, which will assist in further design and testing of the PNIPAM-based hydrogels for cell studies in 3D.

Finally, findings of this project will broaden the understanding of MSC behaviour within 3D biomimetic environment, and the effect of 3D synthetic milieu on differentiation potential of MSCs. Taken together, outcomes of this study will form a contribution for vitally important area of tissue engineering research – understanding of MSC behaviour within 3D biomimetic environment.

3 Hydrogel scaffolds: PNIPAM synthesis and characterisation

3.1 Introduction

Unprecedented need for replacement organs (Organdonation.nhs.uk 2014), which is hugely unmet, has stimulated research into organ repair by means of scaffolding materials. Decades of active research has resulted in a plethora of materials that hold a great potential for tissue engineering strategies (Roux & Ladavière 2013; Hutmacher 2000; Lee & Mooney 2001). Central idea of the scaffold use is to provide an ECM-like environment, that would stimulate tissue repair and function restoration (Daley et al. 2008). Scaffold systems, primarily targeted towards soft (i.e. non-mineralised) tissue repair, are widely represented in the tissue engineering field by hydrogels from natural polymers (e.g. collagen (Winer et al. 2009), gelatin (Dolatshahi-Pirouz et al. 2014), fibrin (Ahmed et al. 2008), alginate (Domm et al. 2002), agarose (Aizawa & Shoichet 2012), chitosan (Hong et al. 2007)) and synthetic polymers (e.g. poly(ethylene glycol) (Burdick & Anseth 2002), poly(N-isopropylacrylamide) (Lapworth et al. 2011), poly(N, N-diethylacrylamide) (Idziak et al. 1999), poly(N-vinylcaprolactam) (Laukkanen et al. 2004), poly(vinyl alcohol) and poly(acrylic acid) (Lee et al. 1996)).

Hydrogels, formed by both polymer types, represent various modes of gelation. However, few hydrogels stand out due to their unique thermo-sensitive and state-reversible properties. Thermo-sensitive properties are exhibited by poly(methyl vinyl ether), poly(N-vinylcaprolactam) and poly(N-isopropylacrylamide) amongst many (Schmaljohann 2006). Hydrogels, which demonstrate LCST properties, are most suitable for biological application, as the gelation process takes place after gradual increase in temperature. Whereas, upper critical solution temperature (UCST) gels often require large amounts of heat energy to denature original gel structure and liquefy the gel, making these materials less suitable from the processing aspect, as well as for cell release from the structure and injection therapies. Problematic applicability of UCST gels can be exemplified by agarose and gelatin gels, where the hydrogel first has to be heated above 60˚C in order to denature the original structure, followed by cooling to form a gel (Hunt & Grover 2010).

Whereas some polymer hydrogels, that demonstrate LCST, undergo phase transition at physiologically relevant temperatures, therefore being of a greater interest for tissue engineering applications: for example poly(N, N-diethylacrylamide), poly(methyl vinyl ether) and poly(N-vinylcaprolactam) (Schmaljohann 2006). This list would not be complete without PNIPAM, the most studied thermo-responsive polymer with a distinct LCST point at ~31˚C in its original formulation (Scarpa et al. 1967).

The solution-gel transition process in PNIPAM is orchestrated by enthalpy-driven hydrogen bond disruption between the hydrophilic functional groups and the surrounding solvent. This phase-transition mechanism is a product of PNIPAM's amphiphilic nature, where hydrophobic isopropyl group is counteracting hydrophilic and polar amide group (Rimmer et al. 2009). Amide groups form hydrogen bonds with surrounding aqueous phase, where isopropyl group are avoiding contact with water and represent the force that drives collapse of the chain when hydrogen bonds with amide groups are broken. At temperatures below LCST polymer chains are relaxed and fully hydrated. However, when the temperature is increased past LCST point, hydrogen bonds between water molecules and amide groups are disrupted and hydrophobicity of isopropyl groups is starting to prevail, chain contraction into globular shape occurs (in order to minimise contact with water). The final result of this process manifests in collapse and entanglement of the polymer chains, producing in physically cross-linked network (Zeng et al. 1998; Liao, Zhang, et al. 2011; Rimmer et al. 2007).

Phase transition properties of PNIPAM were first noted by Scarpa et. al., where water-dissolved polymer was precipitating from a solution at 31^{o} C (Scarpa et al. 1967) . This report was shortly followed by work of Heskins and Guilette, confirming phase transition of PNIPAM and providing a detailed polymer characterization (Heskins & Guillet 1968).

Over the years various approaches were employed to alter transition temperature of PNIPAM, where most recently functionalisation with hydrophilic or hydrophobic moieties and addition of surfactants has been shown to provide great level of control over the LCST point (Chung et al. 1998; Wu & Zhou 1996). In addition, work of our

group has shown that by controlling degree of branching and functionalisation with polar groups it is possible to fine-tune LCST point of PNIPAM (Rimmer et al. 2007).

However, after reaching the LCST temperature PNIPAM hydrogel demonstrates further progression of the gelation processes, which in heating up stage is expressed as continuous shrinkage of the structure via solvent expulsion, known as syneresis (Gan et al. 2010). Where during cooling process, a lag in dissolution is often observed – i.e. dissolution takes place at temperatures below original LCST point. Such process is known as hysteresis (Cheng et al. 2006). Both of these processes are affected by the molecular weight of the polymer, degree of branching and introduction of hydrophilic or hydrophobic functional groups. Hydrophilic modification of PNIPAM leads to reduction or ablation of syneresis (Gan et al. 2010). Addition of the hydrophilic groups is also known to improve stability of the PNIPAM gels (Rimmer et al. 2007).

3.2 Study rationale

From the array of available hydrogels, PNIPAM is highly suitable for biological application due to its' thermo-responsive nature, lack of batch-to-batch variability and control over synthetic composition, virtually–absent cytotoxicity (Cooperstein & Canavan 2013), readiness for functional (Hopkins et al. 2009) and mechanical modification (Chung et al. 2006), controlled porosity (Galperin et al. 2010), suitability for cell expansion (Lei & Schaffer 2013), and ability to release encapsulated drugs (Zhang et al. 2009) and cells (Lapworth et al. 2011).

At the same time, rapid advances in the field of multipotent cell biology helps to understand what chemical and mechanical stimuli are effecting cells *in vivo* (Jones & Wagers 2008; da Silva Meirelles et al. 2008). By fine-tuning the surrounding environment of the cell, a control over cellular fate can be obtained (Engler et al. 2006; Pek et al. 2010; Giobbe et al. 2012). This insight in to regulation of cell and tissue development is of fundamental importance for treatment of degenerating diseases. Therefore, it is crucial to create a truly physiologically-relevant hydrogel scaffold that will match the biological needs of the multipotent cell.

The core objective of this study is to design, synthesise, characterise and validate a fully synthetic scaffolding material with highly amenable and thermo-sensitive nature, which would support viability of encapsulated cells.

Lack of cell-encapsulating scaffold, that would provide control over synthetic architecture with functional group presentation, has been a driving force behind this project. Highly branched architecture, contrary to dendrimer (England & Rimmer 2010), is more practical to synthesise, also providing versatility of functional modification. Despite active research of the highly branched polymers in the last two decades, complete understanding of how these materials can be utilised in the biomedical application has not been reached due to continuous discovery of control factors of cellular development (Yang et al. 2014) and molecular signalling factors (Colombres et al. 2008).

Outcomes of this scaffold-focused study are expected to provide a synthesis protocol for a novel cell-culture-suitable material with highly functional architecture. In addition, understanding of the mechanical and structural properties of this material, which will be obtained as a result of this study, will be of substantial importance for analysis of encapsulated cell behaviour during *in vitro* experiments.

3.3 Materials and methods

3.3.1 Branched PNIPAM synthesis

Previously, successful highly branched poly(N-isopropyl acrylamide) (HB PNIPAM) polymer synthesis was demonstrated by our group (England & Rimmer, 2010; Hopkins et al., 2009). In brief, 25 molar equivalents (m. e.) of NIPAM were reacted with 1 molar equivalent of RAFT agent to produce a highly-branched polymer with average number of 25 NIPAM units per branching point, formed by RAFT agent.

Also, one molecule of RAFT gives rise to one RAFT-functionalised chain end. Theoretical conversion is 100%, where in practice it will be lower. To account for this variability, number of functional ends were calculated as follows:

1g of polymer (NIPAM:RAFT) = $Moles_{PNIPAM}$ x (M_r NIPAM) + $Moles_{RAFT}$ x (M_r RAFT)

For a PNIPAM:RAFT=25:1 ratio (with 100% (theoretical) conversion):

$$1g = 25\ Moles_{RAFT} \times (113.1) + 1\ Moles_{RAFT} \times (259.1)$$

$$1g = 2827.5\ Moles_{RAFT} + 259.1\ Moles_{RAFT} = 3086.6\ Moles_{RAFT}$$

$$Moles_{RAFT} = 1g/3086.6 = 3.2398 \times 10^{-4} \text{ moles per 1 g of polymer}$$

For a PNIPAM:RAFT=25:1 ratio (with X (actual) conversion, confirmed by NMR)

$$1g = 25\ Moles_{RAFT} \times (113.1) \times Y + 1\ Moles_{RAFT} \times (259.1)$$

Y = ratio between PNIPAM and RAFT NMR signal

$$1g = 2827.5\ Moles_{RAFT} \times Y + 259.1\ Moles_{RAFT}$$

$$Moles_{RAFT} = 1g/(2827.5 \times Y + 259.1)$$

Prior to synthesis of the 4-vinylbenzyl-pyrrolecarbodithioate RAFT agent, pyrrole (99%, Sigma-Aldrich, UK) was distilled over calcium hydride (95%, Sigma-Aldrich, UK) under reduced pressure and kept at 4 °C with molecular sieves. 50 g (74.53 mmol) of distilled pyrrole was added dropwise over 30 min to a rapidly stirring mixture of sodium hydride (3 g, 125 mmol; 60%, in mineral oil dispersion; Sigma, UK) and anhydrous dimethylformamide (10 ml, DMF; from Grubbs solvent purification system). This solution was stirred for 30 min at room temperature, followed by cooling down to 0˚C with an ice bath. Carbon disulphide (5.68 g, 74.59 mmol; ≥99.5%, Sigma-Aldrich, UK) and DMF (10 ml) were added dropwise over 10 min at 0˚C to form a dark red solution, which was stirred for 30 minutes at room temperature and cooled to 0˚C again thereafter. Further, 4-vinylbenzyl chloride (11.37 g, 74.49 mmol; 90%, Sigma-Aldrich, UK), distilled under reduced pressure, and DMF (10 ml) were added dropwise over 20 min. The formed brown solution was allowed to steer for 16 hours at room temperature. Distilled water (80 ml) and diethyl ether (80 ml; Laboratory Reagent Grade, Fisher, UK) were added to the stirred solution. The organic layer was separated and the aqueous layer extracted with diethyl ether (3 x 160 ml). Collected extracts were dried over magnesium sulphate (Sigma-Aldrich, UK), followed by filtration and rotary evaporation of the excess solvent. Obtained brown oil was purified by flash chromatography on a silica column with n-hexane as an eluent. (Yield = 7.03g, 36.6%)

1H NMR ($CDCl_3$, rt, 400 MHz): δ/ppm 4.6 (2H, s, Ar-CH2-S-); 5.3 (1H, d, vinyl); 5.8 (1H, d, vinyl); 6.3 (2H, m, =CH-, pyrrole); 6.7 (1H, dd, vinyl); 7.7 (2H, m, N-CH=, pyrrole); 7.4 (4H, s, C6H4-)

To increase purity, N-isopropyl acrylamide monomer (NIPAM, 97 %, Sigma-Aldrich, UK) was recrystallized from 40/60 hexane/toluene mixture 3 times. Highly branched PNIPAM was synthesised by dissolving N-isopropyl acrylamide monomer (9.834 g, 86.646 mmol;), RAFT agent (0.9 g; 3.474 mmol) and 4,4′-Azobis(4-cyanovaleric acid) (ACVA) (0.57 g; 2.029 mmol; Sigma-Aldrich, UK) in dioxane (40 cm^3; Sigma-Aldrich, UK). Formed solution was transferred into an ampule, where it was subjected to 4 cycles of pump-assisted freeze-thawing cycles at 10^{-3} mbar pressure during freezing, followed by sealing of the ampule with the blow torch. Polymerisation process was carried out in a water bath at 60˚ C for 12 hours,

forming a viscous but still pliable product. Collected product was precipitated into cold diethyl ether three times, followed by gentle N_2 blow-drying and two days in vacuo at room temperature, providing 79.36% product recovery.

1H NMR ($CDCl_3$, rt, 400 MHz): δ/ppm 1.14 (br s, isopropyl -CH(CH_3)$_2$), 1.44 – 2 (br m, overlapping, polymer backbone CH_2 and CH), 3.72 (br m, PNIPAM NH-CH), 4 (s, br, 1H $(CH3)_2C\underline{H}$-) 6.35 (s, 2H, N-pyrrole-H_b), 6.4-7.2 (br m, overlapping), 7.68 (br d, 9 Hz, 2H, N-pyrrole-H_a)

Chain ends of the HB PNIPAM were functionalised with 4,4′-azobis(4-cyanovaleric acid) (ACVA, 98%, Sigma-Aldrich, UK) in order to achieve carboxylic acid chain-ends. 20 molar equivalents (m.e.) of ACVA were dissolved in dry DMF and reacted with 1 molar equivalent RAFT in HB PNIPAM for 24 hours at 70˚C under N_2 atmosphere. 20 m.e. of ACVA were added twice more under the same conditions.

Unreacted excess of ACVA and traces of DMF were removed by triple ultrafiltration through a cellulose filter with 3000 molecular weight cut-off. Polymer product, dissolved in DMF, was added to 250 ml mixture of 90%:10% ethanol:deionised water, under positive pressure of N_2 gas at 4 atmospheres, reducing the mixture to 50 ml. 250 ml of EtOH:H_2O were added and the ultrafiltration process was repeated twice more, where post-filtration fraction was freeze-dried.

To prepare resulting polymer for amino acid coupling, highly branched PNIPAM (3.17g), functionalised with ACVA, was dissolved in DMF (45 ml), followed by addition of dissolved dicyclohexyl carbodiimide (DCC, 0.5155 g, 4.479 mmol; 99%, Sigma-Aldrich, UK) and N-hydroxysuccinimide (NHS, 0.90187 g, 4.371 mmol; 98%, Sigma-Aldrich, UK). DCC and NHS were dissolved in 10 ml of DMF. Formed solution was stirred under nitrogen atmosphere for 24 hours at room temperature. Reaction by-product dicyclohexylurea (DCU) was filtered off. Traces of reagents and DMF were removed from the product by ultrafiltration process, repeated twice, followed by freeze-drying.

3.3.2 RRR synthesis

Peptide synthesis was performed in-house on an automated synthesizer PSW100 (Chemspeed Technology, Switzerland). Wang resin (2000 mg; Novabiochem, Germany) was swollen in DMF (25 ml) overnight by vortex at 350 rpm. Following DMF aspiration, for the first α-amino group deprotection, 20% piperidine (99%, Sigma-Aldrich, UK) / 80% DMF mixture (30 ml) was added to the swollen resin for 15 minutes under gentle (100 rpm) vortex. Deprotection mixture addition and vortex step was repeated once more.

Further, deprotection mixture was aspirated by vacuo. Traces of piperidine were removed by six washes with DMF (30 ml), with 100 rpm vortex for 1 minute during every wash. For the coupling step arginine (Pbf)-OH (4.0864 g in 12.6 ml of DMF; Fluorochem, UK), HBTU (9.557g; Apollo Scientific, UK) and 2-MBT (4.221 g; Sigma-Aldrich, UK) in 12.348 ml of DMF were added to the deprotected resin, followed by DIPEA (2.195 ml; Apollo Scientific, UK). The coupling reaction was performed for 1 hour with stirring at 350 rpm. In order to improve reactivity, identical amounts for arginine (pbf)-OH, HBTU, 2-MBT and DIPEA were repeatedly added, followed by 1 hour of stirring. Resin was washed with DMF (30 ml) six times.

The cycle of double deprotection and double coupling, described above, was repeated once more in order to complete peptide chain extension. After chain extension, the resin was washed 6 times with DMF, 6 times with DCM and 6 times with methanol.

Cleavage of the extended peptide sequence from the resin and side-chain protective group removal was done by addition of 90/10 trifluoroacetic acid (TFA, 99%, Sigma-Aldrich, UK) /dH_2O (125 ml) and stirring for 4.5 hours. The cleaved resin was separated from the cleavage cocktail and peptide product by filtration. TFA was removed from the mixture by rotary evaporation, where peptide product was recovered by precipitation into cold diethyl ether. The peptide trituration was repeated 5 more times, followed by rotary evaporation of diethyl ether and freeze-

drying from dH_2O and 0.5% acetic acid mixture. Recovered peptide was stored at -20˚C.

3.3.3 Tri-arginine (RRR) addition

2.5 g of NHS and DCC functionalised PNIPAM were mixed with 150 ml of ultrapure water and stirred over ice for 20 minutes under nitrogen atmosphere. 600 mg of RRR peptide (mixture of R , RR and RRR sequences; RRR sequence fraction is present at 73.1%; Figure 7) were dissolved in 75 ml of dH_2O and added to stirring polymer solution, followed by immediate addition of 25 ml of phosphate buffer (0.1 M pH 8.5; resulting concentration 0.01 M). Reaction was allowed to proceed for 16 hours, with the ice bath warming up to room temperature during the reaction time. Collected reaction solution was ultra-filtered 3 times and freeze-dried, as described above.

1H NMR ($CDCl_3$, rt, 400 MHz): δ/ppm 1.14 (br s, isopropyl -CH(CH_3)$_2$), 1.44 – 2 (br m, overlapping, polymer backbone CH_2 and CH), 3.72 (br m, PNIPAM NH-CH), 4 (s, br, 1H $(CH3)_2CH$-) 6.35 (s, 2H, N-pyrrole-H_b), 6.4-7.2 (br m, overlapping), 7.68 (br d, 9 Hz, 2H, N-pyrrole-H_a)

3.3.4 Nuclear magnetic resonance (NMR) characterisation

NMR spectra was obtained from Bruker Advance 400. 20 mg of polymer sample were dissolved in 1.5 ml of chloroform-d (99.8 atom % D, Sigma-Aldrich, UK).

3.3.5 Gel permeation chromatography (GPC) characterisation

Molecular weight of PNIPAM+RRR was determined by GPC with DMF eluent for mobile phase. GPC setup consisted of a Polymer Laboratories LC1150 pump and Viscotek TDA 300 refractive index detector. Mobile phase was eluted through 3x30 cm PL gel mixed-B columns (Polymer Laboratories, UK). Poly(methyl methacrylate) standards (Polymer Laboratories, UK) were used for calibration of the instrument and data was analysed by using Cirrus software package.

3.3.6 Zeta potential and particle size characterisation

Zeta potential analysis was performed on ZetaPALS instrument (Brookhaven Instruments, USA) with heat controlled sample holder. The PNIPAM and PNIPAM+RRR samples were prepared in 1 mM potassium chloride (KCl, 99%, Sigma-Aldrich, UK) (solution at 0.025 and 0.1 mg/ml concentration respectively. Particle size analysis was conducted on the same instrument, where polymer samples were prepared in 10 mM KCl at identical concentrations as for the zeta potential measurement. Every plotted value is an average of 3 analysis cycle results with 10 runs in every cycle.

3.3.7 Cloud point measurement with UV-visible spectrophotometry

LCST quantification was performed on 0.05-0.1 wt% polymer solutions in ultrapure water by using Varian CARY3-bio UV-visible spectrometer. All samples were subjected to sequential heating and cooling steps at 1˚C/min rate. Change in solution absorbance was recorded at 500 nm wavelength. Temperature point, at which collected turbidimetry data would cross 1% absorbance reference line, was considered to be an LCST point during heating step. Identical measurement was done during the cooling step in order to quantify amount of hysteresis in the system.

3.3.8 Scanning electron microscope (SEM)

Samples of 5 wt% PNIPAM+RRR were prepared in ultrapure water and basal cell culture media (i.e. DMEM media containing 1% penicillin/streptavidin (10,000 U/mL; Life Technologies, UK), supplemented with 10% foetal bovine serum (FBS; Gibco, Life Technologies, UK). Polymer solutions were deposited drop wise on the etched copper plates followed by heating to 37˚C and maintained at this temperature for 30 seconds to allow complete gelation to occur. Following gelation, polymer samples on the copper plates were promptly transferred into liquid nitrogen. Further, samples were freeze-dried overnight at -60˚C, following stepwise elevation of temperature by 10˚C every 30 minutes until temperature was normalised to room temperature. Dried polymer samples were fractured and sputter coated with Pd/Au. SEM analysis was performed with field emission JSM-7600F SEM (Jeol, USA) with accelerating voltage set to 3kV.

3.3.9 Infra-red (IR) spectroscopic analysis of the NIPAM polymers

Fourier transform infrared (FTIR) spectra of PNIPAM and PNIPAM+RRR (10 wt%, prepared in deionised water) were collected using a Golden Gate™ single reflection attenuated total reflectance (ATR) module (SpectraTech) coupled with a Thermo Nicolet Nexus FTIR spectrometer. Every collected spectrum was averaged 64 times at 4 cm^{-1} resolution. Prior every measurement 5 minute temperature equilibration hold was applied. ATR-FTIR spectra were processed with Omnic v6.1 ATM (ThermoNicolet) software.

3.3.10 Phase transition analysis with micro-scale differential scanning colorimeter (µDSC)

Temperature dependent phase transition of PNIPAM and PNIPAM+RRR, dissolved in deionised water at 1.5 mg/ml concentration, was analysed on differential scanning micro calorimeter (GE Life Sciences). Prior analysis, polymer solutions were degassed and cooled down to 5˚C. Heating and cooling cycles were repeated 20 times at 1˚C/min rate. Data analysis was performed with MicroCal Origin Software.

3.3.11 Rheological behaviour analysis

Rheological analysis of the PNIPAM+RRR in aqueous solution was performed on AR-2G cone (40 mm; 2˚) and plate viscometer (TA Instruments, USA). Heat flow in the Peltier plate was controlled by a Julabo F24 water bath. Samples at 2.5, 5 and 10 wt% concentrations were analysed at a fixed strain rate of 2.5, 1 and 3.5 Hz respectively and controlled temperature rate of 1˚C/min. Elastic (G') and plastic (G'') moduli were recorded, where crossover between G' and G'' considered an onset of the gelation process.

3.3.12 Tri-arginine (RRR) peptide purity assessment with liquid chromatography mass spectrometry (LC-MS).

Synthesised RRR peptide was fractionated on a Kinetex™ 2.6 µm HILIC 100 Å (50 x 2.1 mm; Phenomenex®) liquid chromatography column, followed by time of flight mass spectrometry analysis using following settings: 70% acetonitrile / 30 % 100 mM ammonium formate (pH 3.2) at 0.5 ml/min.

3.4 Results

3.4.1 Polymer synthesis

Highly branched (HB) PNIPAM was synthesised via the RAFT route, a reliable method of radical polymerisation that provides high degree of control over the reaction. Initial PNIPAM polymerisation and further functionalisation with RRR peptide sequence is shown in Scheme 1.

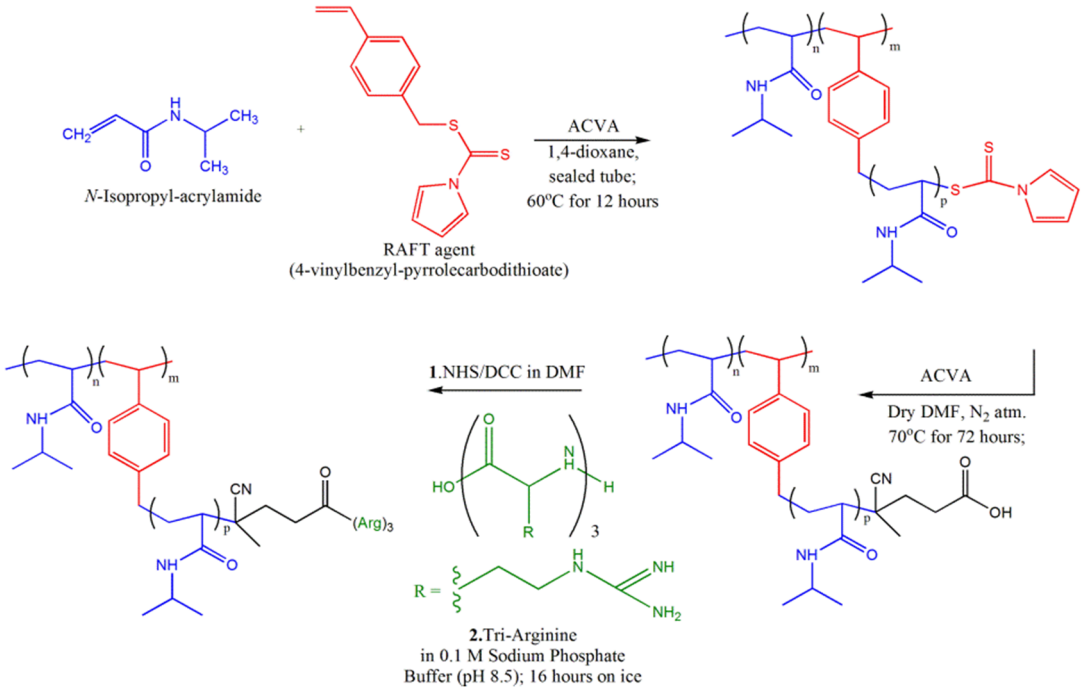

Scheme 1: HB PNIPAM and RRR functionalisation steps

Molecular weight and number distribution of the initial polymer was assessed by GPC, where obtained data is summarised in the table below (Table 5).

Table 5: Molecular weight of parental PNIPAM (i.e. no COOH or RRR chain ends)

M_p	M_n	M_w	PDI
46755.67 (g/mol)	17933 (g/mol)	58817 (g/mol)	3.28

In-house synthesised RRR peptide was not fractionated due to high product losses during liquid chromatography separation. The liquid chromatography and mass spectrometry tandem analysis identified the proportion of RRR peptide sequence to be equal to 73.12% of the total product. Whereas RR an R sequences were represented at 22.77% and 4.1% respectfully (Figure 7). Initial separation of the peptide fractions has demonstrated loss of yield below required. Therefore, the

collected peptide product was used as a mixture of tri-peptide (RRR), di-peptide (RR) and mono-peptide (R).

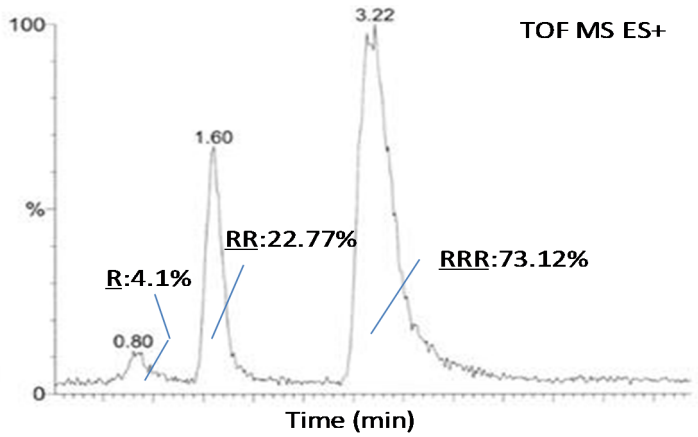

Figure 7: HPLC-MS analysis of RRR collected product, where 3 peptide fractions were identified, with 73.12% of the product composition represented by RRR.

Prior to addition of the RRR peptide functionality to carboxylic acid ended HB PNIPAM, polymer solubility in water was poor. Hydrogels, prepared in water, were contracting and expelling most of the entrapped water in the period of 20 minutes at 37˚C. However, following RRR functionalisation, solubility of the polymer improved and formed hydrogels, which retained structural integrity after prolonged incubation periods with a minimal expulsion of water (Figure 8).

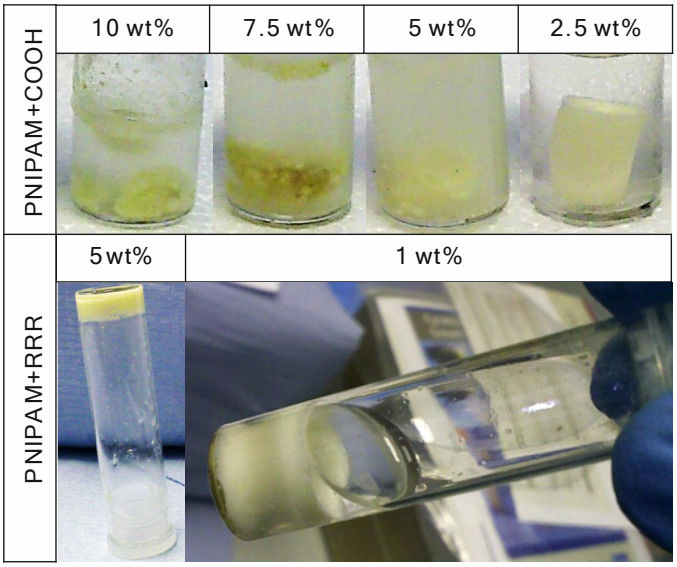

Figure 8: Solubility and water expulsion by carboxylic acid (COOH) and peptide (RRR) functionalised PNIPAM at various concentrations. After functionalisation with RRR peptide, polymer hydrogels became self-supporting at a sufficient concentration (i.e. 5 wt%).

After heating the sample beyond the gelling point, PNIPAM+RRR, prepared in water at 5wt% concentration, forms a self-supporting gel with high micro-porosity (Figure 9). Hydrogel reconstitution in serum-supplemented cell culture media results in increased pore size and more randomised network structure.

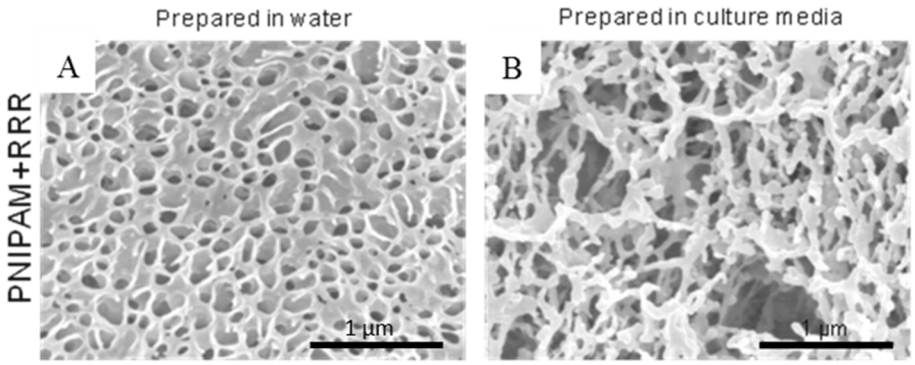

Figure 9: SEM micrographs of a freeze-dried and fractured PNIPAM+RRR, prepared in deionised water (A) or cell culture media (B). The accelerating voltage was set to 3kV.

3.4.2 Uv vis: LCST and hysteresis window determination

Alongside with gelation stability (Figure 8), functionalisation of PNIPAM with RRR sequence has increased lower critical solution temperature (LCST) from 18˚C to 24˚C, as the turbidimetry analysis demonstrates (Figure 10). Whereas hysteresis window has widened up from 4.5˚ C to 6.5˚ C after RRR sequence addition.

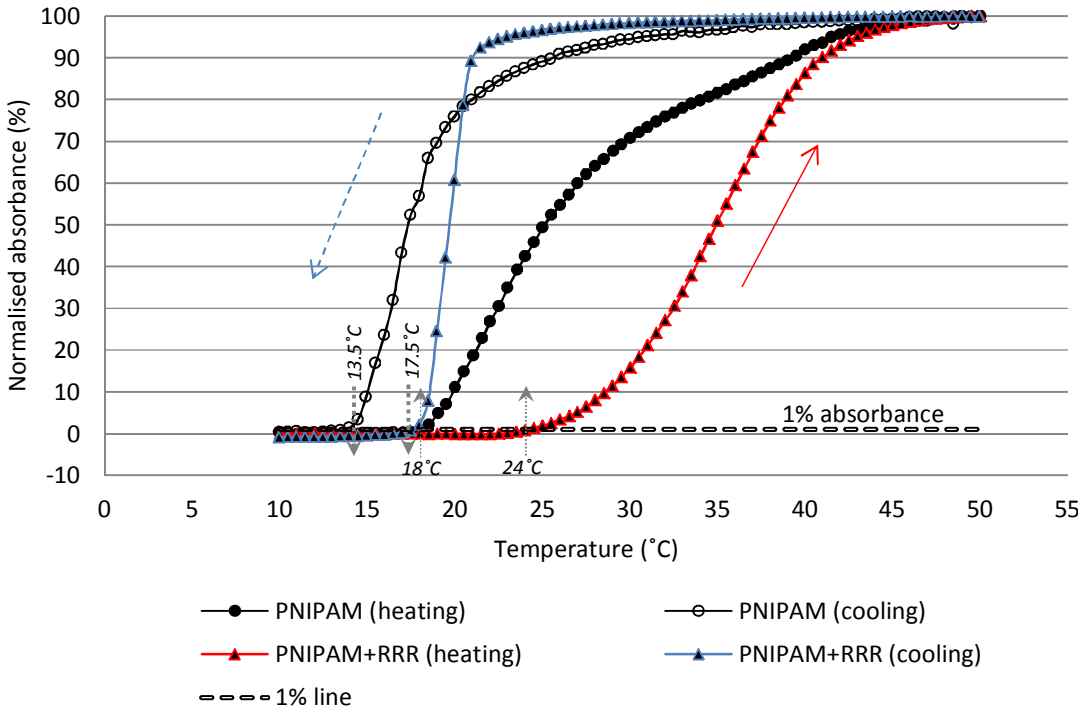

Figure 10: UV-Vis analysis of parental and RRR functionalised PNIPAM in aqueous solution. The onset of LCST process for non-functionalised (parental) HB PNIPAM was at 18˚C, and addition of the RRR peptide to the polymer has increased LCST onset point of the polymer to 24˚C. Dissolution points were 13.5˚C and 17.5˚C in the parental HB PNIPAM and the PNIPAM+RRR, respectively.

3.4.3 µDSC: detailed analysis of the phase transition

Heat input, required for solution-gel transition to occur, has been recorded by µDSC (MicroCal VP-DSC; GE Healthcare) for both parental and RRR functionalised PNIPAM in aqueous solution and at identical concentration (Figure 11). During heating and cooling cycles parental PNIPAM demonstrated a single peak appearance (17.77˚ and 17.15˚C, respectively), whereas PNIPAM+RRR has shown two clear peaks during heating step (at 22.34˚ and 27.49˚C) and two crossing over peaks during cooling, with dominant peak centre at 24.19˚C. In addition, heat flow requirement for the transition to take place in PNIPAM+RRR sample is 19-fold lower than for parental polymer sample.

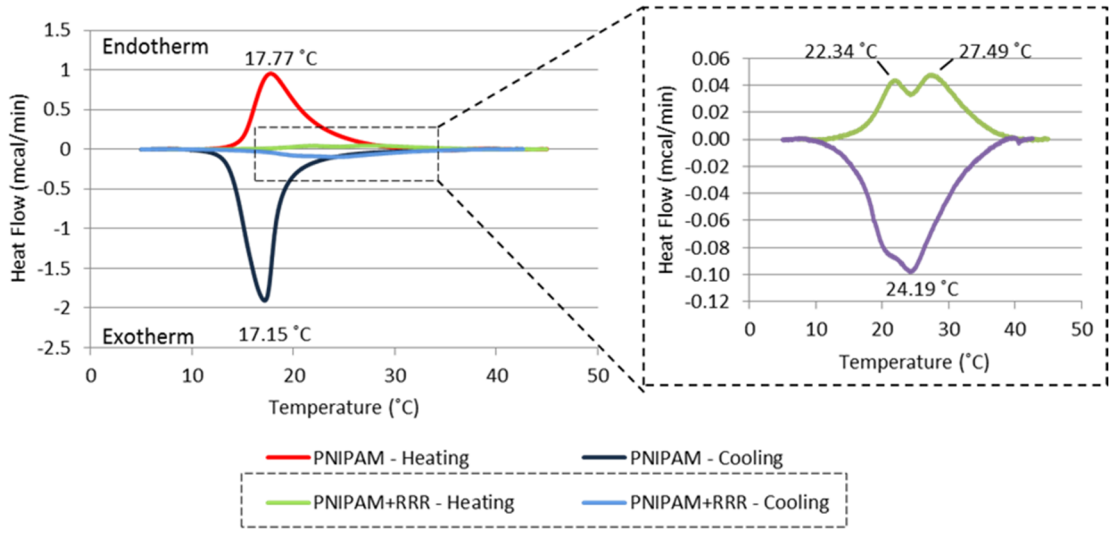

Figure 11: Thermal analysis of the solution-gel transition in parental and RRR functionalised PNIPAM. Selected dotted area shows an enlargement of plotted data for PNIPMA+RRR with higher resolution in y-axis.

3.4.4 Zeta potential and particle size: colloidal stability and dehydration effect

Zeta potential measurement is a convenient way to elucidate polymer interaction with the solvent, flocculation parameters, colloidal stability and polymer adsorption by means of determination and tracking of the effective charge at the surface of the particle. PNIPAM polymer, as a colloidal solution, is also known to demonstrate change in particle conformation, from opened (i.e. coil) to closed (i.e. globule) after passing the LCST point (Hopkins et al. 2009). As a result of this conformational change hydrophobic isopropyl group is becoming more prevalent at the interface with the solvent. Hydrophobic bond formation between colloidal bodies of the polymer takes places. If the hydrophobic forces are overpowering and concentration of the polymer is too high, most probably flocculation and precipitation will occur. Such colloidal aggregation can be analysed by particle size analysis at different temperatures.

Zeta potential of parental PNIPAM (i.e. polymerised NIPAM monomer into HB variant, without functionalisation with carboxylic acid) was initially analysed at 0.1 mg/ml concentration, identical to the concentration used during UV-Vis analysis (Figure 10) and matching concentration of PNIPAM+RRR sample during zeta potential and particle size measurement (Figure 14). However, 0.1 mg/ml concentration was not fully suitable for particle size measurement due to count rate being much higher than the recommended testing range. Therefore, parental

PNIPAM sample at 0.025 mg/ml was used for zeta potential and particle size measurement.

Zeta potential analysis of parental PNIPAM at 0.025 mg/ml demonstrated particle charge of -5.78 and -5.26 mV at 15 and 20˚C, respectively (Figure 12A). Whereas at following measurement point (at 25˚C), particle charge is equal to -8.82 mV. Therefore, in the 20 to 25˚C range a change in the trend of the plot is observed, suggesting that the LCST point lies in the 20-25˚C range. After 25˚C temperature point, zeta potential charge continues to decrease, and by reaching 37˚C, zeta potential is equal to -11.2 mV (Figure 12A).

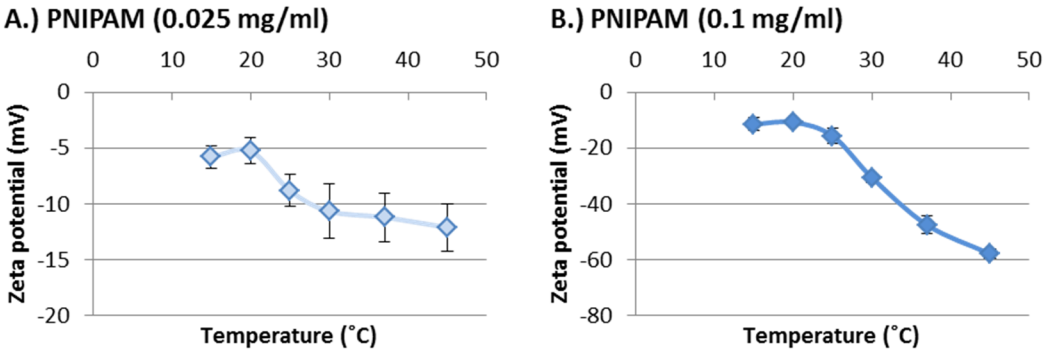

Figure 12: Zeta potential measurement of parental PNIPAM at 0.025 (A) and 0.1 mg/ml (B) concentrations and temperatures from 10 to 45˚C. Change in the trend of the plot is observed in the 20-25˚C range in both samples, where increase is concentration results in the increase of the response magnitude. n=3.

Parental PNIPAM at 0.1 mg/ml concentration has demonstrated change of trend in the 20-25˚C range, identical to 0.025 mg/ml sample (Figure 12A and B). However, by 37˚C zeta potential is equal to -47.56 mV, demonstrating an effect of the concentration on zeta potential.

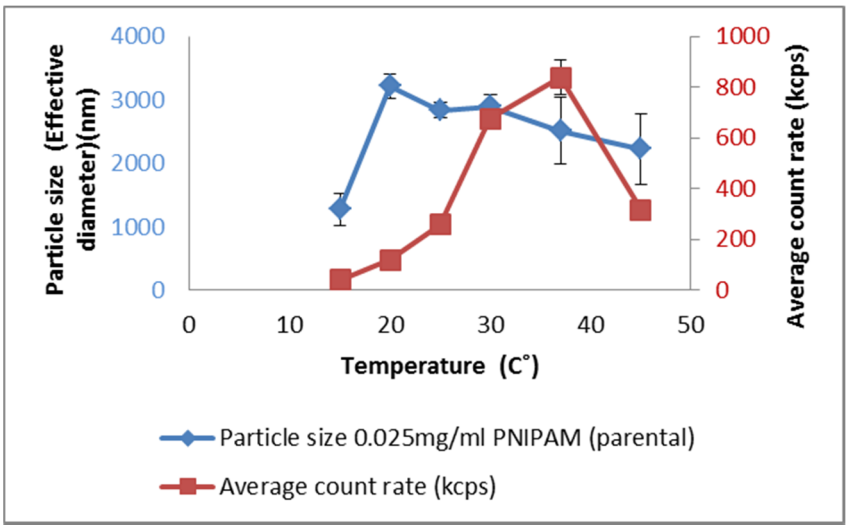

Figure 13: Particle size and average count rate in parental PNIPAM (0.025 mg/ml). n=3.

During particle size analysis of the parental PNIPAM a rapid increase of the particle size was observed between 15˚C and 20˚ temperature points, where effective diameters of the particles were 1272.2 and 3215.6 nm, respectively (Figure 13). Such behaviour can be explained by a low particle count rate in this particular temperature range, and as a consequence, inability of the instrument to detect particle size accurately. In addition, 500-1000 thousand counts per second is a recommended range.

However such prompt increase in particle size can also be explained by a rapid aggregation of the dispersed polymer particles during temperature increase. Therefore, particle sizes of 1272.2, 3215.56 and 2509.13 nm at 15, 20 and 37˚C, respectively, may suggest that by 20˚C polymer particles have formed multi-unit complexes which exhibited progressive aggregation with linear increase in temperature.

Zeta potential measurement in PNIPAM+RRR sample demonstrated a positive charge on the particle surface, where at 20 and 37˚C charges were 19.2 and 31.5 mV, respectively (Figure 14A).

Analysis of the particle size in PNIPAM+RRR has demonstrated a linear decrease in the particle diameter (Figure 14B), however no initial rapid aggregation was observed in the 10-20˚C temperature range, as in parental PNIPAM (Figure 13). In

addition, particle size at 20˚C was 460.37 nm and 238.13 nm at 37˚C, what demonstrated a 1.9-fold decrease in diameter.

In addition, zeta potential signal of parental PNIPAM becomes more positive with increase in temperature (Figure 14), where parental PNIPAM samples demonstrates an opposite effect – originally negative values are becoming more negative (Figure 12). Such difference in polarity is attributed to highly polar nature of PNIPAM+RRR, when compared to parental PNIPAM.

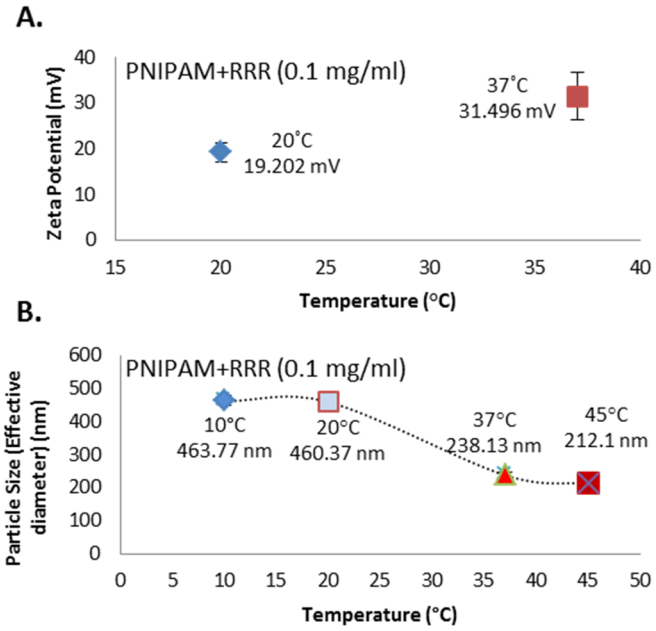

Figure 14: Zeta potential and particle diameter of PNIPAM+RRR solution. At 0.1 mg/ml PNIPAM+RRR demonstrates an increase in zeta potential past 30 mV with increase in temperature, what suggest colloidal stability of the polymer at 37˚C (A). Particle size of the same polymer has reduced sharply after 20˚C, representing a 1.9-fold diameter shrinkage by 37˚C (B). n=3.

3.4.5 Infra-red spectroscopic analysis

The phase transition mechanism of PNIPAM involves changes in vibrational energy of the chemical bonds, where the attenuated total reflectance Fourier transform infrared spectroscopy (ATR-FTIR) is a particularly robust method for quantitative analysis of these changes.

The ATR-FTIR approach was chosen because of its high sensitivity to change in functional group environment and change in molecular interactions as a function of temperature.

PNIPAM-based systems have been previously characterised by FTIR spectroscopy, where PNIPAM specific peaks were assigned. Most common functional groups used are PNIPAM characterisation are: amide 1, amide 2 and antisymmetrical methyl stretch (ν_{as}(CH)). (Maeda et al. 2000; Sun et al. 2007; Sammon et al. 2006)

In order to study phase transition mechanism of a highly branched PNIPAM and its' peptide-functionalised derivative, amide 1, amide 2 and antisymmetrical methyl stretch region (ν_{as}(CH)) were used to track change in their chemical environments with increase and decrease of the temperature (Figure 15).

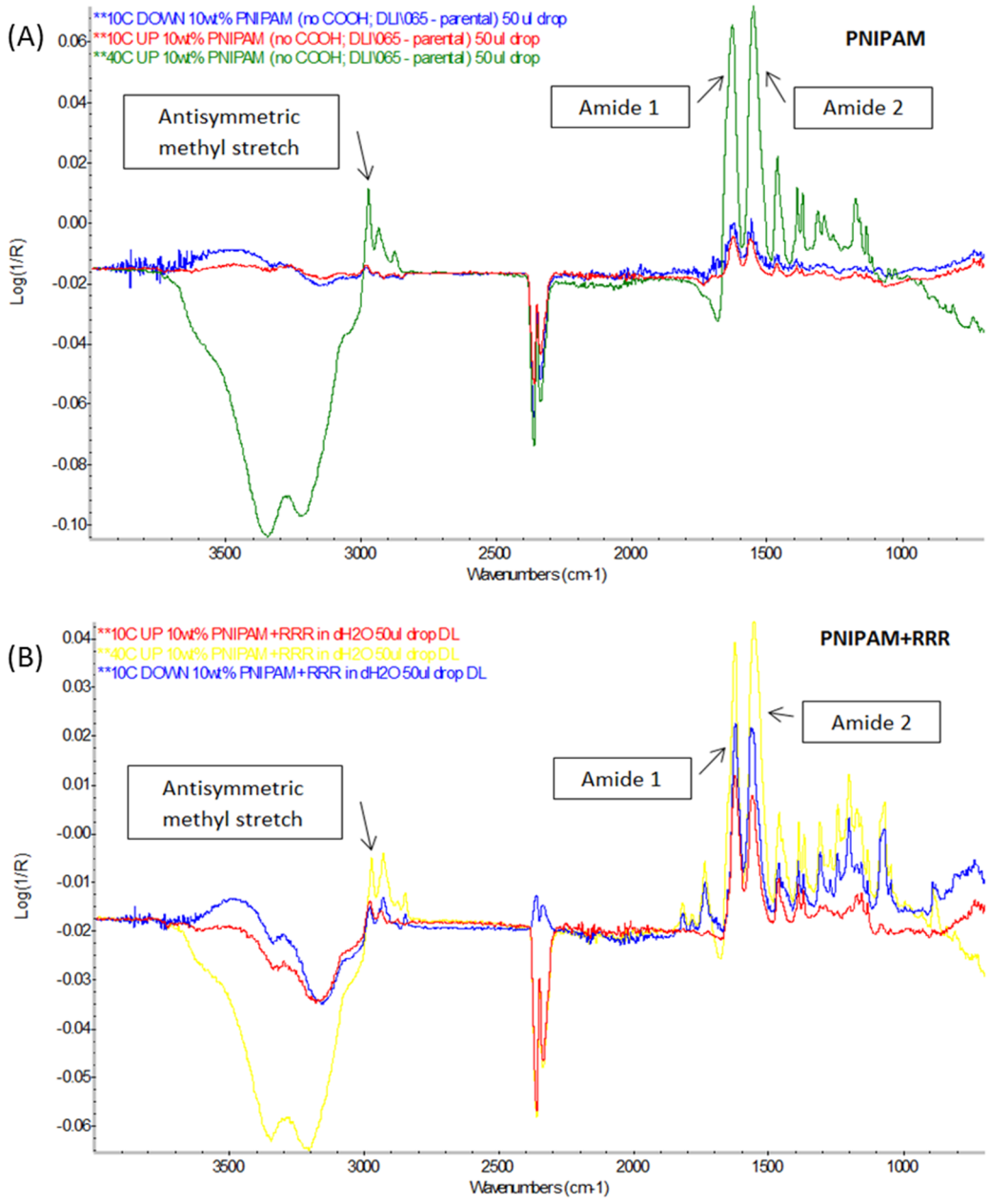

Figure 15: ATR-FTIR spectra of 10 wt% HB PNIPAM:non-functionalised (A) (parental) and RRR-functionalised (B) during 10˚C and 40˚C of the heating stage, and during 10˚C of the cooling stage. Regions of interest (antisymmetric methyl stretch, amide 1 and amide 2) are emphasised.

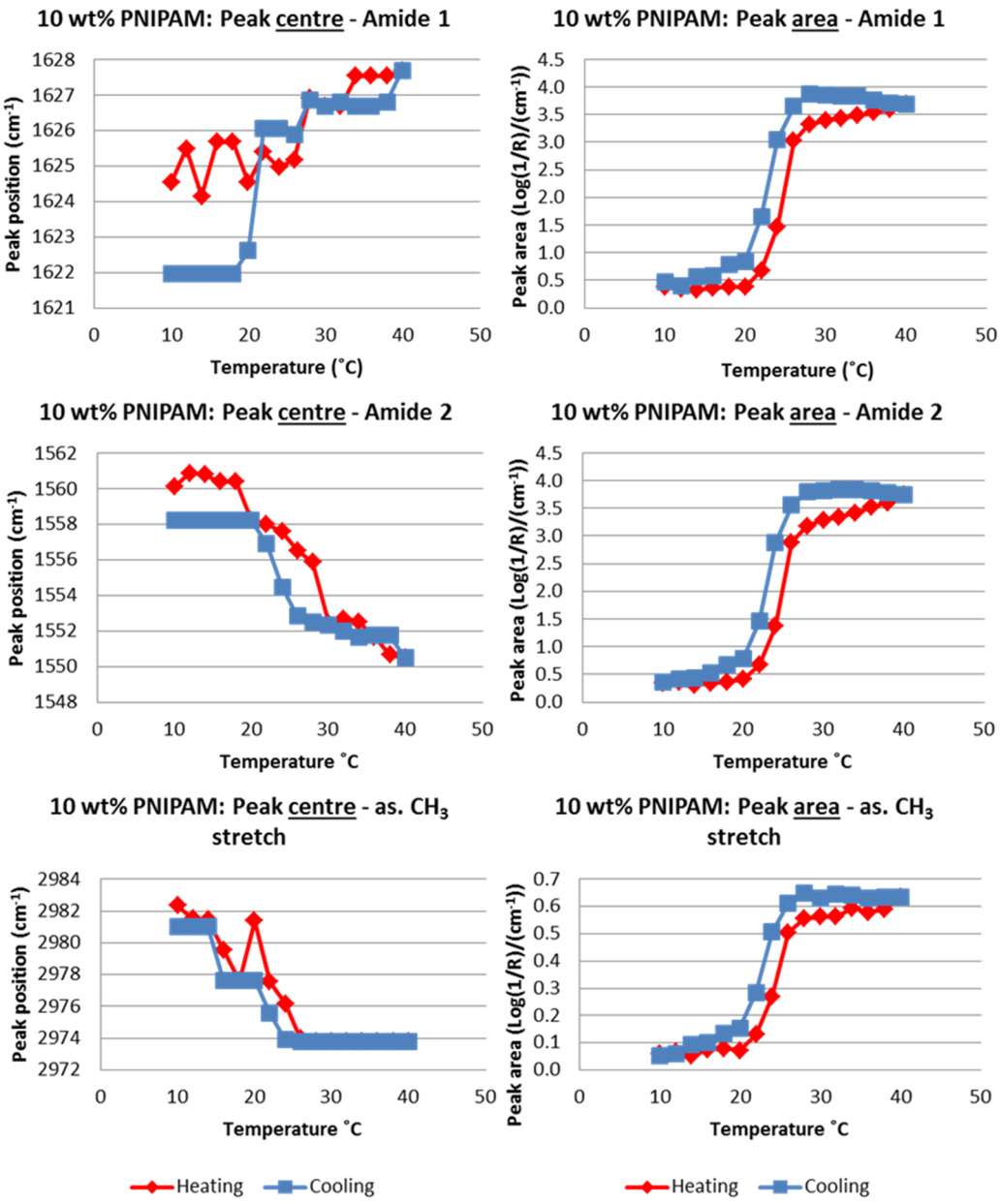

Figure 16: Quantitative assessment of bond vibrational energy between non-functionalised PNIPAM polymer chains and the solvent (i.e. water) via ATR-FTIR analysis. Left column represents positional shift of the peak centres in amide 1, 2 and CH_3 antisymmetric stretch regions of parental PNIPAM (10 wt%) during heating and cooling stages (10˚C - 40˚C - 10˚C); right column provides measurement of area under the peak for the same regions of interest.

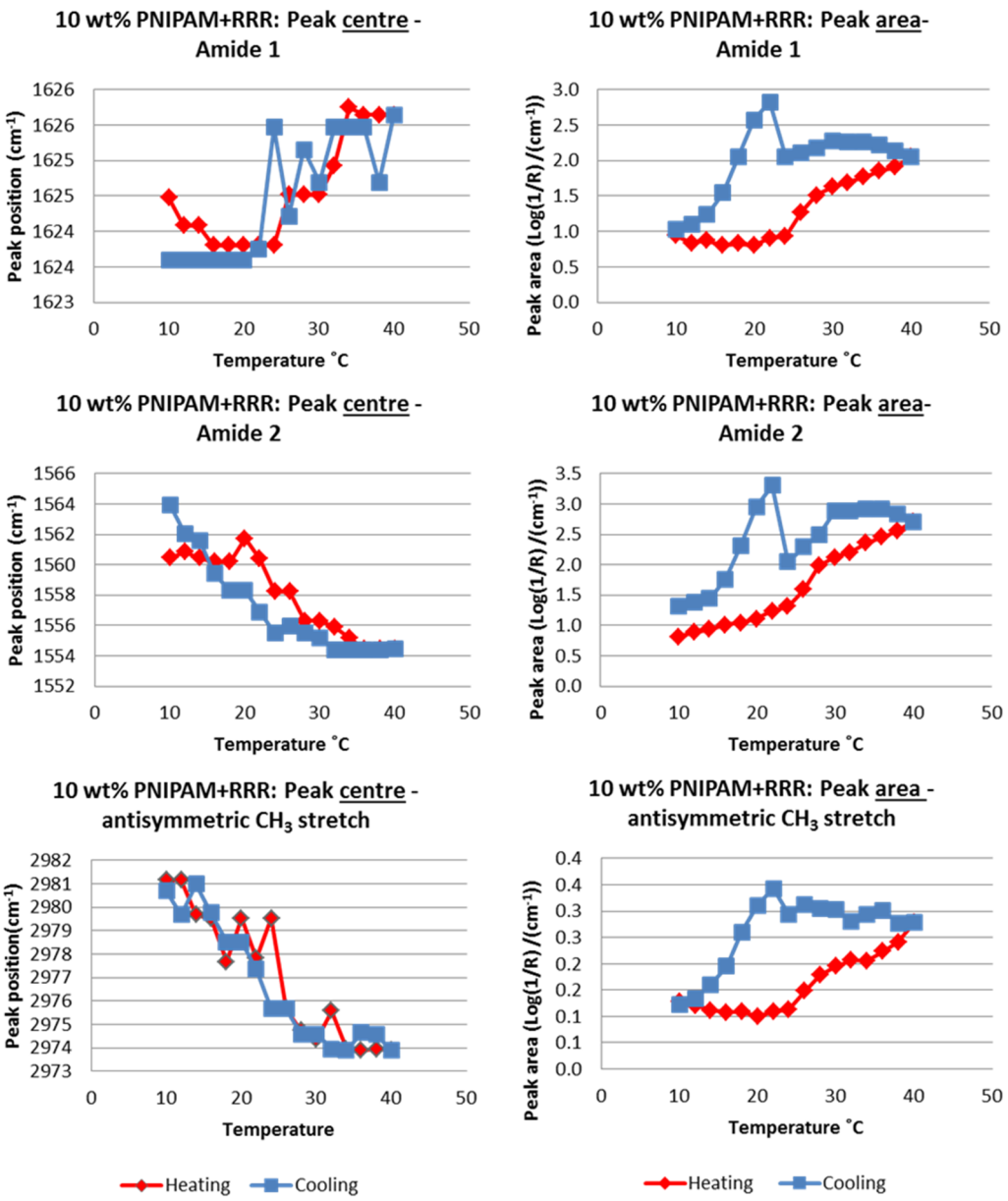

Figure 17: Quantitative assessment of bond vibrational energy between RRR-functionalised PNIPAM polymer chains and the solvent (i.e. water) via ATR-FTIR analysis. Left column represents positional shift of the peak centres in amide 1, 2 and CH_3 antisymmetric stretch regions of PNIPAM+RRR (10 wt%) during heating and cooling stages (10˚C - 40˚C - 10˚C); right column provides measurement of area under the peak for the same regions of interest.

Regions of interest: amide 1, amide 2 and antisymmetrical CH_3 stretch were tracked during heating stage from 10˚C to 40˚C with a 2˚C step, and back to 10˚C during cooling. Shifts in the peak centres and area under the curve for parental PNIPAM and PNIPAM+RRR are plotted in Figure 16 and Figure 17, respectively.

Analysis of the peak positioning in PNIPAM-associated functional groups during heating and cooling stages has identified peak centre shifts, summarised in Table 6.

Table 6: ATR-FTIR analysis summary of parental PNIPAM and PNIPAM+RRR in aqueous solution. Peak shifts in PNIPAM-characteristic IR regions were analysed during heating from 10˚ to 40˚C with 2˚C step, and cooling back to 10˚C.

Summary of the peak shifts	Stage	Amide 1	Amide 2	ν_{as}(CH)
10 wt% PNIPAM	*Heating*	3 cm^{-1} ←	10 cm^{-1} →	8 cm^{-1} →
	Cooling	5.5 cm^{-1} →	8 cm^{-1} ←	7 cm^{-1} ←
10 wt% PNIPAM + RRR	*Heating*	1.5 cm^{-1} ←	8 cm^{-1} →	7 cm^{-1} →
	Cooling	1.5 cm^{-1} →	10 cm^{-1} ←	7 cm^{-1} ←

3.4.6 Rheology: hydrogel's visco-elastic properties under oscillatory shear force

Majority of studies that have assessed mechanical properties of the two-dimensional or three-dimensional culture substrates have used measure of stiffness, most commonly known as Young's modulus (Legant et al. 2010; Discher et al. 2005; Trappmann et al. 2012; Balaban et al. 2001). During Young's modulus measurement, tested material is under a tensile loading, where uni-axial stress and strain is measured. Whereas, in the cone and plate viscometry, utilised in the presented study, sinusoidal shear (oscillatory) force is applied. Collected information of the ratio between shear stress and shear strain is known as a shear modulus, which also provides a measure of material stiffness.

Application of the oscillatory force in the cone and plate viscometer allows to measure stress-response of visco-elastic materials, such as PNIPAM hydrogels, with high sensitivity. Despite the difference in the mode of force application in shear and Young moduli, both of these moduli are calculated in closely-related manner.

During oscillatory testing of PNIPAM+RRR, complex modulus (G*), a direct measure of material stiffness or total rigidity, was obtained. G* is a summation product of absolute value of elastic (G') and viscous (G") components of the tested material. G' is often referred to as a storage or elastic modulus, as it describes material rigidity when it is exposed elastic deformation. Where G", known as a viscous modulus, is used as an indicator of viscous flow in the material. In addition, G', as a measure of elasticity, is often reported together with G* to describe material performance under mechanical stress. (Rheologyschool.com 2013)

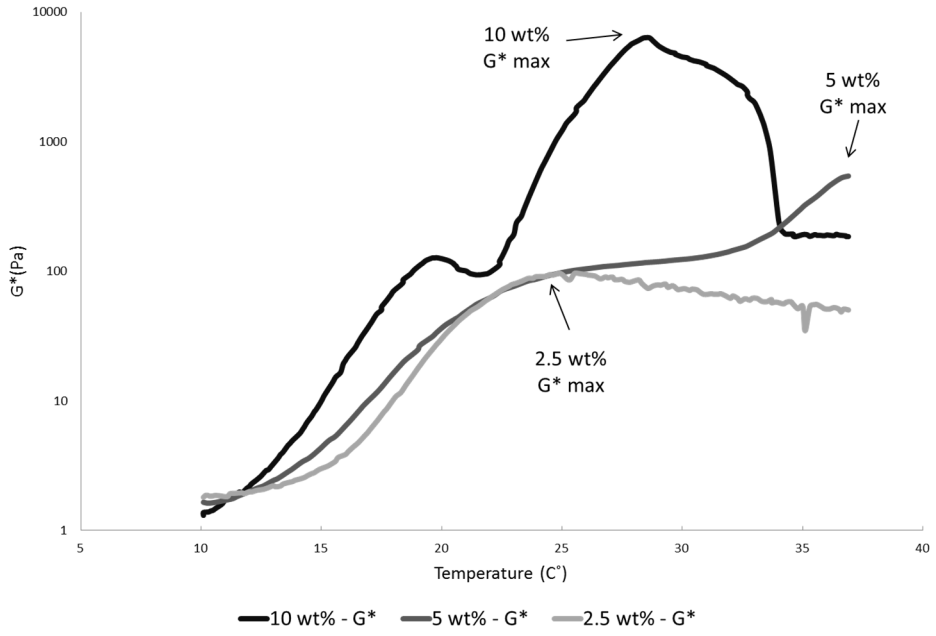

Figure 18: Total rigidity of the PNIPAM+RRR hydrogels is represented by the complex modulus (G*), which can be seen in the temperature scan plot at 2.5, 5 and 10 wt% polymer concentrations.

Complex modulus (G*) was chosen to represent overall mechanical stability of the PNIPAM+RRR sample, as it is a direct measure of material's rigidity (performance under stress). Maximal values of G* for 10, 5, 2.5 wt% samples are 6334 Pa (at 28.6 ˚C), 542.3 Pa (at 36.9 ˚C) and 96.7 Pa (at 25.6 ˚C) (Figure 18). As expected, 10 wt% sample has demonstrated highest rigidity, but at physiological temperature of 37 ˚C this value was reduced down to 184.97 Pa – a 34-fold drop. Such prompt drop in material rigidity can be explained by loss of traction between polymer and the cone due to rapid expulsion of water out of the polymer network at high sample concentration. Where 5 wt% sample was found to show maximal rigidity at 37 ˚C

(542.3 Pa). 2.5 wt% sample has showed a slight drop in rigidity at 37˚C, equating to 50.25 Pa (1.9-fold decrease).

Similarly to G*, G' and G" were plotted to demonstrate solution-gel phase change, indicated by G' and G" cross over (Figure 19). Cross over between the elastic moduli (G') and the plastic moduli (G") is considered as an onset point for the gelation process of PNIPAM hydrogels (Liao, Zhang, et al. 2011). Therefore, gelation onset temperatures for 2.5, 5 and 10 wt% PNIPAM+RRR samples were 18.8˚, 17.3˚ and 16.4˚C, respectively. This observation demonstrated inverse relationship between hydrogel concentration and the onset temperature of the gelation processes.

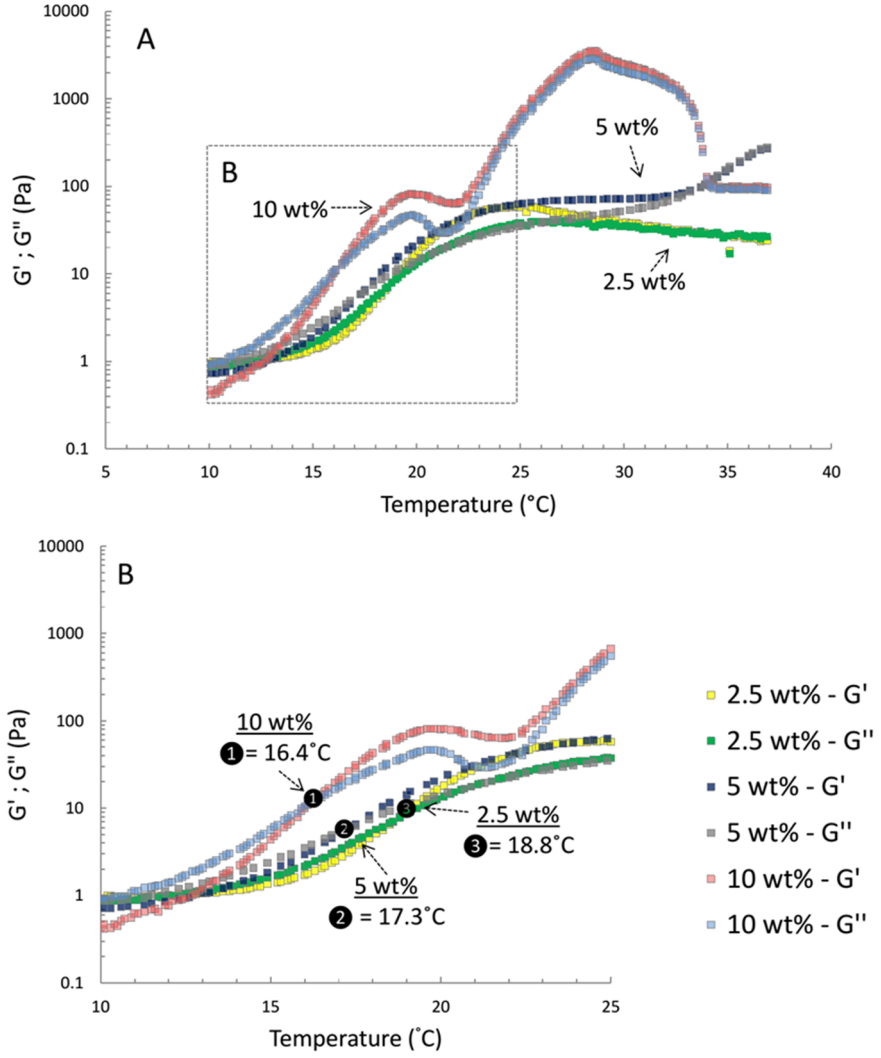

Figure 19: Rheological properties of PNIPAM+RRR in aqueous solution, at 2.5, 5 and 10 wt% hydrogels concentrations, were tested on a cone-plate viscometer. A temperature scan of all three concentrations is represented in (A), where (B) provides a closer look at the region where G' and G'' gelation-related cross-overs are taking place.

Similarly to G*, not all maximal G' values were obtained at 37˚C. Maximal G' value for 2.5 wt% sample was 58.7 Pa at 24.9˚C; for 5 wt% sample maximal G' value was 266.5 Pa at 36.9˚C; for 10 wt% maximal G' was equal to 3497 Pa at 28.6˚C. At the same, G' values at physiologically-relevant temperature (i.e. 37˚C) were as follows: $G'_{37^{\circ}C}$ at 2.5, 5 and 10 wt% were 23.92, 266.5 and 95.43 Pa. Presented values of G* and G' are collated in the Table 7 below.

Table 7: A summary table of PNIPAM+RRR performance under shearing oscillatory force and during gradual heating (1 ˚/min). Observed G* and G' maximal and physiological values are presented at corresponding temperatures.

PNIPAM+RRR in dH_2O	Concentration (wt%)	Maximal value		Modulus at physiologically relevant temperature (i.e. at 37˚C) (Pa)
		Modulus (Pa)	Corresponding temperature (˚C)	
G*	2.5 wt%	96.7	25.6	50.25
	5 wt%	542.3	36.9	542.3
	10 wt%	6334	28.6	184.97
G'	2.5 wt%	58.7	24.9	23.92
	5 wt%	266.5	36.9	266.5
	10 wt%	3497	28.6	95.43

3.5 Discussion

In recent years, particularly during the last decade, a marked increase in research of non-linear polymers was observed due to the fact that the new levels of polymer complexity can provide exploitable properties of the material in the biomedical field (Jikei & Kakimoto 2001; Hopkins et al. 2009; Carter, Rimmer, et al. 2005; Lapworth et al. 2011). The key driving force for spurring up the interest was the discovery of new polymerisation methods, such as reversible addition−fragmentation chain-transfer polymerization (RAFT) (Chiefari et al. 1998). Discovery of these methods allowed convenient synthesis of polymers with highly-branched architecture.

Three core properties of a highly-branched polymer have an instrumental effect on the properties of the end polymer. These properties are degree of branching, chain end functionality and repeat unit structure (England & Rimmer 2010).

Degree of branching is directly correlated with amount of available RAFT agent. Reduction in RAFT presence results in decrease of degree of branching and generally lower number average molecular weight (Rimmer et al. 2007). Also, the level of polymer branching effects the ability of the polymer chains to slide past one another, what in turn affects the intermolecular force balance and is manifested in the bulk physical polymer properties.

During PNIPAM polymerisation, repeat unit propagation is done by using RAFT monomer, which is a dithioate ester with alkene functionality (Rimmer et al. 2007). Alternative polymerisation method, based on atom transfer radical polymerisation (ATRP), will also yield a highly branched PNIPAM but with different repeat unit structure and LCST point of 36˚C (Allı et al. 2012).

Linear polymers provide basic functionality, where monomers often offer only two bonding sites essential for chain propagation. Whereas highly branched polymers, PNIPAM+RRR designed in this study being a great example, provide a highly tunable mechanism of controlling number of reaction sites on every accessible chain of the polymer structure (Hopkins et al. 2009). As a result, further functionalisation with molecules of interest (e.g. peptides) in a controlled manner becomes possible.

3.5.1 Highly branch polymer synthesis and initial functionalisation

NIPAM monomer polymerisation with RAFT-based method resulted in product with number and weight average molecular weight of 17933 and 58817 g/mol, respectively (Table 5). These molecular values are lower than in the product previously synthesised by Lapworth, from whom the original synthesis protocol was adopted (Lapworth 2009). Number and weight average molecular weight of the product, synthesised by Lapworth, was 33942 and 114863 g/mol, respectively. Such deviation in the current study can be explained by following factors: substitution of the original 4,4'-azobis(isobutyronitrile) (AIBN) initiator for more reactive 4,4'-azobis(4-cyanopentanoic acid) (ACVA) initiator; reduction in polymerisation time from 48 hours to 12 hours; reduced use of ACVA initiator (i.e. 1.7-fold molar equivalent difference between RAFT and ACVA; NIPAM:RAFT:ACVA=25.045:1:0.5844).

Collected product, the highly branched parental PNIPAM, demonstrated a rapid increase in absorbance at 17.5˚C during UV-Vis turbidimetry analysis (Figure 10). However, during initial dissolution of the parental PNIPAM poor solubility was observed. In order to improve solubility of the polymer, pyrrole carbodithioate end groups were reacted with ACVA, producing carboxylic acid functionality. Due to hydrophilic and polar properties of the carboxylic acid, solubility of the polymer was greatly improved. However, at concentration, sufficient for gel formation, very active syneresis was observed in all PNIPAM+COOH samples tested (Figure 8).

Syneresis in hydrogels presents a substantial barrier for utilisation of this hydrogel for cell culture purposes (Gan et al. 2010). To overcome this barrier, highly branched architecture of PNIPAM+COOH was further functionalised with extremely polar and hydrophilic peptide sequence - tri-arginine. Introduction of the tri-arginine peptide sequence was thought to provide an impetus for retention of hydrogen bonds between water molecules and hydrophilic groups. As a result, peptide functionalised PNIPAM demonstrated substantial retardation in water expulsion from the hydrogel: minimal syneresis was observed in 5 wt% sample, and even gel formation was noted in 1 wt% sample (Figure 8).

Syneresis is a long-standing issue with non-functionalised PNIPAM architecture. A well-established route to syneresis reduction is co-polymerisation of NIPAM with acrylic acid (AA) (Gutowska et al. 1992; Gan et al. 2010). Where the current study reports successful synthesis of a new chemical moiety – HB PNIPAM+RRR addition, which was not previously reported Scheme 1: Scheme 1). It is worth noting, that HB PNIPAM was functionalised with an arginine peptide mixture, dominated by RRR sequence (i.e. 73.12%) (Figure 7).

Presence of the RRR peptide functionality had a substantial effect on the gelation properties of the HB PNIPAM. Along with reduction of syneresis, LCST point has been shifted from 18˚C to 24˚C after peptide addition, and was complemented by extension of the hysteresis window (Figure 10). From the position of practicality, liquification of the hydrogel at a lower temperature due to extended hysteresis window is very beneficial – during *in vitro* experiments, flexibility in sample manipulation and handling will be greater.

Turbidimetry analysis for LCST point identification is a routine method in PNIPAM studies (Duan et al. 2006). In the current study UV-vis analysis was supplemented by highly sensitive methods, μDSC and ATR-FTIR, for elucidation of PNIPAM's gelation mechanism on a molecular level.

3.5.2 SEM: architecture and porosity

An essential parameter of a cell-supporting material is porosity, presence of which will ensure nutrient delivery and waste removal from the cells (Lawrence & Madihally 2008). Snap-freezing and dehydration of the PNIPAM+RRR hydrogels, followed by imaging of the fracture surface with scanning electron microscope (SEM) allowed to assess structural organisation and porosity of the gel (Figure 9).

Preparation of the hydrogel with culture media had a substantial effect on pore size and organisation, when compared to one prepared with water. Change in hydrogel architecture is contributed to presence of serum in the media – a rich source of protein, such as bovine serum albumin (BSA), may affect intrachain interaction and aggregation process of the polymer chains during phase transition.

It is clearly seen that the porosity is interconnected, however, volumetric or percentile quantification of the hydrogel porosity was not possible to perform. In the future work, this issue will be addressed by employing beads of nano and micro scale and known size to be used as reference for pore measurements.

Qualitative assessment of the pore size in PNIPAM+RRR hydrogel, prepared with cell culture media, suggests the range of the pores to be ca. 0.5 – 1 µm in diameter. Taking in the account the diameter of encapsulated MSCs in 3D, represented by 18 to 30 µm range (data not shown; personal observations), it is valid to assume that there will be no void between a cell and the scaffold structure. However, this level of porosity and pore size should be sufficient for nutrient influx and waste removal, and in this regard, preparation of the hydrogel with serum-rich culture media is of great benefit.

3.5.3 Conventional DSC vs µDSC of HB PNIPAM and HB PNIPAM+RRR

Thermo-responsive property of the PNIPAM polymer is based on chain aggregation and coil-globule transition, accompanied by solvent expulsion, during heating process beyond LCST point.

Whereas at temperatures below LCST point polymer chains are relaxed and reside in their hydrated state. High degree of sensitivity to changes in energy requirements provided by µDSC has been employed to analyse phase transition mechanism in PNIPAM-based polymers (Graziano 2000).

Importantly, PNIPAM architecture has a major impact on the gelation mechanism (Chung et al. 2006; Sammon et al. 2006). DSC analysis of PNIPAM polymers has commonly revealed an endothermic single peak around 32˚ C point and a single exothermic peak at ca. 30-31˚C during cooling phase (Maeda et al. 2000; Ding et al. 2005).

µDSC analysis of PNIPAM+RRR has provided observations, that differs with established understanding of the phase transition (see above). Parental PNIPAM has demonstrated conventional endothermic peak at 17.77˚C during heating cycle (Figure 11). Where PNIPAM+RRR sample at the same concentration presented two

distinct peaks at 22.34˚C and 27.49˚C. Throughout literature review no studies were identified where DSC analysis would show two endothermic and exothermic peaks in the heating cycle. However, two studies been found to show exothermic spectra with double peak appearance in linear and block PNIPAM co-polymers, during the cooling phase of the DSC analysis (Ding & Zhang 2006; Lu et al. 2013). Exothermic spectrum from PNIPAM+RRR demonstrates a broad peak, consisting of two overlapping peaks with highest intensity at 24.19˚C. In order to identify centres of the overlapping peaks, spectral de-convolution is required and will be addressed in the future work.

Furthermore, Ding and Zhang have analysed state transition behaviour of PNIPAM in dilute and semi-dilute aqueous solutions with DSC microcalorimeter. In that study a bimodal transition during cooling process, represented by two exothermic peaks, was observed (Ding et al. 2005). The first peak, at 31^{o} C, was assigned to the disruption of the additional intrachain hydrogen bonding, which has formed between chains at the collapsed state, while polymer macromolecules were maintained at temperatures above LCST point. The second peak, at 30.2^{o} C, was attributed to dissolution of the collapsed chains. This bimodal behaviour was recorded in a dilute sample when temperature scanning rate was lower than 0.328 ^{o}C/min. At higher scanning rates bimodal acitivy was not detectable, suggesting kinetic control of the process. In addition, performing heating cycles at rates as low as 0.03˚C/min did not show any signs of bimodal nature of the coil-globule transition process. This observation highlighted validity of their original hypothesis, which stated that during cooling stage globule-coil transition commences with intrachain hydrogen bonding disruption, followed by gradual dissolution from outer layer to the interior (Ding et al. 2005).

Follow up study by the same authors has further elucidated the mechanism of collapsed globule-coil transition throughout cooling stage. During solution heating past LCST point PNIPAM chains associate together to form large aggregates; where during cooling process polymer aggregates are swollen first, prior to inner chain egression from the swollen core and dissolution in surrounding solvent as individual chains (Ding & Zhang 2006).

In addition, detection of the intrachain hydrogen bonding in collapsed globules provides mechanistic explanation of the hysteresis process. Extra hydrogen boding, that has partly caused bimodal relaxation mechanism in PNIPAM during cooling, has been identified in the collapsed state of PNIPAM chains, and it is attributed to the dehydration process (Cheng et al. 2006). Also, dehydration, driven by increase in temperature, has caused shortening of the average interchain distance, what in turn creates a lag between LSCT of heating and cooling stages, which is manifested as hysteresis (Ding et al. 2005; Cheng et al. 2006; Ding & Zhang 2006). Compilation of the observed facts about hysteresis from bimodal transition, during the cooling stage of DSC, suggests a following conclusion: hysteresis phenomenon is caused by the additional time required for the relaxation and reversion of polymer aggregates into their hydrated state and regaining of chain-solvent equilibrium.

In the current study hysteresis has also been observed in highly branched PNIPAM during UV-vis, DSC and FTIR analysis (Figure 10, Figure 11 and Figure 17). Furthermore, micro calorimetric DSC analysis of the PNIPAM+RRR has revealed bimodal transition in heating and cooling cycles (Figure 11). Extensive literature search shows that such transition mechanism was not documented previously. Comparison of DSC spectra from PNIPAM and PNIPAM+RRR demonstrates absence of multiple peaks in either endotherm or exotherm in PNIPAM (parental) sample, what suggests that presented functionality of PNIPAM+RRR can be attributed to RRR peptide addition. Further investigation is required to elucidate underlying transition mechanism that resulted in a double peak spectrum of the endotherm signal in PNIPAM+RRR sample.

By taking in consideration collected data in the current study and the theories, proposed in the literature, it can be hypothesised that RRR peptides provide amphiphatic properties to the branched polymer chains, what may result in a better retention of water molecules in the aggregating polymer globules. As a results, initial coil-globule organisation and dehydration can be attributed to the first peak on the DSC endotherm (at 22.34 ^{o}C), where the second peak (at 27.49 ^{o}C) is likely to represent an energy barrier that requires additional input of heat energy in order for the system to achieve colloidal stability. In addition, out of the 20 essential amino acids arginine has the ability to form most of hydrogen bonds (Luscombe et al.

2001). This property of arginine provides further insight into bimodal phase transition mechanism in HB PNIPAM+RRR.

PNIPAM chain dehydration during heating is described by two processes: interchain association and interchain contraction, where first process incurs lower cost of conformational entropy, compared to the second process (Ding & Zhang 2006). Therefore, during heating cycle, the earliest endothermic peak should represent interchain association, if a bimodal spectrum is presented. I assume identical sequence of interchain processes to take place in the HB PNIPAM+RRR sample.

By comparing DSC spectra from both samples at identical concentrations, parental HB PNIPAM and HB PNIPAM+RRR, substantial difference in heat flow intensity is observed (Figure 11). Considering that the heat flow measurement provides quantitative insight into how much thermal energy is required for phase transition to occur – it is possible to show that the heat energy requirement for the phase transition in HB PNIPAM+RRR is 19 times lower, when compared to parental HB PNIPAM. Thus, this observation allows to conclude that the RRR peptide addition lowers requirement in the heat energy to produce an equilibrated globule structure.

3.5.4 Zeta potential: colloidal stability and peptide effect on particle size

To further understand how structural stability of the hydrogel was affected by peptide functionalisation and provide predictions on hydrogel performance during *in vitro* testing with cells, zeta potential and particle size of parental HB PNIPAM and HB PNIPAM+RRR were measured.

Initial difference between functional groups of parental HB PNIPAM (Figure 12) and HB PNIPAM+RRR (Figure 14A) was reflected in zeta potential measurement, where parental polymer carried negative net charge in contrary to positive charge of the peptide functionalised polymer. Increase in temperature has resulted in corresponding increase in zeta potential. Commonly, zeta potential progression past +/-30 mV suggests formation of a stable colloidal suspension, that will not flocculate and precipitate (Malvern Instruments Ltd n.d.). Colloidal stability of HB PNIPAM+RRR was confirmed, as the zeta potential at 37˚C was equal to 31.496

mV. Whereas, analysis of parental HB PNIPAM does not give a clear conclusion: when parental polymer sample is tested at concentration, identical to HB PNIPAM+RRR, zeta potential was equal to -47.56 mV at 37˚C, suggesting colloidal stability; however, this concentration was not optimal for the instrument. After concentration optimisation, parental sample demonstrated zeta potential of -11.203 mV at 37˚C, opposing previous assumption regarding colloidal stability. As the initially tested concentration was not optimised, the zeta potential result should be disregarded for this particular concentration.

Along with zeta potential, particle size of HB PNIPAM (Figure 13) and HB PNIPAM+RRR (Figure 14B) was also measured. In both of the samples identical trend was observed – with increase in temperature particle size is gradually decreasing. This observation is consistent with prevailing view of PNIPAM gelation, where fully relaxed and hydrated coil structure condenses into compact globular structure at phase transition temperature (Maeda et al. 2000).

3.5.5 Infra-red spectroscopy: closer look at the hydrogen bond formation between polymer and solvent

During DSC data analysis bimodal phase transition was identified in PNIPAM+RRR, and in order to gain a greater insight into causes of this phenomenon, a descriptive analysis method was required.

The attenuated total reflectance Fourier transform infrared spectroscopy (ATR-FTIR) became a method of choice because of its' high sensitivity to change in functional group environment and change in molecular interactions as a function of temperature (Sammon et al. 2006).

The aforementioned mechanism of phase transition of PNIPAM involves changes in vibrational energy of the chemical bonds, where ATR-FTIR is a particularly robust method for quantitative analysis of these changes.

More precisely, ATR-FTIR looks into interaction between molecule and infra-red spectrum of radiation at a broad range of wavelengths, where raw data is being

converted from a time domain into frequency domain by means of Fourier transformation.

Vibration of the molecular bonds is often compared to vibration in spring-connected system and described by Hooke's law of harmonic oscillation (Figure 20). Knowledge of the reduced mass value and the bond strength between the atoms can suggest where particular bond stretches can be found on the FTIR spectra.

$$(1)\ f = \frac{1}{2\pi}\sqrt{\frac{k}{\mu}} \qquad (2)\ \mu = \frac{m_1 * m_2}{m_1 + m_2}$$

Figure 20: Hooke's law model of a harmonic oscillation process. (1) describes frequency of the oscillating body, where the constant *k* defines the stiffness of the spring. (2) provides information on the effective mass of a two-body system, also known as reduced mass value.

PNIPAM-based systems have been previously characterised by FTIR spectroscopy, where PNIPAM specific peaks were assigned. Most common functional groups used are PNIPAM characterisation are: amide 1, amide 2 and antisymmetrical methyl stretch (ν_{as}(CH)). (Maeda et al. 2000; Sun et al. 2007; Sammon et al. 2006)

The amide 1 peak mostly describes stretching vibrations of the carbonyl (C=O) bond and is often found in the 1600 -1700 cm^{-1} range , where amide 2 is mainly representative for in-plane N-H bond bending, but it is more complex than amide 1, as C-N stretching is often integrated in this peak. Amide 2 is often found in the 1510-1580 cm^{-1} range (Jabs n.d.). Whereas, antisymmetric stretch of the methyl group (i.e. $-C(CH_3)_2$ of the isopropyl group) is commonly found at a higher wavenumber position (e.g. 2982 cm^{-1}) (Maeda et al. 2000).

In order to study phase transition mechanism of a highly branched PNIPAM and its' peptide-functionalised derivative, amide 1, amide 2 and antisymmetrical methyl stretch region were used to track change in their chemical environments with increase and decrease of the temperature.

As previously mentioned, PNIPAM can form hydrogen bonds between water molecules and the amide functional groups via C=O and NH linkages. Bond shifts in

these functional groups by more than 4 cm^{-1} to the higher and lower wavenumbers, respectively, were found to indicate a reduction in hydrogen bonding between the amide functional groups and water molecules (Maeda et al. 2000; Sammon et al. 2006).

Moreover, it has been previously demonstrated that the shift towards higher wavenumber in the ν_{as}(CH) peak is indicative of the increase in the hydrophobic interaction between PNIPAM polymer chains (Maeda et al. 2000; Sammon et al. 2006). Such observation is consistent with the coil-globule transition mechanism, which is observed during PNIPAM gelation (Wang & Wu 1999).

In the current study, presented analysis of PNIPAM polymer demonstrates peak centre shifts in all 3 regions of interest: amide 1 and 2, and ν_{as}(CH). Quantification of the shifts in the parental PNIPAM (Figure 16) and PNIPAM+RRR (Figure 17) samples is summarised in the Table 6.

After comparing shifts in amide 1, 2 and ν_{as}(CH), for both PNIPAM samples, it can be clearly seen that the amide 1 peak demonstrates a shift in the expected direction, towards higher wavenumbers. However, the observed shift values for amide 1 are below the set signal resolution of 4 cm^{-1}, what diminishes significance of the shifts in this particular band. Whereas, amide 2 and ν_{as}(CH) bands demonstrate a substantial magnitude of peak shifting in expected directions (i.e. 7-10 cm^{-1}, towards lower wavenumbers), and where amide 2 region was particularly responsive to the temperature change.

Additionally, modification of the PNIPAM polymer with RRR peptide sequence did not have a substantial effect on the magnitude of the peak shifting.

Alongside with peaks shift analysis, area under the curves for the same peaks was also quantified, as it provides complementary data on the nature of the hydrogen bonding (Sammon et al. 2006). Due to horizontal architecture of the ATR accessory, increase in band intensity can also be related to gelation of the polymer, as during aggregation process water is being expelled from polymer branches and the formed gel comes into a closer contact with the ATR crystal, resulting in increase of

intensity. Therefore, the change in the band intensity is indicative of the onset of the gelation process, as well as polymer relaxation-disaggregation, during which, process of hysteresis is commonly observed (Ding et al. 2005; Wang & Wu 1999).

Analysis of the peak areas for both polymer samples demonstrates an increase in area as a function of temperature (PNIPAM: Figure 16; PNIPAM+RRR: Figure 17). The peak area analysis in the parental PNIPAM sample showed an interesting curve shape, which closely resembles the UV-Vis data curves.

One of the primary reasons for employing IR spectroscopic analysis was to elucidate origins of the double-peak μDSC spectra in the PNIPAM+RRR sample (Figure 11).

By correlating highest temperature points from DSC data, that represent phase transition in PNIPAM and PNIPAM+RRR, with quantified FTIR data presented above, a correlation table was compiled to demonstrate if the infra-red spectroscopy data is in agreement with DSC and UV-Vis results (Table 8).

When DSC data is compared to UV-vis, both data sets appear to be in an agreement, where the onset of phase change during heating is consistent in both methods of analysis (Figure 11 and Figure 10).

In summary, the polymer hydration and hydrogen bond formation in PNIPAM and PNIPAM+RRR was investigated by ATR-FTIR studies at variable temperatures. Shifts towards the higher wavenumber in the amide 2 and the ν_{as}(CH) region confirmed hydrogen bond disruption, an expected part of the solution-gel transition process. Moreover, shift in the peak position of the ν_{as}(CH) band towards lower wavenumbers during heating stage is indicative of a hydrophobic interaction between polymer branches.

Furthermore, a comparative analysis between UV-Vis, DSC and FTIR results suggested that FTIR data matches the observations made with other two methods only partially. However, FTIR measurements of the peak area are representative of the solution-gel transition mechanism, particularly in the parental PNIPAM sample.

Onset of a sharp phase transition in parental PNIPAM sample takes place at very similar temperature, as seen in DSC and UV-Vis spectra.

Table 8: DSC peak data correlation with FTIR data

	Heating			
	PNIPAM	PNIPAM+RRR		
	Peak	**Peak 1**	**Trough**	**Peak 2**
µDSC correlation with ATR-FTIR	*17.76˚C*	*22.34˚C*	*24.31˚C*	*27.48˚C*
Amide 1 (peak centre)	X	X	0.7 cm^{-1} peak shift (←)	X
Amide 1 (area)	X	X	Onset of the peak area increase	End of the onset
Amide 2 (peak centre)	8 cm^{-1} shift (→); linear, in few data points	2 cm^{-1} shift (→)	X	End of shift at 28˚C
Amide 2 (area)	ca. 18-20˚C onset of the rapid peak area increase	X	Onset of the peak area increase	End of the onset at 28˚C
A.s. CH3 (peak centre)	4 cm^{-1} shift (→); note, may be due to noise	X	From 2 to 5 cm^{-1} peak shift (→)	X
A.s. CH3 (area)	X	X	Onset of the peak area increase	X (Peak area increase continues in a linear fashion)

In order to further elucidate phenomenon of a double peak response, seen in the DSC data from PNIPAM+RRR, a peak fitting around the 1600-1100 cm^{-1} region is required. The peak fitting process would help to identify presence and the effect on the strength of hydrogen bonding, provided by the multiple amide functional groups of the arginine peptide.

3.5.6 Rheology: a dynamic mechanical analysis of PNIPAM+RRR at various concentrations

Hydrogen bond re-organisation, intrachain interaction and phase transition processes are manifested in mechanical properties of PNIPAM+RRR hydrogel on a macro-scale, which can be assessed with rheological analysis. Understanding of the mechanical properties in the hydrogel is of principal importance for this project, as numerous biological studies demonstrated key contribution of the cell culture substrate stiffness in directing differentiation fate of the cell (Pek et al. 2010; Engler et al. 2006; McBeath et al. 2004).

One of the earliest studies on network formation within linear PNIPAM hydrogel was done by Zheng and colleagues, setting out key requirements for representative rheological analysis of PNIPAM (i.e. linear viscoelasticity framework)(Zeng et al. 1998).

Rheological parameters of three PNIPAM+RRR concentrations (2.5, 5 and 10 wt%) were assessed. In order to represent data from the viscoelastic strain region, strain and frequency settings were optimised for all three concentrations. As a result, dynamic mechanical analysis with constant frequency and varying temperature of the sample, also known as a temperature sweep, was performed to show phase transition temperature and viscoelastic properties of all three concentrations (Figure 18 and Figure 19).

3.5.7 Rheology correlation with previous characterisation methods

Each of the characterisation methods, used in this study, has provided different insights into gelation mechanism of PNIPAM+RRR. Fundamental parameter like LCST was defined differently by each method, where UV-vis predicted LCST at 24 ^{o}C (Figure 10), DSC at 22.34/27.49 ^{o}C (Figure 11) and viscometry at 16.4, 17.3, 18.8 ^{o}C in 10, 5, 2.5 wt% samples, respectively (Figure 19B). It is difficult to do a direct comparison between all three methods due to difference in the nature of analysis method and concentrations.

Most importantly, rheological analysis has provided an understanding, what mechanical stiffness can be expected from the hydrogel at 37˚C, a physiologically relevant temperature. Results of the rheological analysis are collated in Table 7.

Analysis of rheological data for PNIPAM+RRR suggests that all three concentration samples undergo expected solution-gel transition and hydrogel network formation, where increase in concentration leads to lowering of the LCST point. Such observation is attributed to more rapid polymer chain collapse and dehydration processes at higher polymer concentrations caused by higher number of chains in the solution and shorter interchain distance.

According to rheological results (Figure 18 and Figure 19), 5 wt% sample demonstrates obscene of syneresis that led other two concentration to G* reduction after certain temperature point, indicating loss of traction with the hydrogel due to water expulsion. In addition, complex modulus (G*) of the 5 wt% sample was highest at 37˚C and being equal to 542 Pa.

Knowledge of the complex and elastic moduli of PNIPAM+RRR at 37˚C (Table 7) allows comparison of this particular hydrogel with other bio-compatible hydrogels. For example, Chung and colleagues has synthesised a semi interpenetrating polymer network (sIPN) on the basis of linear PNIPAM, functionalised with acrylic acid and enzymatically sensitive peptide sequences (Chung et al. 2006). Resulting hydrogel with complex moduli range of 100-200 Pa (G* depended on the peptide concentration) has shown an increase in osteoblast proliferation with increase in complex modulus. Induction of bone regeneration was also observed in *in vivo* rat femoral ablation model, but only when peptide-functionalised hydrogels were used. (Chung et al. 2006)

Another study by Pek and colleagues involved use of polyethylene glycol-silica nanocomposite gel with RGD functionality. Results of the study demonstrated an increase in neural (ENO2), myogenic (MYOG) and osteogenic (Runx2, OC) transcription factor expression when MSCs were cultured in 7, 25 and 75 Pa gels, respectively. (Pek et al. 2010) This study highlights importance of hydrogel stiffness, where a material with stiffness of 7 Pa can direct differentiation of MSCs.

4 MSC behaviour in 3D and hydrogel encapsulation

4.1 Introduction

4.1.1 Cells in 3D

As all cells in the human body are residing in 3D environment, and are constantly exposed to mechanical and chemical gradients, it is crucial to account for numerous parameters during model system design, including: cell-cell and cell-matrix interaction (Cukierman et al. 2001; Chung et al. 2006; Bissell et al. 1982; Ingber 1997), mechanical properties of the 3D substrate (Winer et al. 2009; Yang et al. 2014), nutrient supply and waste removal (inter-connected porosity) (Lawrence & Madihally 2008; Kraehenbuehl et al. 2011; Yow et al. 2009), bio-activity (Lutolf, Lauer-Fields, et al. 2003) and bio-degradability (Galperin et al. 2010) of the culture substrate.

Numerous platforms which are designed to test cell behaviour in 3D are currently available (Meng et al. 2014; Pampaloni et al. 2007). These 3D platforms can be divided into two sub-groups: mechanically soft (normally gel-based environment that is designed to match mechanical properties of the soft tissues) and mechanically rigid (often consists of non-organic components and demonstrates high ultimate stress, which is required to match weight-bearing requirements, set by the skeletal system). The soft systems include spheroids (cell aggregates), culture on micro carriers, alginate microencapsulates, thermo-reversible hydrogels and nanostructure scaffolds composed of self-assembling peptides, amongst others (Table 9). Whereas rigid systems are mainly represented by non-organic porous scaffolds like bioglass and hydroxyapatite (HA) based materials (Willerth & Sakiyama-Elbert 2008), and non-porous substrates and scaffolds with engineered nano-pillar-patterned surface (Fu et al. 2010). Each method is unique as it provides different levels of biological complexity and density of information that can be collected during the experimentation process.

In addition, soft scaffold and organoid (scaffold-free) systems in comparison with mechanically rigid culture and implant systems are advantageous in terms of cell behaviour analysis by currently available imaging methods (Pampaloni et al. 2007;

Dickinson 2006). In most cases, soft-type scaffolds are more translucent, which eases the imaging methodology. Also, cell seeding in soft gels is more efficient (i.e. cell seeding is not dependent on the scaffold geometry) and the encapsulation or seeding process is often rapid.

4.1.2 Scaffolds, particularly hydrogels, drive revolution in understanding cell-cell, cell-matrix interactions and tissue formation.

Over the years numerous test models have been designed for the analysis of MSC behaviour in 3D environment. The list below is not exhaustive, but it represents main testing solutions from a range of soft scaffolds (Table 9):

Table 9: Mechanically soft 3D culture systems

3D culture method	Unique benefits
Cell aggregates (spheroids) (Frith et al. 2009; Kunz-Schughart et al. 2004)	Low material and running costs
Microcarriers (Meng et al. 2014)	Better cell quality and high purity can be provided due to effective mass and gas transfer.
Alginate microencapsulates (Serra et al. 2011)	Provides protection to cells from shear-force induced cell death.
Thermo-reversible hydrogels (Lei & Schaffer 2013; Lapworth et al. 2011)	
Self-assembling peptides (nano-scale scaffolds) (Meng et al. 2014)	Allow introduction of biologically active structural segments (i.e. RGD)
Animal models (Kang et al. 2009)	Collected information is more clinically-relevant
Organotypic explants (Toda et al. 2002)	Original structural and cellular organisation is retained during culture. Collected results are more representative of *in vivo* conditions.
Organ slices (Holopainen 2005)	

Spheroids, microcarriers, alginate microencapsulates, thermo-responsive hydrogels and self-assembling peptides share following benefits: ease of setup and use, scalability and reproducibility. The listed benefits made these platforms more attractive for clinical translation due to highly controlled manufacturing processes that underlay these platforms. Full control over the design of the scaffold is explored by the tissue engineers (Galperin et al. 2010; Cheikh Al Ghanami et al. 2010), where cell-supporting environment is tailored to the needs of a particular cell type and tissue repair process (Bissell et al. 2002).

From the range of mechanically soft scaffolds, PNIPAM-based hydrogels are highly suitable for generation of cell-supporting environments (Lei & Schaffer 2013; Lapworth et al. 2011; Ibusuki et al. 2003). Particularly, the highly-branched sub-class of PNIPAM gels provides the ease of structural modification (highly amenable), highly accessible sites for functionalisation and tight control over the molecular weight, that results in a high degree control of the bulk properties in the resulting hydrogel (England & Rimmer 2010; Hopkins et al. 2009).

Hydrogels represent a subset of mechanically soft scaffolds, where the structural properties are partly determined by the organic nature of the structure. Highly branched polymers like PNIPAM are well suited for mechanical and functional modification to cater for needs of the cells (Rimmer et al. 2007; Nakayama et al. 2007). The required properties of the hydrogel are formed via control of the molecular weight and the degree of branching, attachment of functional groups and other chemical entities (Carter, Hunt, et al. 2005; R England & Rimmer 2010; Lapworth et al. 2011). In this study, PNIPAM with highly branched architecture was designed to encapsulate and provide supporting environment for MSCs. In order to identify an appropriate 3D environment for this cell type, key structural parameters of the bone marrow were considered during the design of the of the highly branched PNIPAM.

Multiple attempts were taken to simulate, at least partially, complexity of the bone marrow environment by use of hydrogel systems, with common ultimate goal to recreate properties of the niche settings (Nuttelman et al. 2005; Aizawa & Shoichet 2012; Giobbe et al. 2012).

The bone marrow is a unique homing environment for myriad of cells and secreted chemical factors. Also, the bone marrow is one of the sites of choice for MSC harvesting, a highly porous, mechanically weak (compared to surrounding cancellous bone tissues (Bayraktar et al. 2004)), with an extensively developed blood supply network. In order to mimic such a complex environment, key structural factors of the bone marrow, which have fundamental effect on cell viability, differentiation and proliferation were selected. The factors that were considered included: inter-connected porosity (Lawrence & Madihally 2008; Galperin et al. 2010), mechanical elasticity (Engler et al. 2006; Pek et al. 2008) and ability to encapsulate cells, providing cell-matrix interaction (Lai et al. 2010; Bissell et al. 2002). The resulting HB PNIPAM+RRR hydrogel system was structurally stable and porous, with no apparent shrinkage and mechanical properties close to value range of soft human tissues, such as brain tissue and bone marrow (Butcher et al. 2009; Higuchi et al. 2013).

4.1.3 PNIPAM modification and MSC differentiation within hydrogels

In the past, PNIPAM-based hydrogels were used as 3D scaffolds for different cell types: hepatocytes (Wang et al. 2011), chondrocytes (Lapworth et al. 2011; Ibusuki et al. 2003) and fibroblasts (Cheikh Al Ghanami et al. 2010), amongst many others (Guan & Zhang 2011). However, MSC's behaviour within PNIPAM environment was assessed very rarely. Available studies in their majority suggest an ability of the hydrogel to successfully encapsulate MSCs (Peroglio et al. 2013; Na et al. 2007; Liao, Chen, et al. 2011), however a high level of syneresis (Gan et al. 2010), optical opaqueness (Lapworth et al. 2011) and limited information on cell viability suggests that structural and functional modifications are required to improve the usability of the PNIPAM hydrogels (Galperin et al. 2010), with micro-environment sensitive cells, such as MSCs (Saleh et al. 2012).

Table 10: Modified PNIPAM-based hydrogels with biomedical potential.

Hydrogel name	Description	Key application properties
PNIPAM-gelatin (Ibusuki et al. 2003)	Gelatin was grafted onto PNIPAM polymer backbone.	Supports cartilage viability and natural phenotype. Mechanical properties are similar to the native hyaline cartilage. Stability of the hydrogel structure is independent of the cell culture period.
PNIPAM-PLGA (Fraylich et al. 2010)	A graft polymer of anionic poly(D,L-lactide-co-glycolide) (PLGA) and cationic PNIPAM	High and interconnected porosity Gels are flexible, with critical yield strain of up to 160%.
PNIPAM-DBA (Vo et al. 2014)	A dimethyl-γ-butyrolactone acrylate (DBA) copolymer with PNIPAM	Calcium-binding properties, coupled with ability to accelerate bone mineralisation within critical size bone defects *in vivo.*
P(NIPA-co-AAm) (Zhang et al. 2009)	A copolymer of acrylamide (AA) and PNIPAM	Formed nanohydrogel particles are efficient at anti-tumour drug (i.e. docetaxel) loading and release *in vivo.*
AHA-g-PNIPAAm (Tan et al. 2009)	A graft polymer formed by coupling of aminated hyaluronic acid (AHA) to PNIPAM through amide bond linkages.	AHA-g-PNIPAAm demonstrates interconnected pores. Viability of encapsulated adipose stem cells (ASC) is supported *in vivo*.
PNIPAM-AA-MMP13-RGD (Chung et al. 2006)	PNIPAM was co-polymerised with acrylic acid (AA) to form interpenetrating polymer network (IPN), which was further functionalised with metalloproteinase-13 (MMP-13) sensitive degradable crosslinker and integrin-binding domain RGD.	Hydrogel stiffness and peptide concentration can be tuned independently to generate cell response. Presence of MMP-13 degradable crosslinker in the hydrogel induces bone regeneration *in vivo*.

From the currently known thermo-responsive hydrogels, PNIPAM-based gels are the most investigated (Delair 2012). To date, numerous PNIPAM-based hydrogels with a plethora of modifications have been designed and synthesised for application in the field of biology (Guan & Zhang 2011; Roux & Ladavière 2013). Table 10 provides examples of modified PNIPAM-based hydrogels with successful application in biological settings and biomedical potential. Various cell types were studied in multitude of PNIPAM hydrogel's architectures. However, very little is known about MSC differentiation in 3D environment of PNIPAM hydrogel. Work of Na et al., Liao et al., Peroglio et al. research groups demonstrates that: i) functionalisation of PNIPAM structure with hydrophilic functional groups will result in an improved structural stability, reduce shrinkage and will allow cellular encapsulation; ii) structural integration of biologically active molecules, like peptides and growth factors, in PNIPAM hydrogels is often required to trigger osteogenesis in 3D environment, in addition to stimulation with common osteo-induction factors (Peroglio et al. 2013; Na et al. 2007; Liao, Chen, et al. 2011).

For instance, Na et al. looked into extent of osteogenic differentiation within PNIPAM hydrogels, functionalised with acrylic acid and mixed with hydroxyapatite (HA), forming a composite. These composite hydrogels were seeded with rabbit MSCs, with or without addition of the osteogenesis stimulator – bone morphogenic protein 2 (BMP-2), and were injected into nude mice for 8 weeks. *In vitro* differentiation experiments were performed as well. After 8 weeks of *in vivo* culture, ALP activity in PNIPAM+AA+HA hydrogels, with added BMP-2, was twice as high, when compared to samples without BMP-2. However, ALP activity in both hydrogel types was significantly higher than in the cell-only controls. Whereas strong mineralisation response was observed only in BMP-2 treated hydrogels, both *in vivo* and *in vitro* settings. (Na et al. 2007) Therefore, this particular PNIPAM-based hydrogel was observed to be osteoinductive. However, to demonstrate noticeable osteogenic differentiation *in vitro* and ectopic bone formation *in vivo*, a potent chemical osteogenic stimulator, such as BMP-2, is required.

Osteoinduction, and particularly osteoconduction, of MSCs and osteoblasts has been previously shown in various functionalised hydrogels as well. Osteogenic differentiation was evidently demonstrated by Chun and colleagues. A

thermosensitive hydrogel poly(organophosphazene), functionalised with GRGDS peptide sequence, was seeded with rabbit MSCs and injected into a nude mouse, where a cell-supporting hydrogel would form. After 4 weeks post-implantation, a sharp increase in osteocalcin gene, a typical marker of late osteogenic differentiation, expression was observed. Furthermore, extensive mineralisation, based on calcium content and collagen type I immuno-staining, also confirmed induction and conduction of osteogenesis in hydrogel-encapsulated rabbit MSCs. (Chun et al. 2009)

Hydrogel functionalisation with peptide sequences is common, particularly with RGD sequence, which is the most researched adhesion-related peptide sequence (Ruoslahti 1996). Yang et al. has covalently bound RGD sequence to the poly(ethylene glycol)diacrylate (PEODA) hydrogel, and encapsulated goat bone marrow MSCs into this conjugated hydrogel via UV cross-linking. After 3 weeks of culture in osteogenic medium, hydrogel-cell composites with 2.5 mM concentration of the RGD peptide demonstrated several-fold increase in OCN and ALP expression. Most interestingly, a minimal concentration (i.e. 1.25 mM) of RGD peptide was required to observe Runx2 expression, as at 0 and 0.025 mM concentration Runx2 expression was not detectable in the MSC-containing hydrogels. At the same time, Runx2 was actively expressed in RGD-free monolayer cultures. Furthermore, Yang and colleagues demonstrated that oversaturation of the PEODA+RGD hydrogel during culture and pre-treatment of the cells with soluble RGD peptide leads to saturation of the RGD receptors on the cell surface, consecutively inhibiting cell-hydrogel attachment. Such adhesion inhibition resulted in complete abolishment of mineralisation, when assessed with calcium assays and von Kossa staining. (Yang et al. 2005)

Osteogenesis of BM hMSCs can be also stimulated by unconventional, but simple method within a hydrogel. Chen et al. has exposed BM hMSCs in monolayers and self-assembling peptide hydrogels (i.e. PuraMatrix™, a RADA peptide sequence-based gel) to a mild heat shock – samples were kept at 41˚C for 1 hour once a week, and at 37˚C thereafter. After ca. 3 weeks of treatment, both 2D monolayer and 3D gel samples demonstrated significant increase in calcium deposition. After 25 days in 3D gel culture, a significant upregulation of Runx2 was observed in hMSCs. In

addition, 24 hours after the heat shock treatment, a significant upregulation in the heat shock protein 70 (HSP70) was detected. (Chen et al. 2012) This study reveals a factor, neither chemical nor structural, which can induce osteogenesis in a culture substrate-independent fashion.

4.1.4 PNIPAM+RRR as a suitable 3D environment model for MSCs

The PNIPAM architecture employed in this study stems from the findings of the Rimmer lab, which showed successful synthesis of highly branched PNIPAM via RAFT route (Carter, Hunt, et al. 2005). Along with design of a novel chemical architecture, biocompatibility and cell analysis studies were performed. Lapworth and colleagues have used a PNIPAM-based co-polymer with comb architecture to encapsulate chondrocytes in 3D (Lapworth et al. 2011). Where Hopkins and colleagues have demonstrated that a highly-branched PNIPAM with RGD functionality can be used as a trypsin-free method for cell detachment in monolayer culture (Hopkins et al. 2009).

The work of Hopkins et al. has demonstrated the biocompatibility of HB PNIPAM+RGD and dermal fibroblasts in 2D monolayer culture. Therefore the highly branched architecture via RAFT synthesis method was chosen for fabrication of PNIPAM for further MSC encapsulation.

Functionalisation of a HB PNIPAM with tri-arginine (RRR) sequence was performed to increase water retention in the structure, resulting in reduced gel syneresis and retention of the stable 3D architecture.

Stable 3D architecture is one of the initially set out prerequisites for the MSC scaffold design. Along with promise of successful encapsulation, HB PNIPAM presents the following advantages for cell culture in three dimensions.

- HB PNIPAM has a sharp phase transition at biologically relevant temperatures (Carter, Rimmer, et al. 2005). Attachment of hydrophilic groups results in an increase of transition temperature, where hydrophobic group attachment has an opposite effect (Tao & Yan 2010).

- Highly branched architecture of PNIPAM provides numerous reaction sites on each chain, where the degree of branchness is controlled by the number of available RAFT agents (Hölter et al. 1997; Carter, Rimmer, et al. 2005). Virtually full control over hydrogel's structural design allows parameter optimisation for the needs of the encapsulated cells, such as mechanical properties and LCST point, where these parameters can be manipulated via functional groups addition and feed control (Rimmer et al. 2007).
- Due to the nature of the RAFT polymerisation reaction, where the available monomer is exhausted during controlled polymerisation, and consecutive ultra-filtration steps during purification stage, the resulting PNIPAM polymer has a low monomer content, suggesting virtually zero toxicity (Chiefari et al. 1998; Carter, Hunt, et al. 2005; Scales et al. 2006).
- The colloidal structure of PNIPAM, together with rapid hydrogen bond formation and disruption during change of temperature, is responsible for solution-gel and gel-solution transition (Ding et al. 2005; Cheng et al. 2006; Ding & Zhang 2006). When the colloidal nature of PNIPAM is coupled with highly-branched architecture and a highly polar RRR sequence, the resulting gel produces a highly-hydrated and mechanically supporting 3D milieu - properties shared by the natural ECM (Tibbitt & Anseth 2009; Chen 2010).
- As the temperature is lowered past the gel's LCST point, the polymer chains undergo relaxation steps where the intra-gel hydrogen bonds are broken, allowing the colloidal structure to revert to a non-aggregated state, which in turn will trigger cell release from the hydrogel (Lapworth et al. 2011; Wang et al. 2011).
- The branched architecture of PNIPAM+RRR generates inter-connected pores, which are of paramount importance for cellular nutrient and waste transport within 3D environment.

4.1.5 Work rationale

The *in vivo* environment of the MSCs is extremely complex. Therefore, assessment of the MSC behaviour on 2D surfaces is limited and non-representative of MSC's natural environment (Table 2). Ability to study single cell or micro-tissue (spheroid) behaviour and development in 3D environment is of paramount importance for

design of the cell therapies (Jakob et al. 2012), cancer treatment (Martin et al. 2008) and tissue repair (Pampaloni et al. 2007).

On the basis of the chemical characterisation, HB PNIPAM+RRR hydrogel holds a great promise in generating MSC specific environment, owing to the following features: *in vivo*-like physical molecular bonding, mechanical properties in the range of the soft tissues, highly hydrated structure and chemical functionalisation ability. Therefore, encapsulation of MSC spheroids and single cell suspensions in HB PNIPAM+RRR would provide an adjustable platform for studying MSC behaviours in *in vivo*-like 3D environment.

4.1.6 Hypothesised performance of PNIPAM+RRR hydrogel in biological settings

Based on the literature review of PNIPAM and chemical characterisation of the HB PNIPAM+RRR (Section 3.1 and 3.4), it can be hypothesised that:

i) HB PNIPAM+RRR hydrogel allows rapid MSC encapsulation and subsequent release after temperature drop below the LCST point.

ii) HB PNIPAM+RRR hydrogel is biocompatible with MSCs, with high cell viability during long term cultures.

iii) MSC culture within the 3D HB PNIPAM+RRR environment may stimulate osteogenic or adipogenic differentiation.

4.1.7 Importance of the study

Assessment of HB PNIPAM+RRR hydrogel biocompatibility will help to validate applicability of this material for tissue engineering. Also, findings on MSC phenotype changes (proliferation and differentiation) within 3D hydrogel will contribute towards fundamental understanding of multi-potent cell behaviour in *in vivo*-like environment. In addition, analysis of differentiation capacity in MSC's within 3D will aid in identification of factors that affect the cell fate decision-making process.

Finally, exploration of links between mechanical properties of the hydrogel and cell motility within 3D will help to advance current understanding of scaffold design, what in turn will allow to emulate *in vivo* conditions as close as possible.

4.2 Materials and methods

4.2.1 MSC extraction and culture

Primary human MSCs were isolated from femoral heads or knee plates, removed during joint-replacement operations. Both tissue types were received following informed consent from the donors. Cell isolation from the femoral heads was performed by removal of the bone marrow and expansion in cell growth media (Dulbecco's modified eagle medium (DMEM; GIBCO No: S41966-052) (with 4.5 g/l glucose) containing 100 U/ml penicillin (Life Technologies, UK), 100 μg/ml streptomycin (Life Technologies, UK) and 15% foetal bovine serum (FBS; Gibco, Life Technologies, UK)) in 75 cm^2 flask (Corning, UK) at 37˚C and 5% CO_2 atmosphere. Non-adherent cells were removed after 7 days of incubation and the medium was replaced every 3 days thereafter. Upon reaching confluency the cells were passaged at a 1:3 ratio. Cell isolation from knee plates was performed as follows: knee plates were broken up and pieces were placed into tissue culture grade 10 cm^2 Petri dishes (PK200; BD Falcon) and 10 ml of cell growth media was added. After incubation for 7 days at 37˚C and 5% CO_2 atmosphere, knee bones were removed and the medium was replaced every 3 days thereafter. Upon reaching confluency the cells were passaged at a 1:3 ratio.

4.2.2 MSC (single cell suspension) encapsulation and PNIAPM+RRR preparation for cell culture

Freeze-dried HB PNIPAM+RRR was dissolved in ethanol and centrifuged at 315g for 5 minutes. Liquid phase was transferred into a sterile glass Petri dish and left on a heating plate at 37˚C in a cell culture cabinet overnight. The dry product was collected with a sterile scalpel.

The sterilised PNIPAM+RRR polymer solution was prepared at 10 wt.% in cell growth media (DMEM, containing 4.5 g/l glucose, 100 U/ml penicillin, 100 μg/ml streptomycin and 10% FBS). Identical volume of primary MSC suspension at $1x10^6$ cells/ml concentration was added to the polymer solution. The resulting concentration of hydrogel and cells was 5 wt.% and $5x10^5$/ml, respectively.

For 3D environment generation, a hydrogel droplet approach was used, where the surface tension of the culture surface and the volume of the cell-polymer mixture would define geometry of the droplet. For cell-hydrogel droplet formation, 4.5 µl of polymer-cell mixture was placed into wells of a 96-well flat bottomed tissue culture plate (C3595; Corning), followed by incubation at 37˚C and 5% CO_2 atmosphere for 90 minutes lid-side down. A second incubation step of 30 minutes was performed in lid-side up position. In between incubation steps, 200 µl of sterile water was added to each well at the periphery of the plate to minimise medium evaporation. After incubation, 200 µl of pre-warmed osteogenic, adipogenic or cell growth media were added to corresponding sample wells. Cells growth media consisted of glucose (4.5 g/l) and penicillin/streptomycin (100 U/ml and 100 µg/ml, respectively) supplemented DMEM and 15% FBS. Osteogenic media was prepared on the basis of 15% FBS cell growth media with addition of L-ascorbic acid -2- phosphate (50µg/ml), β-glycerophosphate (5 mM) and dexamethasone (10 nM). Media for adipogenic differentiation was prepared with 15% FBS cell growth media containing dexamethasone (1 µM), 3-Isobutyl-1-methylxanthine (IBMX; 500 µM), insulin (1 µg/ml) and indomethacin (100 µM). All of the differentiation-stimulating factors were purchased from Sigma-Aldrich (UK). MSC-only control samples were seeded into identical wells with 200 µl osteogenic, adipogenic or cell growth media at $2x10^4/cm^2$ seeding density. Media were replaced every 3 days thereafter until the end of the differentiation protocol on day 21.

4.2.3 MG63.EGFP culture and encapsulation in PNIPAM+RRR

Fluorescent MG63.EGFP osteosarcoma cells were generated in-house by stable transfection as previously described (Dyson et al. 2007). Prior to hydrogel encapsulation MG63.EGFP cells were cultured on tissue culture plastic (TCP) in basal media at 37^oC and 5% CO_2.

For hydrogel encapsulation, 40,000 MG63.EGFP cells in 12.5 µl culture media (i.e. $32x10^5$ cells/ml) were mixed with 12.5 µl of media containing 1.33 mg of PNIPAM+RRR (i.e. 10.64 wt.%) and seeded into a well of a 96-well plate, forming a cell-polymer solution with 5.32 wt.% final polymer content. After 1 hour incubation

at 37˚C, 150 µl of pre-warmed culture medium was added on top of a newly formed hydrogel. Cell culture media was refreshed every 2-3 days.

4.2.4 Methylcellulose stock solution preparation

MSC spheroids were generated in methylcellulose-containing medium, 6g of methylcellulose (m-0512, 4000 centipoises; Sigma-Aldrich, UK) were autoclaved in a 250 ml flask. Autoclaved methylcellulose was dissolved in 150 ml of pre-heated (60˚ C) DMEM (free from FBS and antibiotics) by stirring for 20 minutes. Further, 150 ml of supplement-free DMEM media was added and the methylcellulose stock solution was stirred for 3 hours at 4˚C, generating a clear and viscous solution. In order to separate undissolved solid fractions, the collected solution was centrifuged for 2 hours at room temperature at 3600 g. The clear and viscous supernatant was collected and stored at 4˚C.

4.2.5 MSC spheroid formation and encapsulation in PNIPAM+RRR

3.35 ml of cell culture media, containing 0.25 wt.% methylcellulose, was mixed with 1 ml of MSC suspension ($8.7x10^5$ cells/ml). Prior to mixing, the suspended MSCs were stained with CellTracker Red CMTPX (Invitrogen) according to manufacturer's protocol. Spheroids containing 30,000 MSCs were formed by placing 150 µl of the methylcellulose-cell mixture in each well of a U-bottomed 96-well plate (FB56412, Fisherbrand) and incubated for 16 hours at 37˚C with 5% CO_2.

Afterwards, individual spheroids were placed into 75µl of cell culture media with 5 wt.% of PNIPAM+RRR within a well of a flat-bottomed 96-well plate (C3595; Corning). 175 µl of cell culture media was added on top of formed hydrogels after 1 hour incubation at 37˚C.

In polymer-free (control) samples, spheroids were placed into U-bottomed 96-well plate wells with 250 µl of cell culture media. Samples were imaged on day 1, 6 and 8.

4.2.6 Cell viability assessment in PNIPAM+RRR hydrogels by Cell Counting Kit 8 assay

Single MSC suspensions were encapsulated in 4.5 µl of polymer-cell mixture with $5x10^5$ cells/ml (for encapsulation method, see MSC (single cell suspension) encapsulation and PNIAPM+RRR preparation for cell culture section). Cell-free hydrogel control samples were formed in identical manner. Further, 200 µl of basal culture media was added to each well with samples, and the plate was incubated at 37˚C and 5% CO_2 for 16 hours.

On the following day, 200 µl of basal culture media was aspirated and 100 µl of fresh culture media with 10 µl Cell Counting Kit 8 (CCK-8, Dojindo Molecular Technologies) was added for an 8.5 hour incubation at 37˚C and 5% CO_2. An identical volume of sterile water was added to periphery wells in order to reduce media evaporation.

After the incubation period, 100 µl of culture media with CCK8 reagent was transferred into fresh 96-well plate and absorbance measurement was done at 450 nm on a microplate reader.

The same hydrogel samples were re-used for this assay, where absorbance data was collected on day 1, 4 and 8. Following absorbance measurement, the hydrogel samples were washed with PBS (magnesium and calcium-free; Invitrogen) twice and 200 µl of basal culture media were added to each well with the samples and incubated until next assay run.

4.2.7 Cell viability assessment in PNIPAM+RRR hydrogels with the Live/Dead assay

Live/Dead assay (Invitrogen) was optimised for 3D settings of the experiment. 2 µM of calcein AM and 20 µM of EthD-1 were prepared in pre-warmed basal culture media, vortexed and added to wells. Prior to the assay, hydrogel-containing wells were washed with pre-warmed PBS. 200µl of the assay solution was added on top of hydrogel-cell constructs in 96-well plates, wrapped loosely in foil and followed by incubation at 37°C and 5% CO2 for up to 10 hours.

4.2.8 Staining of the cells with CellTracker Red

To permit identification and tracking of MSCs in the hydrogel, the cells were fluorescently labelled before encapsulation. $5x10^5$ MSCs/ml were stained with 5µM solution of CellTracker Red CMTPX (Invitrogen), according to the manufacture's protocol.

4.2.9 Encapsulated cell volume and motility analysis

PNIPAM+RRR samples with encapsulated MSCs, and prestained with CellTracker Red as described above, were incubated for 12 days, where media was refreshed every 3 days. The top edge section of the sample well was imaged (z-axis sections of the visible cells) every 4 days on Zeiss LSM 780 multiphoton microscope, where the edge of the well was used as a reference point. Volocity 6.1.1 software (PerkinElmer) was used to create 2 regions of interest, which included 17 non-touching cells. These regions of interest were replicated in every image dataset to measure motility, proliferation and volume of the selected cells.

4.2.10 Release of encapsulated MSCs by cooling

After a period of culturing, MSC-loaded hydrogels in the 96-well plates, covered with 200 µl of culture media, were placed on ice bed and agitated for 16 hours. Undissolved hydrogel fractions were further broken down by pipetting. Collected solution was centrifuged at 315g for 5 minutes, where formed supernatant was replaced by the fresh culture media. The pellet was dispersed in the freshly added media and seeded into 24 well-plate well (SVC7300, Corning). After 3 days of culture at 37˚C cells were assessed.

4.2.11 MSC differentiation staining: donor samples

All differentiation assays were performed on MSCs harvested from the tissues of three donors. Donor tissue details are collated in the Table 11.

Table 11: Details of the tissue samples used for MSC harvesting.

Sample reference	Age on extraction	Gender	BMI	A smoker?	Site of extraction	Tissue condition
FH496	78	Female	21.6	No	Left hip	OA
K89	68	Male	37	No	Left and right knee	Arthritis
K118	62	Male	34	No	Left knee	OA

4.2.12 Osteogenesis and mineralisation: ALP staining

For alkaline phosphate (ALP) activity staining, 1 mg/ml Fast Red TR (Santa Cruz Biotechnology) was pre-weighted and, immediately prior to use, was added to 0.2 mg/ml napthol AS-MX (Sigma) dissolved in 1% N,N-dimethylformamide, followed by addition of 10 ml 0.1 M Tris buffer (pH 9.2). Prior to application, all liquid reagents were pre-warmed to 37˚C.

Before applying the ALP stain, 96 well plates with cell-loaded PNIPAM+RRR hydrogels were rested on a heating platform at 37˚C and hydrogel constructs were washed with PBS twice. The Fast Red stain was filtered through a sterile 0.22 µm filter (Millex 0.22µm, Millipore) and applied onto 3D constructs and cell monolayers for 5 minutes. Afterwards, the stained samples were washed with PBS twice, followed by fixation in 4% paraformaldehyde (PFA, Sigma-Aldrich) for 20 minutes and two PBS washes. Sample wells were filled with PBS and the plates were covered with aluminium foil.

4.2.13 Osteogenesis and mineralisation: von Kossa staining

Samples were washed with deionised water, followed by addition of 1% silver nitrate solution in deionised water for 60 minutes, whilst keeping samples on a light box. Samples were washed three times with deionised water, followed by 5 minute incubation with 2.5% sodium thiosulphate (pH 9.2) at room temperature and double deionised water wash.

4.2.14 Adipogenesis: lipid staining

Cells in monolayers and encapsulated in PNIPAM+RRR hydrogels were treated with basal or adipogenic media for 21 days, with media being replaced every 3 days. On

time-points of day 7, 14, and 21, BODIPY® 493/503 (Molecular Probes®), a stain for natural lipids, was added to wells with media to produce a 0.5 μM final concentration of the stain. After incubation for 30 minutes at 37˚C, media was removed followed by rinsing with PBS. Rinsed samples were fixed with pre warmed 4% PFA for 10 minutes, followed by a triple wash with PBS. All samples were covered with PBS to prevent dehydration of the hydrogels. The sample plate and all reagents used were kept at 37˚C throughout the experiment.

4.2.15 Sectioning

Hydrogel droplet samples, which were used in osteogenesis experiments, but not treated with osteogenesis and mineralisation stains, were sectioned to cross-validate mineral deposition. These samples were fixed with pre warmed 4% PFA in 96-well plate for 10 minutes at 37˚C, followed by triple PBS washes. Further, sample wells were filled with optimal cutting temperature compound (OCT, Tissue-Tek®), followed by snap-freezing in liquid nitrogen. Frozen plates were mechanically broken in order to retrieve the samples. Collected samples were stored at -80˚C overnight prior sectioning. Mounted samples were sectioned at 7 μm thickness and were collected on Superfrost slides (Merck).

4.2.16 Polarised light analysis

Sectioned samples were analysed on Zeiss LSM 510 Meta microscope with polarising filter insert.

4.3 Results

4.3.1 Cell encapsulation in PNIPAM+RRR hydrogels

MG63.EGFP osteosarcoma cells were successfully encapsulated in PNIPAM+RRR and incubated for 8 days (Figure 21). On day 1, cells encapsulated in 3D had a distinct rounded morphology (Figure 21C and D), where MG63.EGFP cells cultured in monolayers on TCP had a typical fibroblast-like appearance (Figure 21 A and B). In addition, encapsulated cells on day 1 were clustered in groups of 2-5 cells (Figure 21C), but by day 4 such associations were no longer observed (Figure 21E). Throughout the culture period of 8 days, the overall majority of encapsulated cells retained a spherical morphology, although some cells started to adopt a fibroblast-like morphology (Figure 21G).

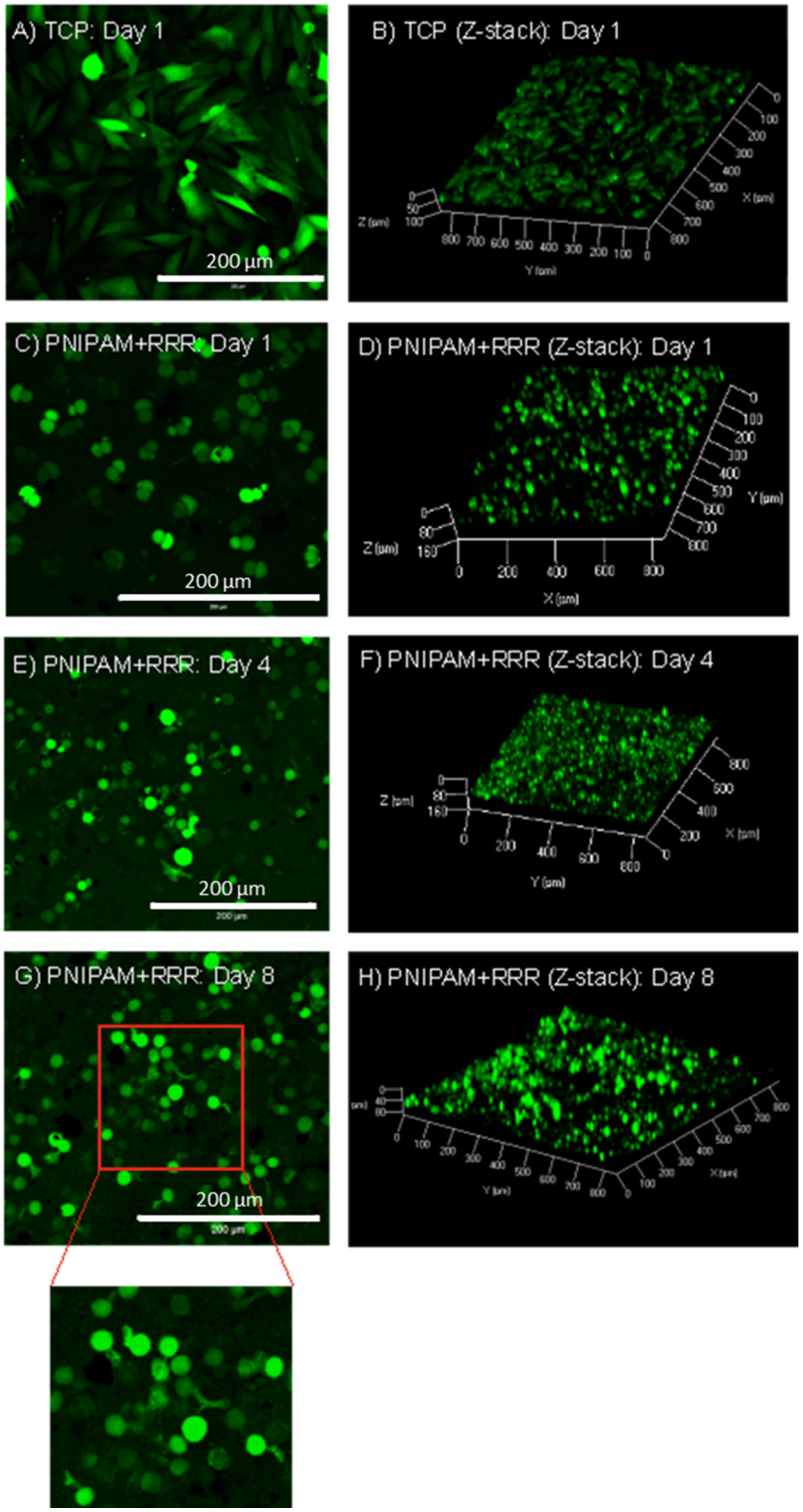

Figure 21: MG63.EGFP osteosarcoma cells, encapsulated in 5wt% PNIPAM+RRR for up to 8 days. Cells, cultured on the well surface, demonstrated typical fibroblastic morphology (A, B). On day 1, hydrogel-encapsulated cells were fully rounded and aggregated into groups of 2-5 cells (C, D). Starting from day 4, cell grouping is minimal (E, F) and small proportion of cells starts to adopt fibroblast-like morphology by day 8 (G crop-in). n=2.

4.3.2 Eencapsulation of MSC spheroids in HB PNIPAM+RRR hydrogel

Encapsulation of MG63.EGFP cells was done to confirm capacity of the PNIPAM+RRR to form a stable 3D hydrogel structure, and verify capability of the confocal microscope to collect fluorescent signal despite opaque appearance of the hydrogel.

The PNIPAM+RRR's ability to generate a hydrogel scaffold was further tested with MSC spheroids in 96-well flat bottom tissue culture plates. Control (hydrogel-free samples) spheroids were cultured in the 96-well U-bottom plates. With progress in culture time, hydrogel-encapsulated spheroids have gradually travelled through the hydrogel structure and made contact with the TCP surface, as confirmed by the fibroblastic morphology of the MSCs on the spheroid periphery (Figure 22: A3 and A4). Concurrently, control spheroids maintained original rounded appearance and demonstrated diameter reduction (Figure 22: B1 and B3).

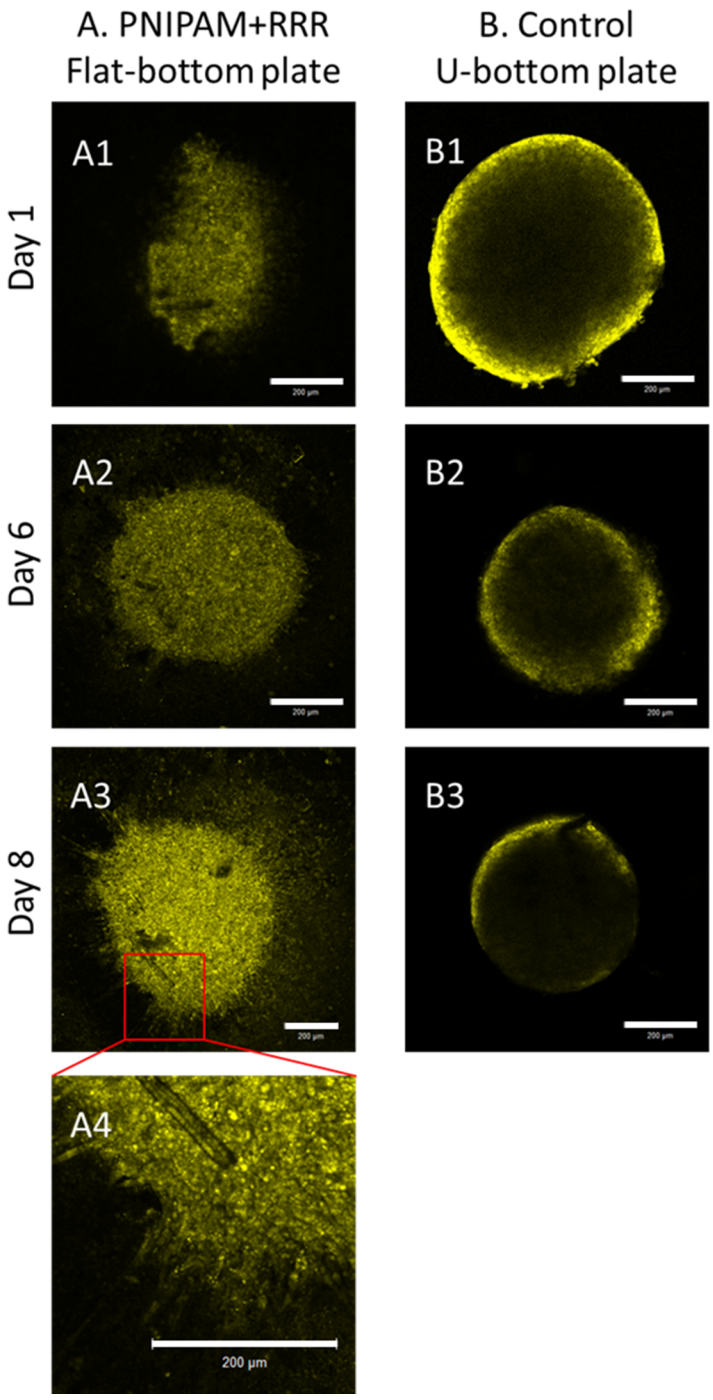

Figure 22: MSC spheroid (30,000 cells) encapsulation in 5wt% PNIPAM+RRR in flat bottom plate (A).Control spheroids (30,000 cells) were cultured in basal media within U-bottom plates (B). Both encapsulated and control samples were cultured for 8 days at 37˚C and 5% CO_2. All cells are pre-stained with CellTracker Red. Colour of the emission channel is changed to yellow for improved contrast. After 1 day of culture, hydrogel-encapsulated spheroid (A1) has a less rounded morphology compared to control spheroids (B1). By day 6, morphological discrepancy is eliminated (A2 and B2). On day 8 encapsulated spheroid is seen to be in contact with the surface of the well, where the cells of the leading edge are adopting fibroblastic morphology (A3 and A4). All scale bars are 200 µm. n=3.

4.3.3 Spheroid encapsulation in U bottom well-plates

Due to the adhesive properties of the tissue culture plastic, the encapsulated spheroids adhered to the surface of the well, with cells adopting a fibroblastic morphology (Figure 22A3 and A4). Therefore, experiments were repeated with using u-bottom plate for both encapsulated and control samples.

Use of non-adherent U-bottom plates has prevented cell adhesion to the plastic surface in hydrogel-encapsulated spheroids (Figure 23A). Therefore, applicability of HB PNIPAM+RRR for MSC spheroid encapsulation was confirmed.

Additionally, control spheroid culture in non-adherent U-bottom well plates results in active spheroid compaction (Saleh et al. 2011). This process affects microscope's laser penetration and results in uneven signal strength across the section of the spheroid. As a result, cells on the spheroid periphery appear to be brighter, than in the centre of the spheroid (Figure 23B). In contrast to control spheroids, hydrogel encapsulated spheroids demonstrated a uniform emission signal across the section of the spheroids during all 16 days of culture (Figure 23A). This observation suggests that the 3D environment of the hydrogel prevents spheroid compaction.

Closer examination of the hydrogel-encapsulated spheroids revealed presence of "voids" in the spheroid's structure, highlighted by the white arrows (Figure 23A). Probability of these "voids" being penetrating hydrogel was tested with "excitation finger printing" approach (data not shown), where a wavelength bandwidth of 200 nm (100 nm below and 100 nm above the original excitation wavelength) was analysed for presence of the autofluorescent signal from the hydrogel. The hydrogel penetration was not confirmed, as HB PNIPAM+RRR was not found to be autofluorescent.

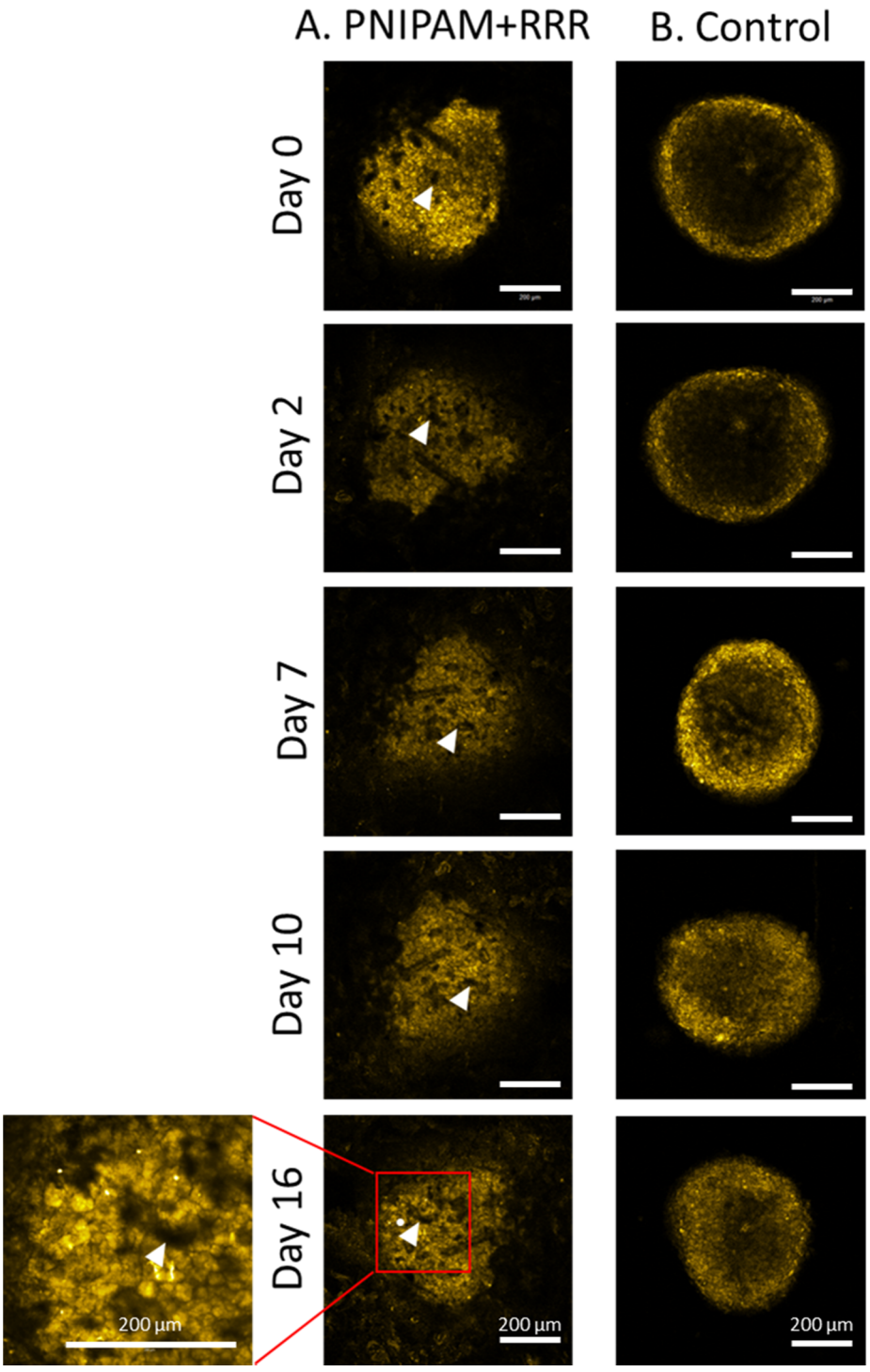

Figure 23: MSC spheroids (30,000 cells) encapsulated within the PNIPAM+RRR hydrogel in a non-adherent U-bottom plate for 16 days (A); identical spheroids cultured in a U-bottom plate without PNIPAM+RRR addition (B). All cells are pre-stained with CellTracker Red. To increase the contrast, colour of the emission channel was set to yellow. After 16 days in culture, encapsulated spheroids did not demonstrate a substantial change in morphology, nor any evidence of fibroblast-like cells on the leading edge of the spheroid. White arrows are pointing at the development of a potential hydrogel-filled void. Excitation fingerprinting analysis did not confirm presence of the polymer of the basis of autofluorescence. All scale bars are 200 µm. n=3.

4.3.4 MSC single cell encapsulation in PNIPAM-RRR hydrogel

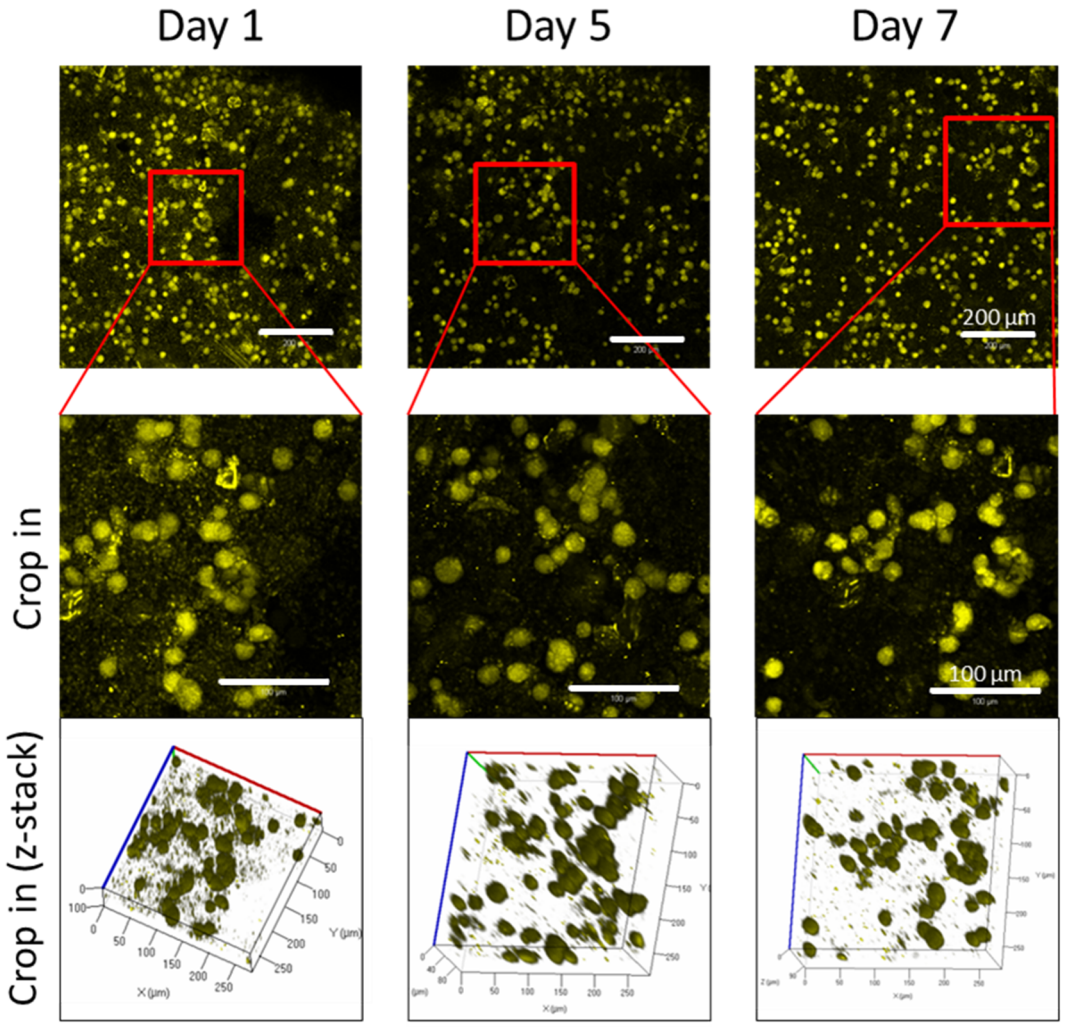

Figure 24: MSCs encapsulated in 5wt% PNIPAM+RRR discs in the cell-adherent flat-bottomed 96 well plate and cultured for 7 days. Cells were pre-stained with CellTracker Red, where emission channel was recoloured to yellow for better contrast. Throughout the culture period, encapsulated cells retained rounded morphology with no signs of adherence to the TCP. At all analysis time-points MSCs were distributed in one plane of the imaged section (see the z-stack of the crop-in section). n=2.

Single MSC suspensions were encapsulated in PNIPAM+RRR and cultured for 7 days, where no cells were observed to adhere to the well plate bottom (Figure 24). Analysis of the z-stack images identified that all CellTracker-stained cells had a rounded morphology and predominantly distributed in one plane of the imaged section (Figure 24 (z-stack)).

4.3.5 Motility of encapsulated primary MSCs

Encapsulated cells were cultured for 12 days, where relative distances between cells in the region of interest were measured on day 1, 4, 8 and 12. The same region was analysed at every time point. After 12 days of culture, encapsulated cells demonstrate no significant motility, retaining rounded morphology and stationary positioning (Figure 25; A).

4.3.6 MSC volume analysis after encapsulation in PNIPAM+RRR hydrogel.

Cells in the region of interest, analysed for change in volume over 12 days, demonstrated multiple responses to hydrogel's 3D environment. Volumes of analysed cells formed three distinct groups, when plotted (Figure 25B). First group (❶), representing cells with initial averaged cell volume of 1075.4 μm^3, presented an increase in cell volume by 65.38% on day 12. Whereas, groups two (❷) and three (❸), having an averaged starting volume of 5790.5 μm^3 and 8275.5 μm^3 respectively, showed a decrease in cell volume with time in culture. Cellular volume in the second group dropped by 23.44%, where in the third group cell shrinkage resulted in 11.06% volume reduction. In all three groups most substantial change in volume was observed on day 4, with following time points showing a steady change in volume.

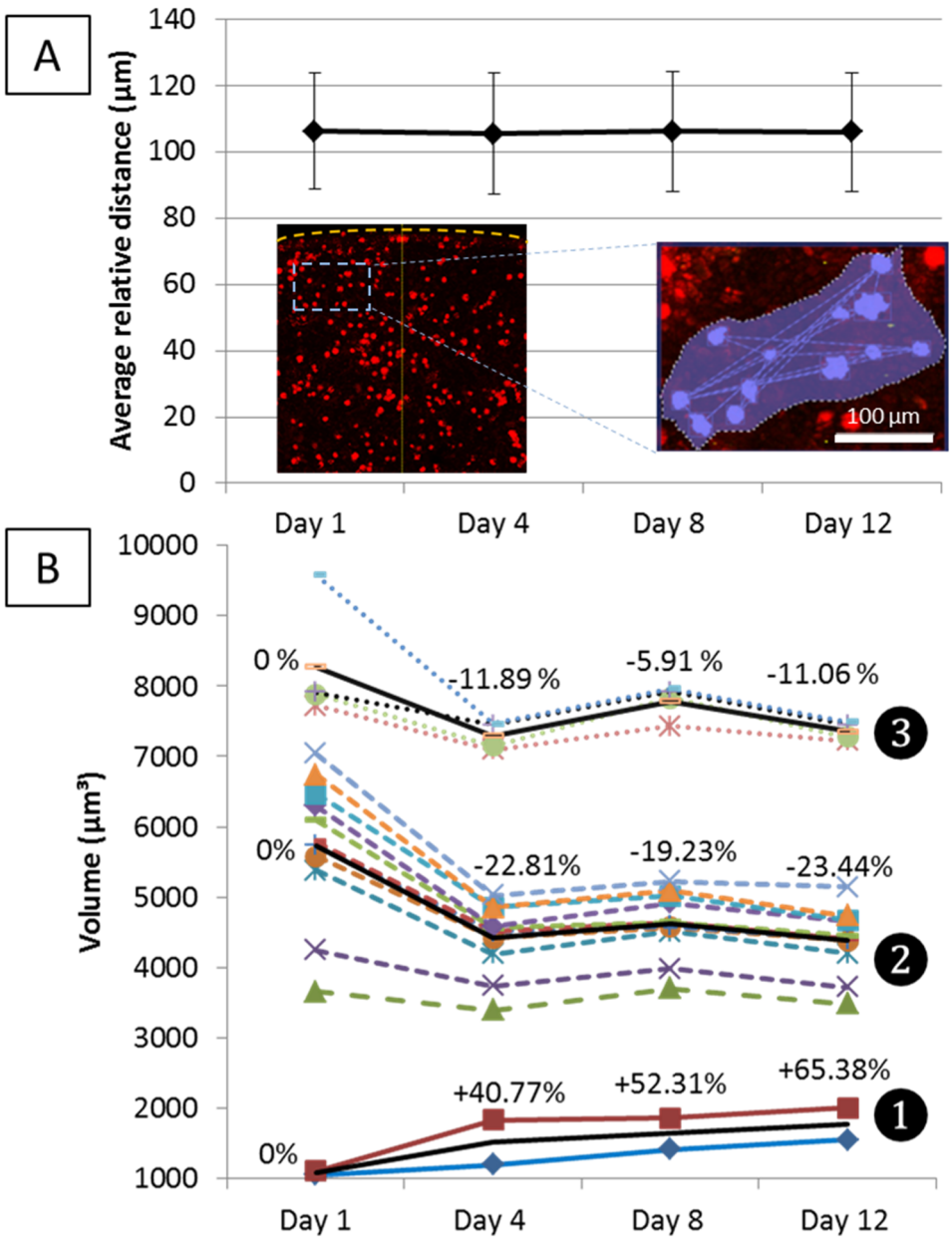

Figure 25: Motility and cell volume tracking of MSCs, encapsulated in PNIPAM+RRR. Identical section of the well, with PNIPAM+RRR-encapsulated and CellTracker Red pre-stained MSCs, was imaged every 4 days (up to day 12) via a z-stack method, to obtain a cell representation in 3D environment. On the basis of the z-stacks, 3D model of every selected cell was virtually rendered with the Volocity software (A, crop-in example), allowing to measure relative distance between the cells (an indication of the cell motility)(A) and volume changes in every individual cell (B). Plotting of the relative distances (A) demonstrated no active motility in encapsulated cells over 12 days. Where the volume-change tracking (B) has identified 3 distinct groups of cells across a broad range of initial cell volumes. Cell groups with the highest starting cell volume (B; groups 2 and 3) are experiencing a cell volume loss, especially between day 1 and 4. The cells with the lowest initial cell volume (B; group 1) are expanding throughout the period of the experiment. n=2.

4.3.7 Cell release from PNIPAM+RRR hydrogels

The theoretical and empirically observed temperature-reversible nature of the HB PNIPAM+RRR during polymer characterisation (Section 3.4.2) was further tested by conducting cell release experiments.

The ability of the HB PNIPAM+RRR hydrogel to release the encapsulated MSCs after period of culture by lowering the temperature below LCST point was tested (Figure 26). Cell release experiment was performed on ethanol-treated and non-treated polymer samples (ethanol treatment method is described in section 4.2.2). After 16 hours of sample plate agitation on ice, both of the HB PNIPAM+RRR sample types were partially dissolved, and the residual hydrogel was mechanically broken down by vigorous pipetting. Cells were precipitated by centrifugation, resuspended in fresh basal media and transferred into a 24 well plate for 3 days of culture. After examination with brightfield microscope of both sample types, ethanol-pretreated and non-treated, the overall majority of the cells were found to be rounded and non-adherent (Figure 26).

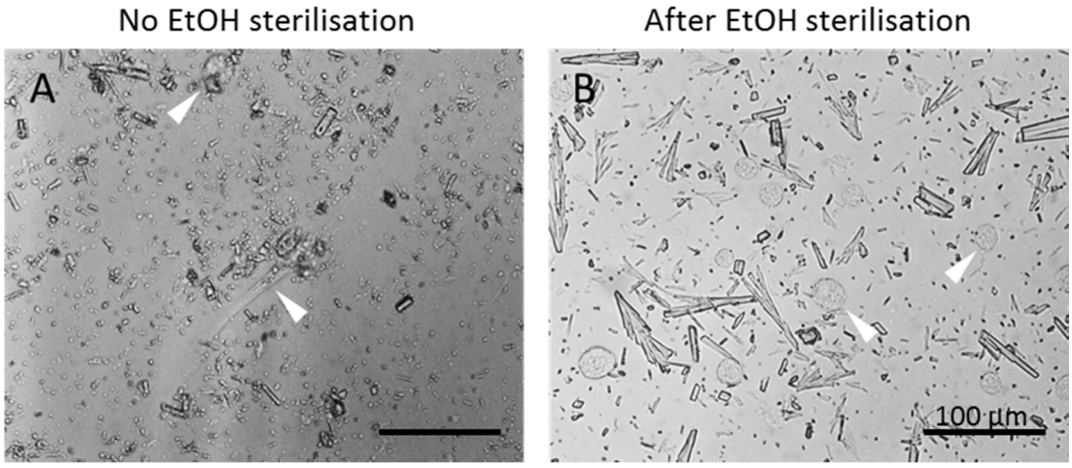

Figure 26: MSC release from PNIPAM+RRR, before and after EtOH sterilization . (A) Encapsulated MSCs ($5x10^5$ cells/ml) were incubated at 37˚C with 5% CO_2 for 16 days in a 96-well plate, followed by 16 hour agitation on ice bed. Undissolved hydrogel fractions were further broken down by pipetting. Collected solution was centrifuged at 315g for 5 minutes, where formed supernatant was replaced by the fresh culture media. The pellet was dispersed in the freshly added media and seeded into 24 well-plate well. After 3 days of culture at 37˚C, cells were assessed. Almost all of the cells were rounded and detached. Very rarely, a fibroblast-like adhered cells were also observed (see white arrows (A)). (B) Prior cell encapsulation, PNIPAM+RRR polymer was dissolved in ethanol (EtOH), spun down at 315g for 5 minutes. Supernatant was collected and transferred into sterilised glass Petri dish. The petri dish was left on coverslip drying plate at 37˚C for 24 hours within a class 2 flow hood. Dried polymer was collected aseptically and used for MSC encapsulation. Encapsulated MSCs ($5x10^5$ cells/ml) were incubated for 6 days. The cell retrieval and following culturing process was identical to the one described above (see (A)). After incubation, cells were rounded and surface-detached (see white arrows (B)). Both scale bars are 100 µm. n=3.

Synthesis process of HB PNIPAM+RRR has produced a soluble polymer by bulk. However, after analysis of the hydrogel under confocal microscope it was noted that a fraction of solid particles and debris is present. Presence of the debris became particularly evident during MSC volume analysis within HB PNIPAM+RRR (Figure 25), as the Volocity software algorithm was recognising more objects for analysis in the region of interest, than the number of cells in the same region of interest. To reduce the number of non-soluble debris, ethanol treatment of HB PNIPAM+RRR was performed. Dissolution of HB PNIPAM+RRR in ethanol and following centrifugation resulted in substantial decrease in amount of debris present with consequent reduction of instances of auto-fluorescence of the gel. In addition, after

solute fractionation, polymer recovery from ethanol was performed in sterile environment what reduces the risk of the cell infection.

4.3.8 MSC viability within PNIPAM+RRR

It was of a paramount importance to determine MSC viability within the PNIPAM+RRR, in order to allow further assessment of cell responses within the hydrogel. MSC viability within same PNIPAM+RRR hydrogels was assessed with Cell Counting Kit 8 (CCK8) assay on days 1, 4 and 8 after encapsulation (Figure 27). Cell-free control hydrogels were treated in identical manner to test the specificity of the assay in this 3D culture system. On day 1, samples with encapsulated MSCs demonstrated substantial difference compared to cell-free samples. However by day 8 change in the absorbance reading from the cell-containing samples, was not substantial when compared to day 1. In addition, on day 8 there was also no substantial difference in absorbance readings between both sample types. Taken together, it can be concluded that the CCK8 assay does not provide definite MSC behaviour within HB PNIPAM+RRR environment.

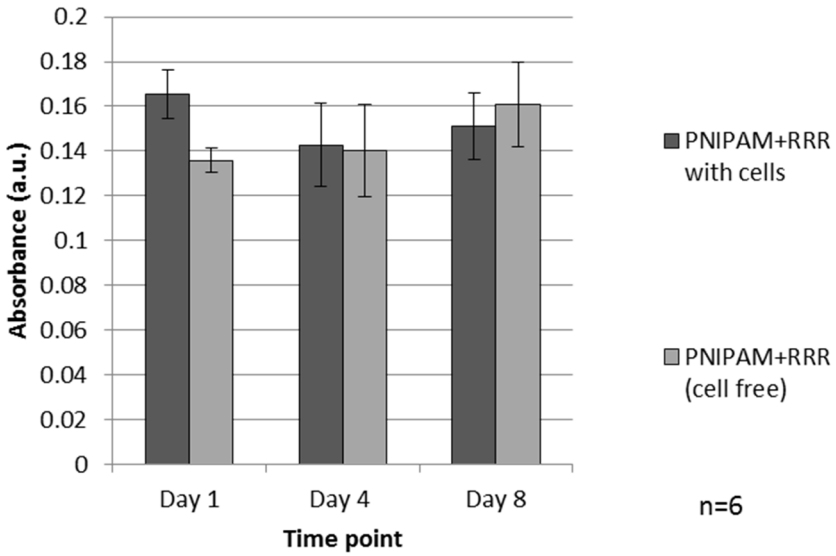

Figure 27: Viability assessment of MSCs in PNIPAM+RRR with the CCK8 assay. K41 MSCs ($0.5x10^6$/ml) were encapsulated in PNIPAM+RRR and treated with CCK8 assay on day 1, allowing to reuse the original samples on day 4 and 8. Cell-free hydrogel samples were treated alongside. After 8 days in culture, cell-loaded hydrogels did not demonstrate enzymatic activity level, substantially differing from the cell-free hydrogels.

In order to obtain reliable viability data, the Live/Dead® staining assay (LifeTechnologies) was used. After optimisation of concentrations and incubation time, samples were imaged with a confocal microscope.

This experiment was designed to assess viability of encapsulated MSCs in ethanol treated and non-treated HB PNIPAM+RRR hydrogel. Application of the Live/Dead® staining assay onto MSCs in monolayer culture demonstrated high assay specificity, where enzymatically active cells showed strong calcein AM signal, together with nucleus-specific EthD-1 staining in the cells with raptured cell membranes (Figure 28A). Concentrations and staining time, used for monolayer control staining, was identical to hydrogel samples.

To validate Live/Dead® dye specificity in hydrogel samples, methanol (MeOH) pre-treated MSCs (i.e. "dead" controls - MSCs with methanol-disrupted cell membranes; Figure 28 B4-6 and Figure 28 C4-6) were encapsulated into hydrogels, identical to ones, used for methanol non-treated MSC (i.e. "live" samples Figure 28 B1-3 and Figure 28 C1-3) encapsulation: ethanol (EtOH)-treated (Figure 28B) and non-treated HB PNIPAM+RRR (Figure 28C).

The EtOH-treated hydrogels with "live" MSCs demonstrated strong calcein AM signal and a minuscule number of EthD-1-stained nuclei (Figure 28 B1-3, see white pointers), suggesting overall active enzymatic activity of MSCs and cell membrane rapture in very few cells through the culture period of 10 days.

Examination of the calcein AM staining in the "dead" controls within EtOH-treated hydrogels showed expected very weak signal on day 1 and 4, and absence of signal on day 10 (Figure 28 B4-6). Whereas with EthD-1 stain no prominent signal was observed, along with low specificity (i.e. cell area highlighted by the EthD-1 dyes was identical to the area of the cell, highlighted by the calcein AM)(Figure 28 B4-6; see white pointers). This observation conflicts with expectation of a strong signal from EthD-1, as all of the cells in this sample had methanol-raptured cell membranes. Therefore, this observation suggests that the EthD-1 dye is unsuitable for identification of the cells with raptured membranes. On the basis of the same

observation it can be concluded that the calcein AM stain, an indicator of enzymatic activity, is a specific marker of encapsulated MSCs viability.

Similarly to “live” MSCs in EtOH-treated hydrogels, non-treated hydrogels demonstrated a strong calcein AM stain within “live” MSCs on day 1 and 4 (Figure 28 C1-2). However, by day 10 very few cells were calcein AM-positive (Figure 28 C3). This observation suggests that the EtOH-treated hydrogels are more suitable for long-term culture of MSCs. Additionally, unsuitability of EthD-1 for damaged cell identification was confirmed again by absence of strong nuclear-specific signal in “dead” control cells within non-treated hydrogel (Figure 28 C4-6).

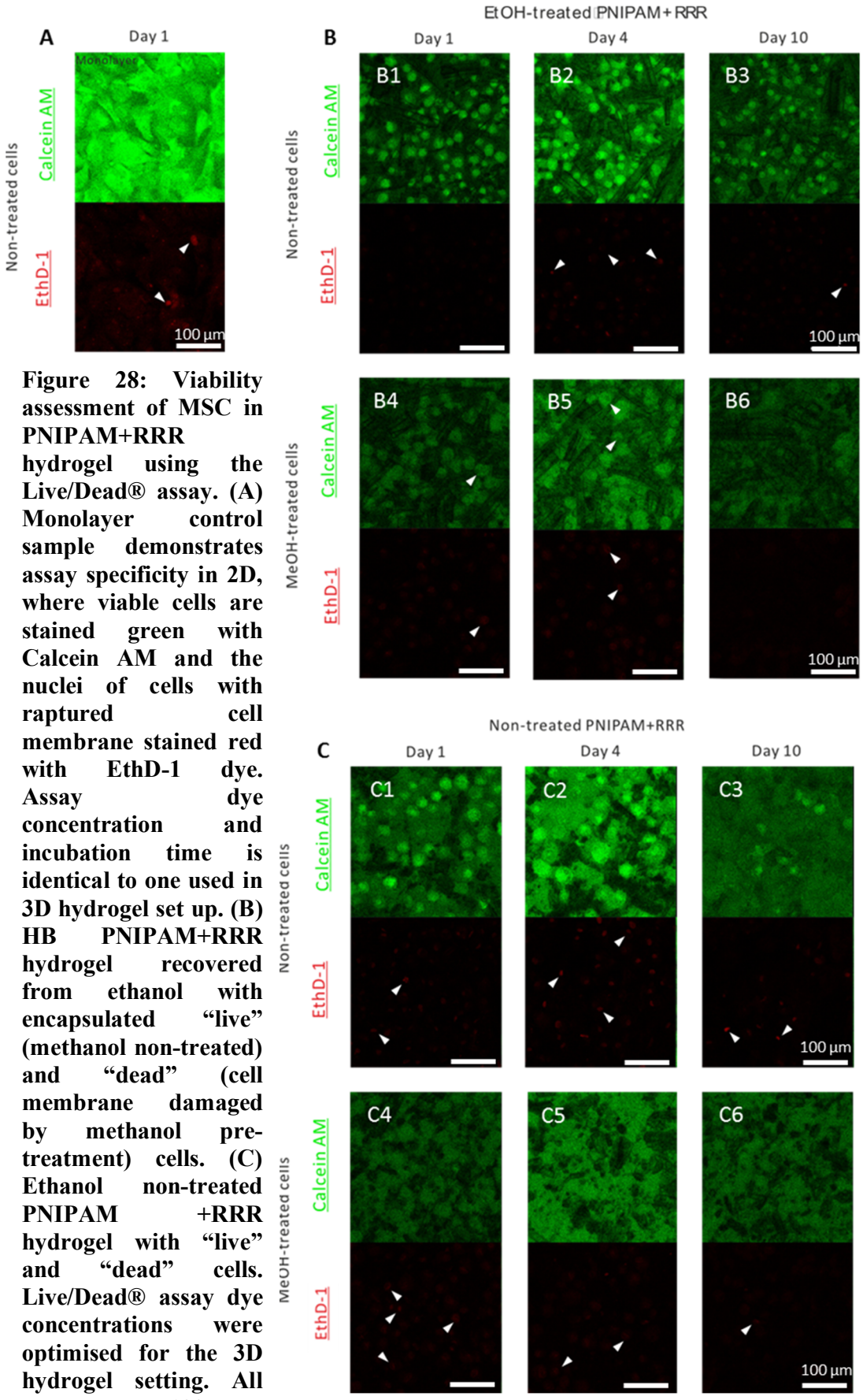

Figure 28: Viability assessment of MSC in PNIPAM+RRR hydrogel using the Live/Dead® assay. (A) Monolayer control sample demonstrates assay specificity in 2D, where viable cells are stained green with Calcein AM and the nuclei of cells with raptured cell membrane stained red with EthD-1 dye. Assay dye concentration and incubation time is identical to one used in 3D hydrogel set up. (B) HB PNIPAM+RRR hydrogel recovered from ethanol with encapsulated "live" (methanol non-treated) and "dead" (cell membrane damaged by methanol pre-treatment) cells. (C) Ethanol non-treated PNIPAM +RRR hydrogel with "live" and "dead" cells. Live/Dead® assay dye concentrations were optimised for the 3D hydrogel setting. All scale bars are 100 µm. n=2

4.3.9 Progression of MSC differentiation in 3D hydrogel

Osteogenic potential in all three donors was assessed by the alkaline phosphatase (ALP) activity assay and the von Kossa staining. Birefringence studies were performed on FH496 and K118 MSCs to validate specificity of the von Kossa stain within the HB PNIPAM+RRR hydrogel environment. In addition, adipogenic potential of K89 and K118 donor cells was also assessed, where lipid deposition was tracked with BODIPY® 493/503 stain.

ALP is a commonly-used marker of osteogenesis, and its' role in osteogenesis was originally confirmed by a study of a genetic disease, which leads to under mineralisation of the bone tissue, known as hypophosphatasia (Whyte 1994). Along with enzymatic activity of ALP, osteogenesis can be also identified by cellular mineral deposition. The von Kossa stain was used to assess level of mineralisation within hydrogel and monolayer cultures. To cross-confirm specificity of the von Kossa stain and indicate calcium deposition, polarised light microscopy, which provides measure of birefringence of the material, was employed. Moreover, progression of adipogenesis in differentiating MSCs is defined by expanding lipid droplet formation within the cells. The main component of the BODIPY® 493/503 stain is a lipid-specific fluorescent compound, which allows visualisation of the lipid-depositing cells in monolayer and 3D settings.

4.3.10 Osteogenesis: ALP enzymatic activity

Osteogenic differentiation capacity of all three donors was assessed within cell-loaded hydrogel and monolayer cultures with the ALP assay on day 7, 14 and 21, after treatment with osteogenic or basal media.

ALP enzymatic activity of the FH496 donor cells was observed in monolayer cultures, where samples treated with osteogenic media demonstrated much higher ALP activity, when compared to control samples, treated with basal media (Figure 29). Whereas, hydrogel-encapsulated MSCs demonstrated high levels of ALP activity throughout the whole culture period and within both treatment conditions: osteogenic and basal (see white arrows).

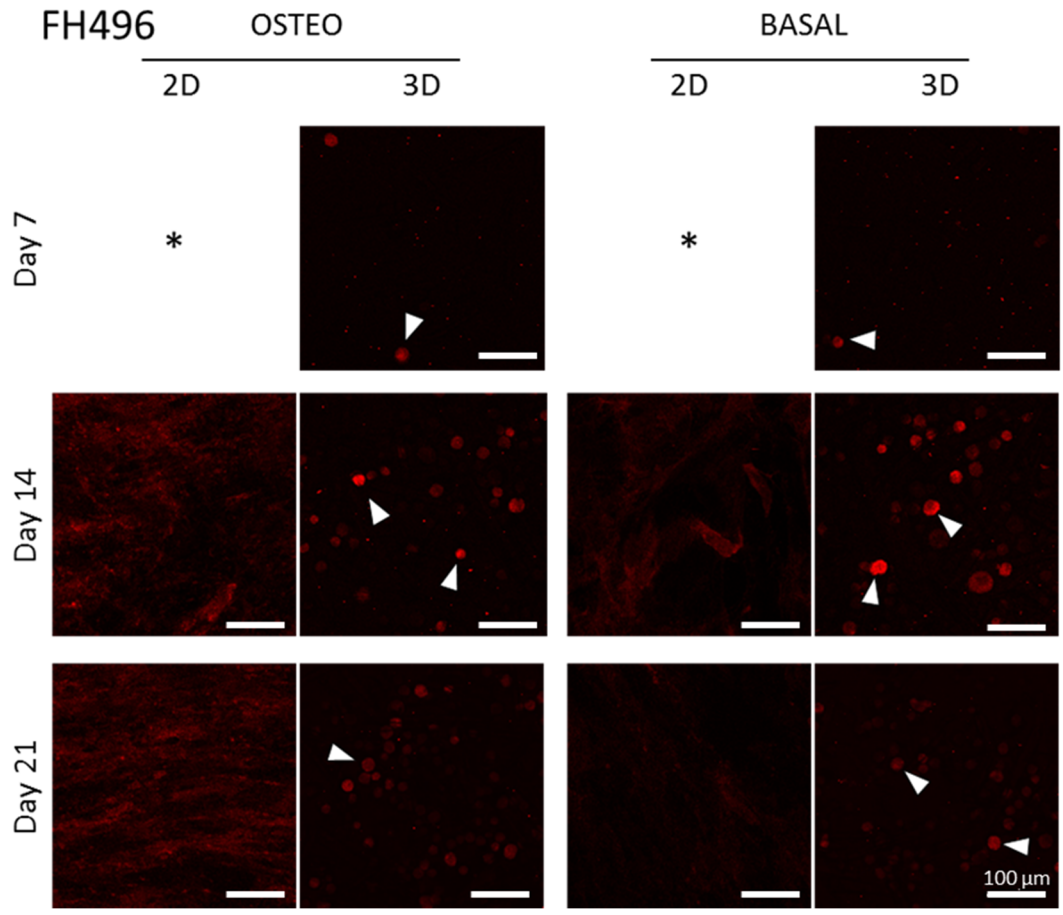

Figure 29: Analysis of ALP activity in primary FH496 MSC monolayers and cell-loaded hydrogel droplets. Samples were exposed to osteogenic differentiation cocktail and control media for up to 21 days. Monolayer cultures in osteogenic conditions demonstrated consistently strong ALP activity on day 14 and 21. Basal monolayers have shown lower ALP activity on the same days. Cell-loaded hydrogels, in osteogenic and basal media, demonstrated strong ALP signals throughout differentiation experiment, with peak activity on day 14 (see white arrows). 2D samples on day 7 have peeled off during pre-imaging washes (*). All scale bars are 100 µm. n=2.

ALP signal wtihin the K89 donor sample followed a pattern, similar to FH496 sample. Monolayer MSCs exhibited ALP acitivty, where the strongest signal was observed on day 15 in samples treated with osteogenic media (Figure 30). Hydrogel-encapuslated MSCs did not show any ALP signal on day 7 in either of the differentiation conditions. However, ALP-positive cells were observed in osteogenic and basal conditions on day 15, as well as day 21 (Figure 30, white arrows).

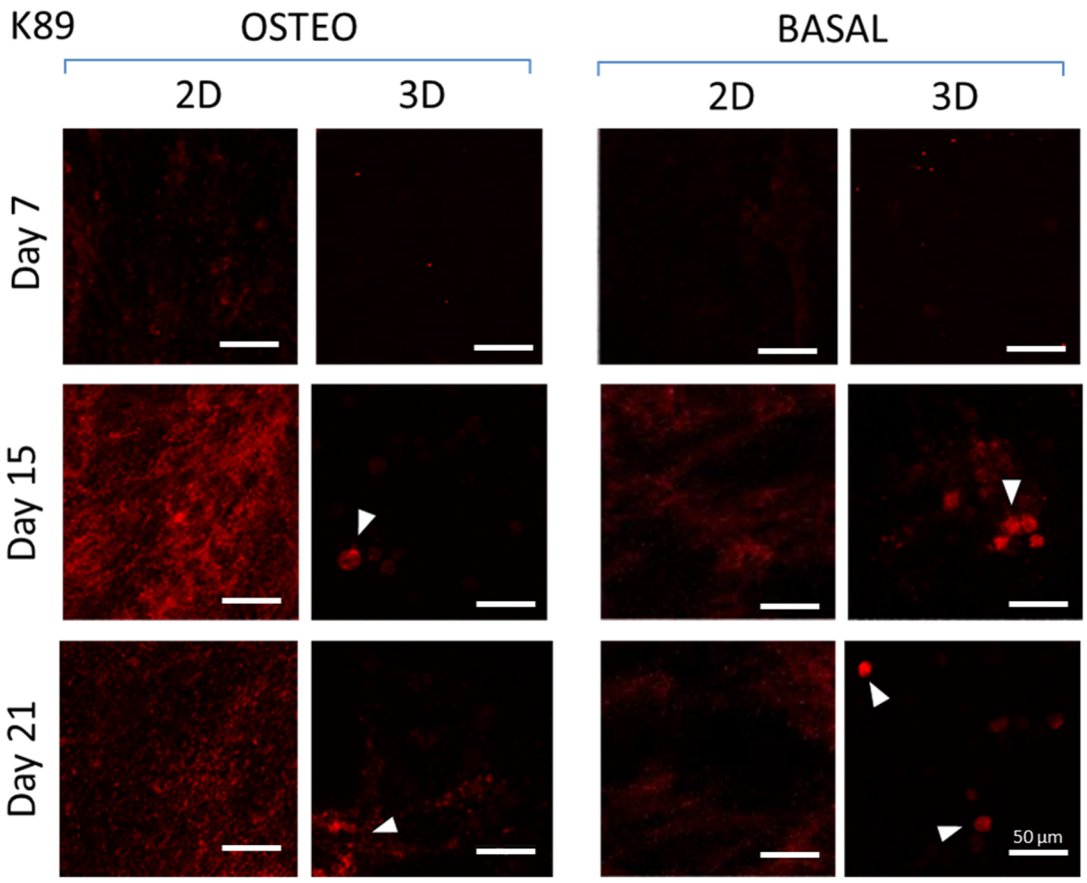

Figure 30: ALP activity in K89 monolayers and cell loaded PNIPAM+RRR hydrogel droplets. Hydrogel-encapsulated cells demonstrate no ALP signal on day 7, and a consistently strong ALP activity on day 15 and 21 in both treatment conditions, osteogenic and basal (white arrows). The ALP activity of varying intensity was also observed in monolayer cultures. In osteogenic condition, strongest ALP signal was seen on day 15. Cells, treated with basal media, have demonstrated very weak ALP signal, peaking at day 15. All scale bars are 50 µm. n=2.

Osteogenic differentiation capacity of MSCs from the K118 sample was analysed in an identical manner to FH496 and K89 samples. ALP-positive cells were only found in monolayer samples, treated with osteogenic media, where ALP activity was most

evident on day 14 and 21 (Figure 31). Neither of the 3D samples, treated with the osteogenic or basal media, had ALP-positive cells.

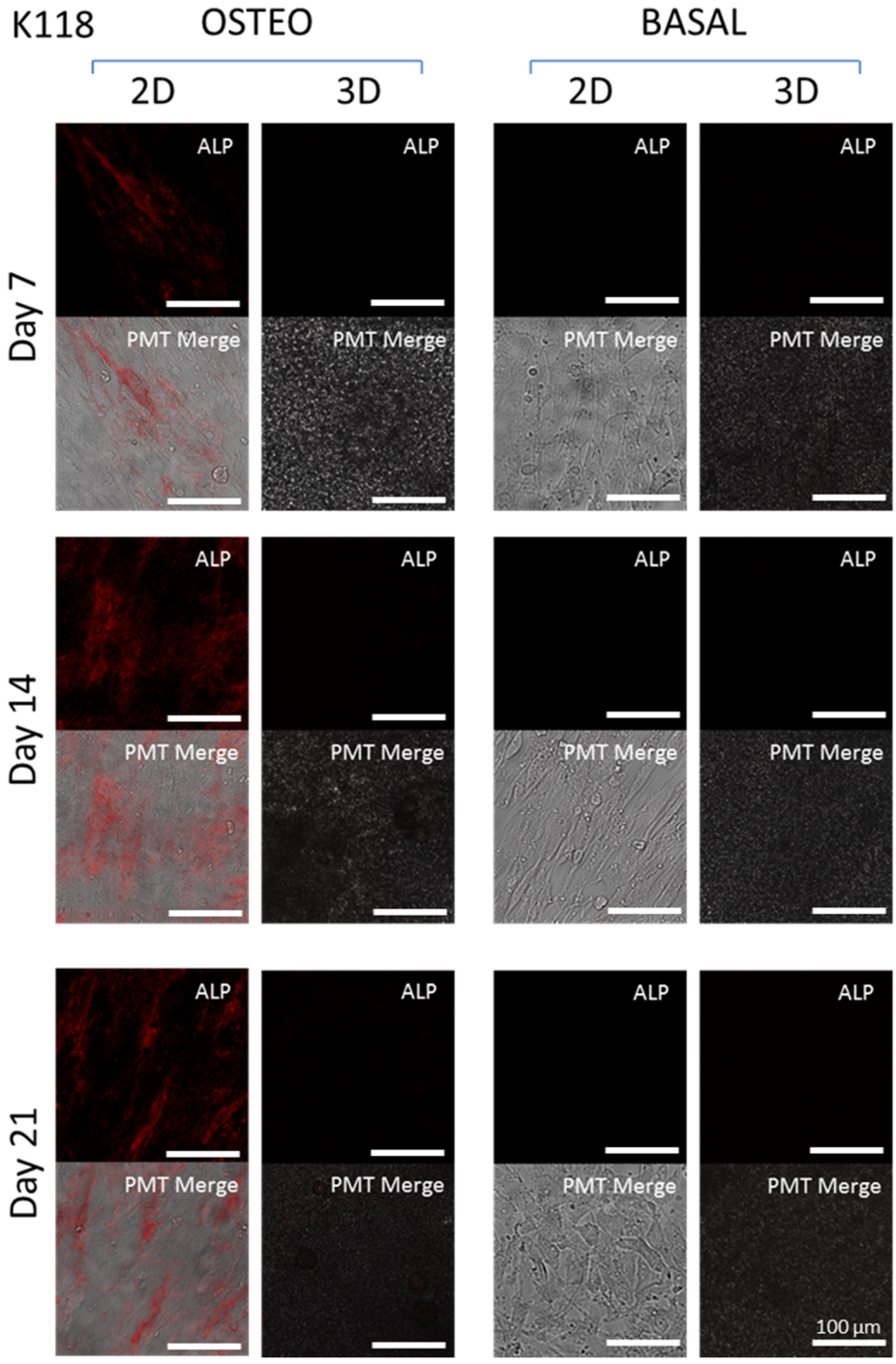

Figure 31: ALP activity within K118 donor cells was only found in osteogenic conditions of monolayer cultures, where most prominent signal was observed on days 14 and 21. The ALP signal channel was merged with photomultiplier tube (PMT) channel to show morphology of the ALP-positive cells and presence of the cells within the hydrogels. All scale bars are 100 µm. n=2.

4.3.11 Osteogenesis: von Kossa mineralisation staining

Mineralisation activity within monolayer and cell-loaded hydrogel samples was tracked with the von Kossa and ALP stains after 7, 14 and 21 days of culture with osteogenic and basal media. Samples, which are von Kossa and ALP positive are represented by brown and pink-red stains, respectively.

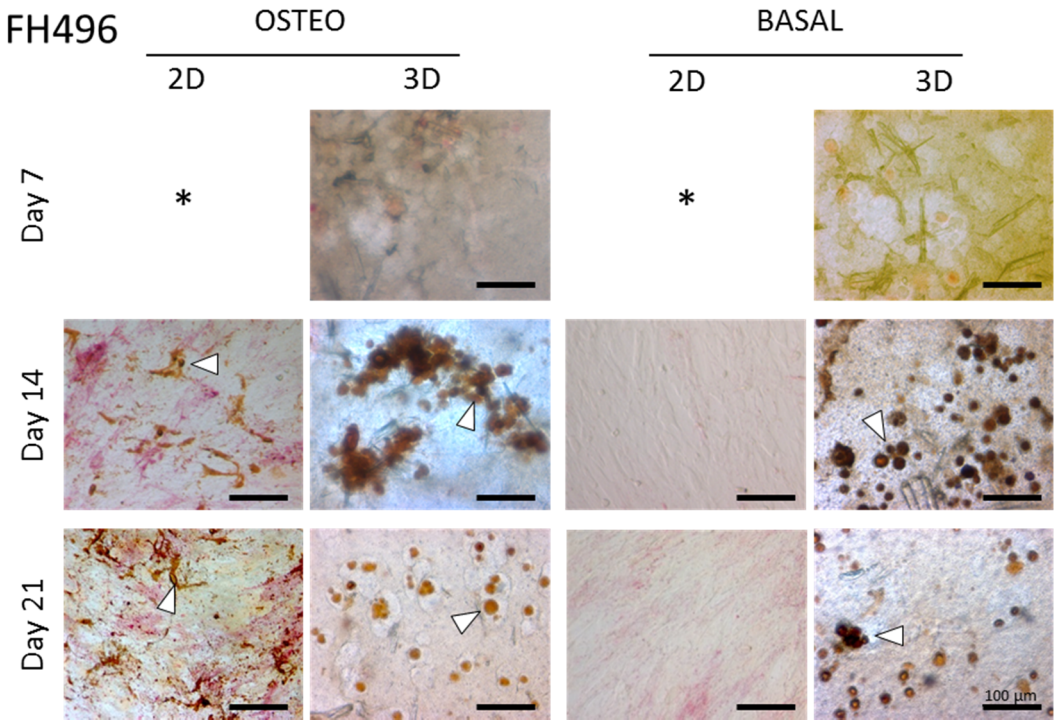

Figure 32: Von Kossa and ALP staining of FH496 MSC monolayers and cell-loaded PNIPAM+RRR droplets. MSC monolayers in basal conditions demonstrated no mineral deposition and minimal ALP activity on day 21. Treatment of MSC monolayers with osteogenic media resulted in strong ALP activity from day 7, with mineralisation onset on day 14 and active mineralisation by day 21. Hydrogel encapsulated MSC single cell suspension in osteogenic and basal conditions demonstrated active mineral deposition on day 14 and 21 (white arrows). 2D samples on day 7 have peeled off during pre-imaging washes (*).All scale bars are 100 µm. n=2

The FH496 donor cells in monolayer culture and basal conditions did not show active mineralisation, however, traces of ALP activity were observed on day 21 (Figure 32). Whereas, monolayer MSCs in osteogenic media demonstrated ALP activity on day 14. Furthermore, progressive mineral deposition was observed on day 14 and 21 (white arrows). No evident ALP signal was detected in either of the cell-loaded hydrogel settings. At the same time, starting from the day 14, strong von

Kossa stain was observed in cell-loaded hydrogels in osteogenic and basal conditions (Figure 32, white arrows).

Von Kossa staining of K89 cell monolayers in basal conditions did not show any mineralisation, where osteogenic conditions promoted active mineral deposition from day 15 (Figure 33). Similarly, hydrogel-encapsulated MSCs in osteogenic conditions demonstrated an onset of active mineralisation on day 15 and omnipresence of von Kossa staining on day 21 (white arrows). Hydrogel samples in basal conditions did not demonstrate von Kossa positive staining up until day 21.

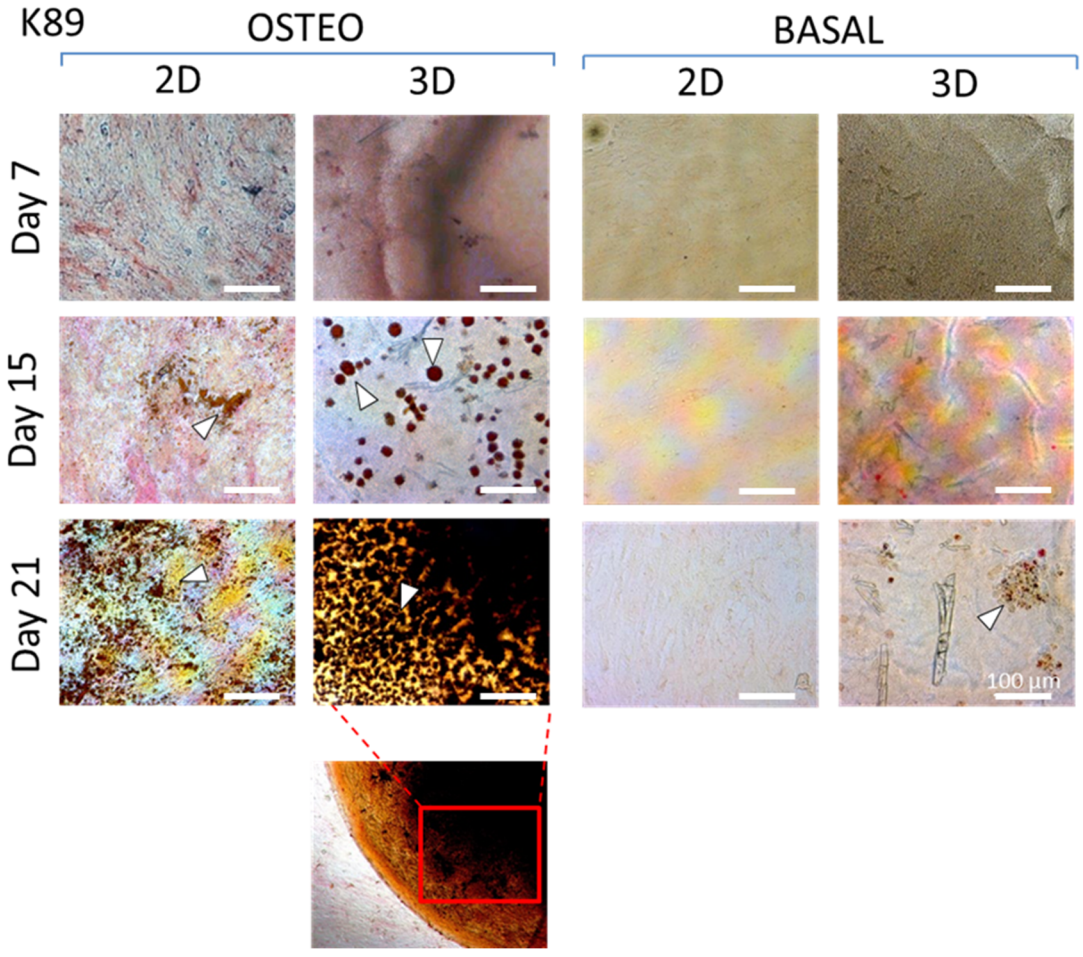

Figure 33: ALP and von Kossa stained K89 MSC monolayers and cel-loaded PNIPAM+RRR droplets. A progressive von Kossa stain was observed in monolayer and cell-loaded hydrogel cultures in osteogenic conditions on day 15 and 21. Where no von Kossa stain was observed in basal media conditioned samples, except for hydrogel-encapsulated samples on day 21. All scale bars are 100 µm. n=2.

Osteogenic potential of the K118 samples was assesed in an identical manner to the FH496 and the K89 donor samples. Progressive mineral deposition in K118 cells was observed only in osteogenic conditions of hydrogel-encapsulated cells on day 14 and 21 (Figure 34, white arrows). Monoloayer cultures in osteogenic conditions demonstrated traces of ALP activity at every analysed timepoint. Monolayer and hydrogel samples showed neither von Kossa, nor ALP staining at any timepoint.

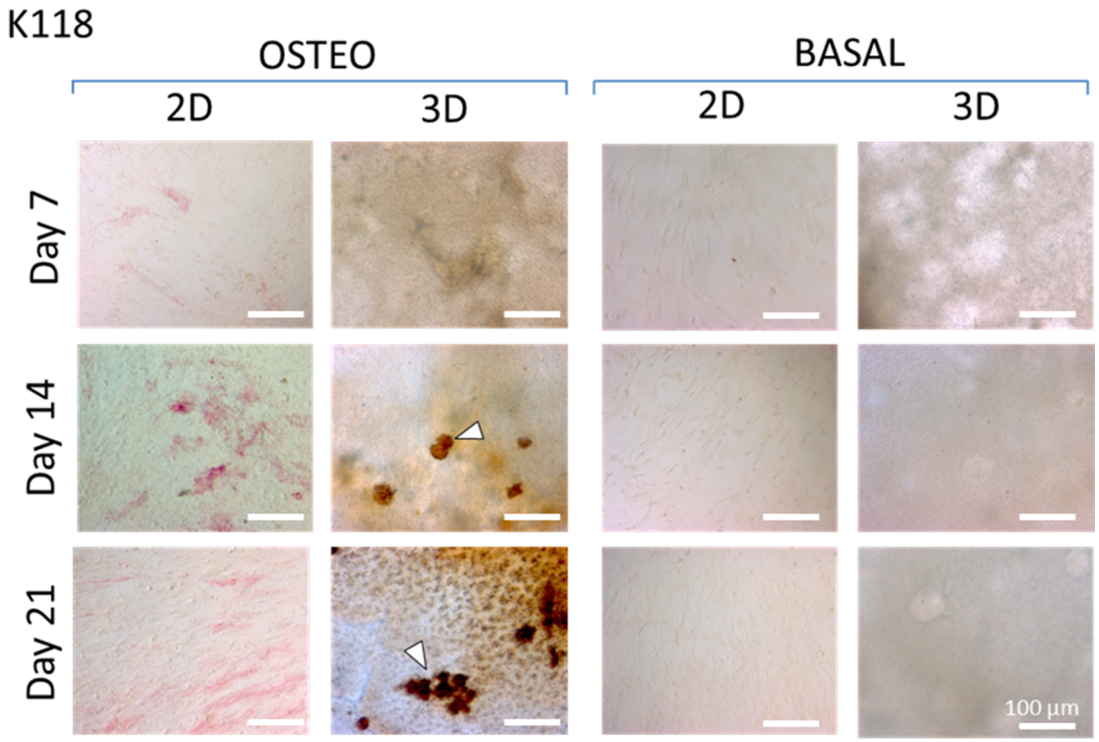

Figure 34: Mineralisation and ALP activity assessment with von Kossa and ALP stain in K118 MSC monolayers and cell-loaded PNIPAM+RRR droplets. Active mineralisation was observed only in hydrogel-encapsulated MSCs on day 14 and 21 (white arrows). Traces of ALP activity were seen in osteogenic monolayer cultures. Neither von Kossa, nor ALP stain was observed in basal media treated sample monolayers and hydrogel-encapsulated cells. All scale bars are 100 µm. n=2.

4.3.12 Osteogenesis: birefringence as the von Kossa stain validation

In order to cross-confirm von Kossa staining results, polarised light microscopy was employed. Prior imaging, cell-loaded hydrogels were sectioned and transferred onto glass slides. In addition, sectioned samples were not pre-stained with any differentiation assays.

Hydrogel samples were collected from two donors: FH496 and K118. Analysis of the FH496 sample under polarised light demonstrated absence of birefringence signal on day 7 in osteogenic conditions, however, already by day 14 a strong birefringent signal was observed (Figure 35, white arrows). Identical response was observed on day 21. Likewise, MSCs in basal hydrogel conditions on day 21 were found to have a clear birefringence signal.

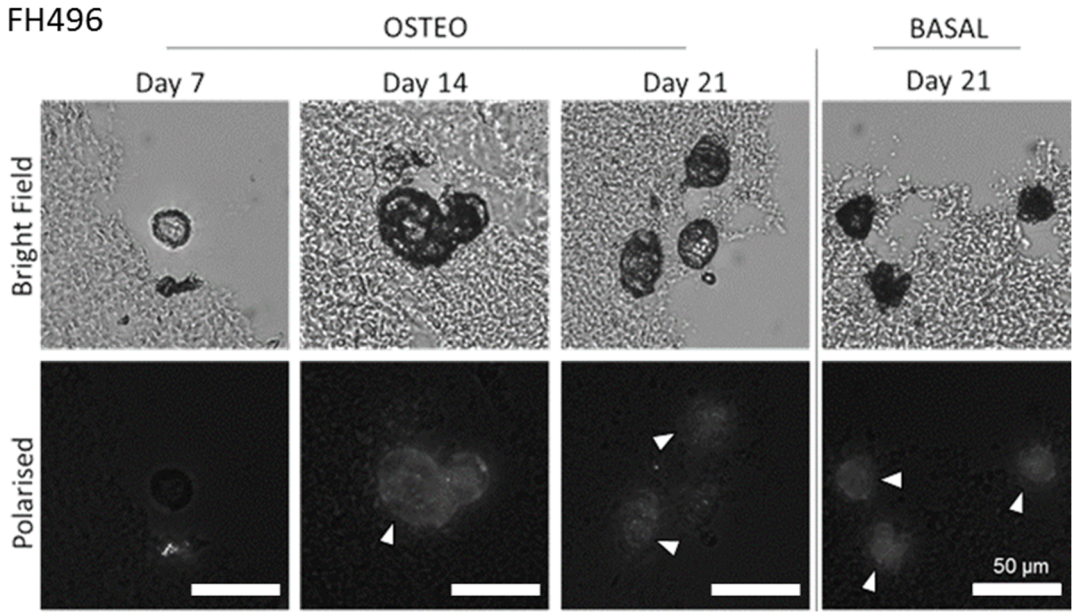

Figure 35: Examination of birefringence effect in FH496 PNIPAM+RRR-encapsulated MSCs under polarised light. No birefringence was observed in MSCs in osteogenic conditions on day 7 under polarised light. Thereafter, on day 14 and 21, a strong birefringence signal was detected (see white arrows). After 21 days of culture in basal conditions, hydrogel-encapsulated MSCs were also found to be birefringent (see arrows). Day 7 and 14 samples in basal conditions were damaged during cryosectioning. All scale bars are 50 µm. n=2.

The response of the K118 cells in osteogenic conditions to polarised light was very similar FH496 cells in the same conditions – birefringent signal was observed on day 14 and 21 (Figure 36, white arrows). However, no signal was collected from samples in basal conditions in either of the days (Figure 36).

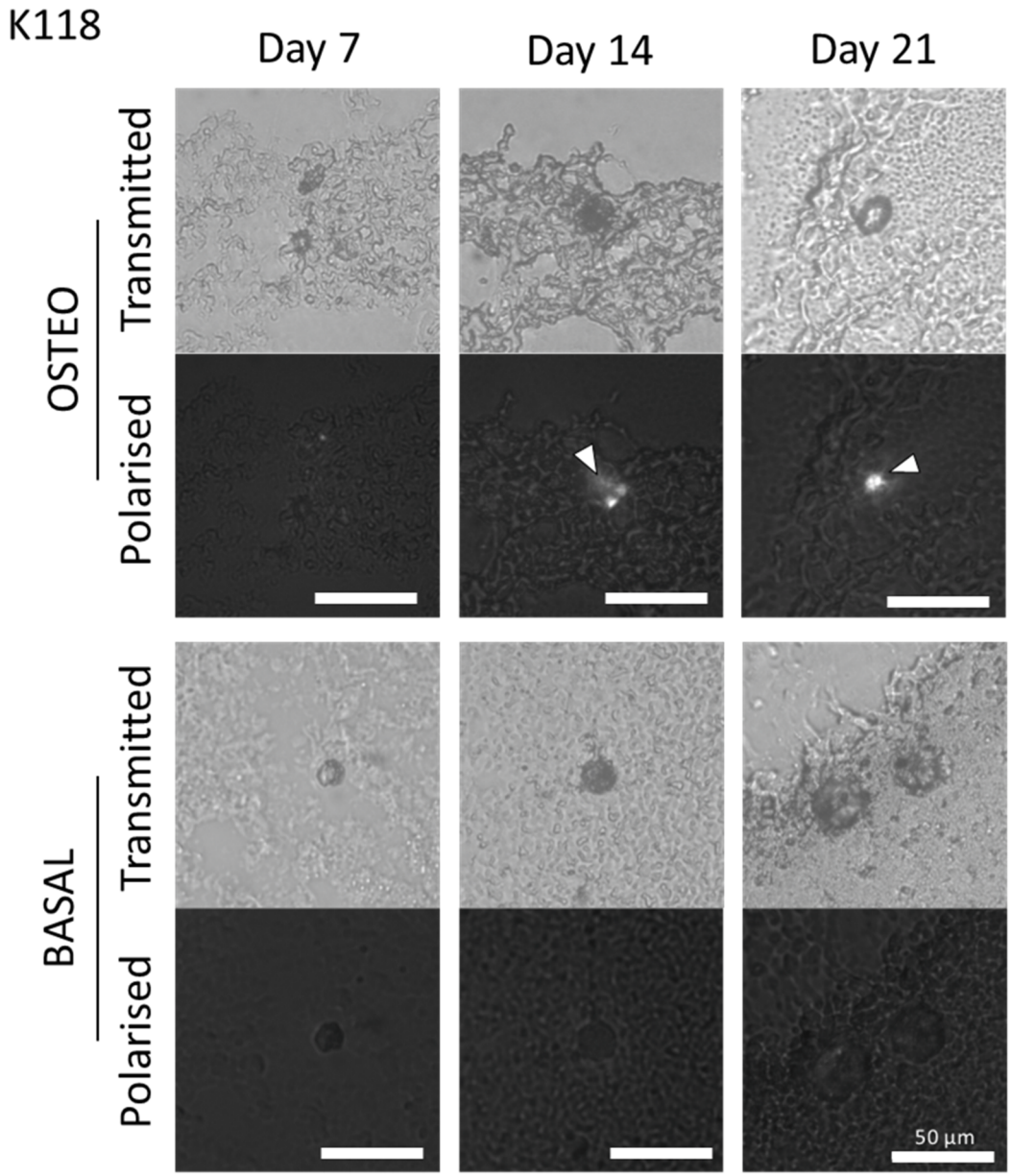

Figure 36: Micrographs of cryo-sectioned hydrogel-encapsulated K118 samples under polarised and transmitted light. No birefringence was observed in basal conditions, where in osteogenic conditions day 14 and 21 samples demonstrated a birefringence signal (white arrows). n=2.

4.3.13 Adipogenesis: BODIPY® staining

Osteogenesis and adipogenesis differentiation in MSCs are mechanistically reciprocal processes (Beresford et al. 1992). According to the collected osteogenesis data, majority of the patient samples are demonstrating active mineral deposition and ALP activity in osteogenic environment, as well as in basal conditions (ALP: Figure 29 and Figure 30; von Kossa: Figure 32 and Figure 33). These observations suggest osteogenesis-inductive effect of the HB PNIPAM+RRR 3D hydrogel environment. Therefore, it can be hypothesised that the same environment will demonstrate adipogenesis-inhibitive properties. To prove or reject this hypothesis, adipogenic potential of the K89 and the K118 donor samples was assessed during 21-day differentiation experiment.

Assessment of the adipogenic potential of the K89 sample MSCs is presented in Figure 37. The monolayer MSCs, which were exposed to adipogenic media for 7 days demonstrated signs of active adipogenesis, by forming spherical structures which were positively stained by tracer for nonpolar lipid - BODIPY® 493/50. By day 21, adipogenic-treated monolayer cells demonstrated widespread lipid vesicle formation within the cells. This observation confirms sensitivity of primary K89 MSCs to osteogenic stimulation.

At the same time, monolayer cells in basal conditions did not produce any visible lipid vesicles, nor were the cells positive to lipid stain at any timepoint. Likewise, hydrogel-encapsulated cells in both, adipogenic and basal conditions did not exhibit any lipid positive staining.

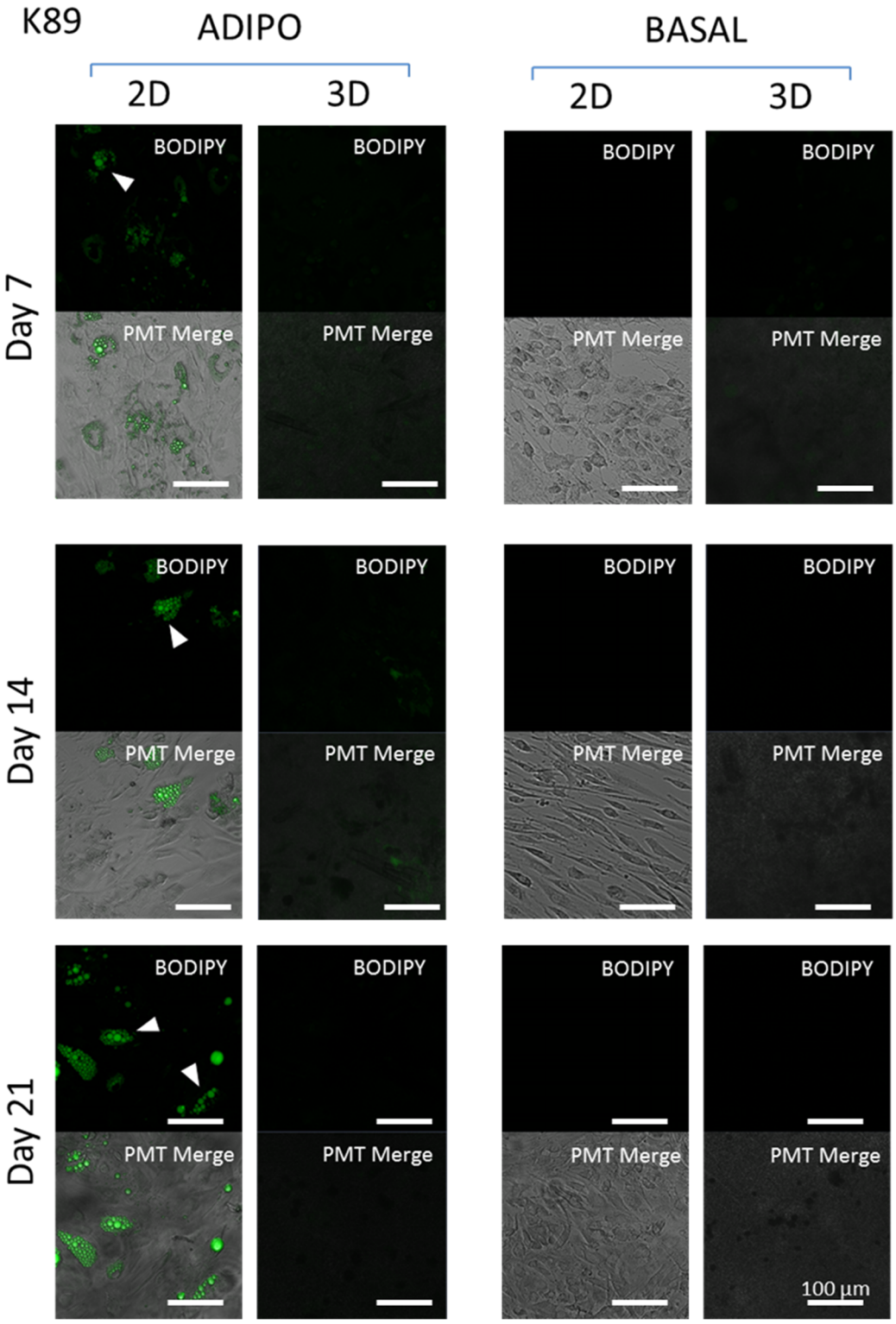

Figure 37: K89 cells in monolayers or PHIPAM+RRR droplets, stained with BODIPY® 493/503 stain for lipid deposits, Both sample types were exposed to adipogenic and basal conditions for up to 21 days. Only cells that have demonstrated adipogenic activity were monolayer MSC cultures in adipogenic conditions (white arrows). The BODIPY signal channel was merged with photomultiplier tube (PMT) channel to show morphology of the lipid-forming cells. All scale bars are 100 µm. n=3.

Adipogenic potential of K118 was assessed in identical manner to K89 sample. Following 21 day treatment with adipogenic media, cells in monolayers did not demonstrate lipid vesicle formation and BODIPY positive staining (Figure 38). Likewise, hydrogel-encapsulated cells were not found to be BODIPY-positive in adipogenic conditions. Identical cell response was observed in 2D and 3D samples treated with basal media.

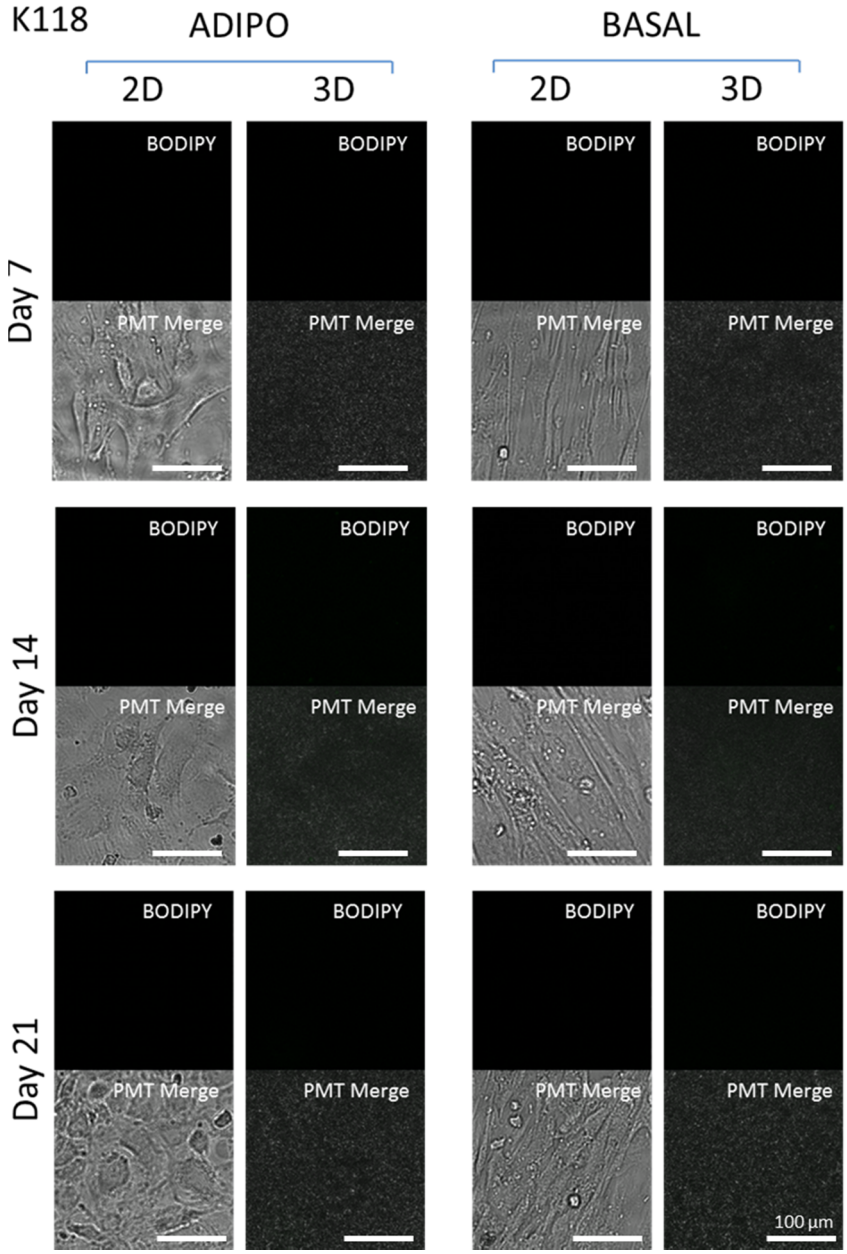

Figure 38: K118 MSCs in monolayers or PHIPAM+RRR droplets, stained with BODIPY® 493/503 stain for lipid deposits, Both sample types were exposed to adipogenic and basal conditions for up to 21 days. No BODIPY-positive signal was observed in either of the samples throughout the differentiation assay. All scale bars are 100 µm. n=3.

4.4 Discussion

4.4.1 Addition of an extra dimension and adaptation to the unique environment

Results of the studies conducted on 2D TCP surface are often misleading in the long run, as numerous factors, which are inherent to *in vivo* conditions in 3D, are not taken in consideration (Meng et al. 2014). One of the key areas that this particular project was designed to cover is extending understanding of BM MSC behaviour in 3D environment, by using PNIPAM-based hydrogel.

PNIPAM as a chemical entity has attracted copious amount of interest from the tissue engineering community due to its phase-transitioning nature (Alarcon et al. 2005; Guan & Zhang 2011; Rimmer et al. 2009; Galperin et al. 2010). Particularly in the last decade, numerous PNIPAM-based solutions for the needs of tissue engineering became available (Gan et al. 2009; Wu et al. 2014; Mazumder et al. 2012). The objective of this project, specifically regarding 3D culture system, was to design a novel, highly tuneable synthetic material, which could be optimised for the needs of MSCs.

The fundamental initiative to design a hydrogel system, based on PNIPAM, was to create an environment which could be used in tissue repair, either by closely mimicking the native environment of the MSCs (i.e. bone marrow or the putative MSC niche) or by directing differentiation.

At the early stage of hydrogel design, highly-branched architecture of PNIPAM was functionalised with tri-arginine peptide. It is important to mention that this architecture of the hydrogel was not previously reported in the literature, and therefore, it was essential to conduct biocompatibility testing that would confirm suitability of HB PNIPAM+RRR for biological application, most importantly with MSCs.

To obtain preliminary understanding of how PNIPAM+RRR hydrogel may perform as a 3D scaffold in cell culture conditions, MG63.EGFP osteosarcoma cells were placed in the gel for 8 days (Figure 21). Cells were successfully encapsulated,

demonstrating rounded morphology, and minimal amount of hydrogel shrinkage was observed.

The core focus of this project is the understanding of the *ex vivo* MSC behaviour in 3D environment. *Ex vivo* MSCs, cultured on 2D TCP, lack structural organisation of the *in vivo* setting. On the contrary, *ex vivo* MSCs, cultured in spheroids, provide an *in vivo*-like morphology, phenotype and cell-cell interaction, representing a better model system of the natural tissue (i.e. force and diffusion gradients are present in spheroids) (Saleh et al. 2011; Kunz-Schughart et al. 2004). In addition, MSC spheroids hold a great promise to be used as building units of artificial organs (Mironov et al. 2009).

Taking in consideration benefits of the spheroidal organisation, MSCs were formed into spheroids and encapsulated in the hydrogel. Spheroids were placed into HB PNIPAM+RRR hydrogel for 8 days in a 96-well flat-bottomed TCP plate (Figure 22). For the first 6 days of culture spheroid encapsulation appeared to be successful, but on day 8 it was evident that encapsulated spheroids regained contact with the surface of the plate and cell growth in monolayer was initiated. An identical spheroid encapsulation protocol was repeated with use of non-adherent U-bottom plates, no adhesion of the spheroid to the surface of the well was observed even after 16 days of culture (Figure 23). Success in spheroid encapsulation was compromised by substantial shrinkage of the gel structure, presumably due to lack of anchorage for the gel and centre-directed pressure imposed on cell-gel composite by the well U-shaped design.

The core focus of this study was the behaviour of the MSC single-cell suspension within 3D environment of the HB PNIPAM+RRR (Figure 24). After 7 days of culture encapsulated MSCs were not found to be adhering to the bottom of the 96-well TCP flat-bottom plate, as no cells have taken up a fibroblastic morphology, but retained their rounded shape. In addition, cells were found to localise themselves at various distances from each other in 3D space of the gel, with majority of the cells organised around one plane, parallel to the TCP surface.

These initial compatibility experiments verified that MSCs can be encapsulated in PNIPAM+RRR hydrogel and observed under multi-photon and confocal microscope, despite its opaque appearance. In addition, MSC morphology was affected dramatically after encapsulation in the hydrogel – flattened fibroblast-like appearance of MSCs, previously cultured on TCP, was replaced by a rounded shape without evident projections.

Cell migration *in vivo* is a complex process, which is accompanied by ECM remodelling via MMPs, cytoskeletal reorganisation and development of the leading edge (protrusion) (Friedl 2004; Petrie & Yamada 2012). Analysis of the relative distances between encapsulated MSCs in identical region of interest (ROI) for 12 days identified virtually no migratory activity in the cells (Figure 25A,C). Most commonly, migrating cells form membrane extensions, also known as protrusions. Hydrogel-encapsulated MSCs did not change the shape substantially and remained rounded.

Cell volume changes in encapsulated MSCs were also analysed (Figure 25C). The particular cell population analysed presented a broad range of cell volumes on day 1, but with progression of time 3 distinct groups of cells were identified (Figure 25B). The majority of the cells demonstrated a reduction in cell volume by ca. 23% after first 4 days in culture, followed by a plateau. Whereas, a small sub-group of analysed cells showed a marked increase in cell volume on day 4 of culture with a further gradual increase in cell volume. Possible explanation for this behaviour by MSCs comes from the fact that the MSC population is heterogeneous and the initial broad range of cell volumes is inherent property of the population.

Moreover, the observation that the starting cell population divided into 3 discrete groups by volume range and demonstrating non-linear volume change with time in culture, suggests that the cells were undergoing active adaptation to new 3D environment (Figure 25B). Interestingly, the volume increase observed in a minority of cells, in contrast to the shrinkage trend observed in the majority of the cells, may suggest that MSCs are remodelling their own cytoskeleton to occupy an optimal cell volume for this particular material. This observation supports the assumption that the

cellular cytoskeleton is constantly remodelling (Rodríguez et al. 2004) in order to facilitate adaptation to the new environment.

4.4.2 MSC release from EtOH-treated PNIPAM+RRR

Key understanding of the hydrogel biocompatibility with MSCs was obtained by conducting cell viability testing. MSCs at their primary stages of culture are selected on the basis of their plastic-adherence property. The initial attempt to assess MSC viability after culture in hydrogel's 3D environment was to be performed by means of cell recovery from the gel. In addition, PNIPAM-based approach to MSC culture was initially chosen because of the thermo-reversible nature of the polymer (i.e. hydrogel structure dissolution takes place after temperature lowering past LCST point and exceeding hysteresis time window), as one of the beneficial properties of this particular polymer.

The thermo-reversible nature and gel dissolution was observed during polymer synthesis and analysis stage (e.g. gelation test, UV-vis, μDSC results; Section 3.4). However, process of cells culture made the thermo-reversible property of the gel less usable, as the hydrogel dissolution was not complete even after 16 hours on the rotating ice bed and mechanical break up was required (Figure 26). This loss of function in PNIPAM+RRR can probably be attributed to protein-rich serum, present in the media, and long term culture process that may have altered dissolution mechanism of the PNIPAM+RRR gel.

Furthermore, analysis of the released cells from both, EtOH-sterilised and non-sterilised, hydrogels types showed that an overall majority of the released cells are rounded and non-adherent (Figure 26). Figure 26A provides an example of an individual MSC reattaching following release from the gel after 16 days of culture and subsequent culture for 3 days. Whereas, Figure 26B exemplifies the majority of MSC being non-adherent with rounded morphology. These observations suggest that the interaction between MSCs and the TCP surface was affected, either via TCP surface modification or the alterations in the MSC surface-binding properties.

Cell adhesion on common tissue culture grade polystyrene is enabled by corona discharge treatment. Following this treatment, initially hydrophobic surface becomes

hydrophilic and negatively charged. This surface modification promotes fibronectin and vitronectin binding, which are present in abundance in the serum-enriched media. Presence of the integrin-responsive sequences, like fibronectin and vitronectin, stimulates cell binding and spreading. (Ryan 2008)

On the other hand, loss of adhesion or development of anchorage independence is often linked to the tumour cells with metastatic potential (Mori et al. 2009). However, loss of adhesion in this particular case can probably be explained by saturation of the TCP surface with polymer and peptide sequences that may have inhibited binding site of integrin receptors. In addition, the recovery conditions after the gel disaggregation were identical to conditions prior disaggregation, where released cells may require some adjustments to the culture settings in order to reinitiate the cell attachment. Moreover, Yang and colleagues has provided evidences, that one week of culture is enough for matrix elasticity to promote MSC commitment to osteogenesis (Yang et al. 2014). The work of Yang and colleagues has demonstrated that MSCs have a mechanical memory, where YAP/TAZ transcriptional activators represent an internal mechanical rheostat, which stores information on previous microenvironments and cell specialisation choices (Yang et al. 2014). Therefore, hydrogel-released cells could be involved in the early differentiation process and are not able to bind to TCP after exposure to a less stiff hydrogel environment.

4.4.3 MSC biocompatibility with HB PNIPAM+RRR

A fundamental requirement of any scaffolding material, which is intended for use in tissue engineering, is its ability to support cell viability. Previous experiments in this study have identified a propensity of encapsulated MSCs to maintain rounded morphology (Figure 24), limited motility and reduction of the volume in the majority of the cells (Figure 25). These observations, taken together, predict lack of active proliferation of the MSCs within PNIPAM+RRR environment.

In order to validate viability of the encapsulated cells, the CCK8 kit was used (Figure 27). An active component of the CCK8, a water-soluble tetrazolium salt, is converted into media-soluble formazan yellow dye by active dehydrogenases in the

cell (Dojindo n.d.). In theory, concentration of the formazan dye is directly proportional to the number of viable cells. However, this dye appeared to be non-optimal for cell viability testing in PNIPAM+RRR hydrogel. After 8 days of culture, cell-free hydrogels have demonstrated identical formazan concentrations, when compared to cell-loaded hydrogels (Figure 27). Such behaviour may be explained by possible retention of the dye within the hydrogel structure.

As the CCK8, a method for cell viability assessment, rendered itself as inappropriate for the HB PNIPAM+RRR system, a qualitative imaging approach was used instead. The Live/Dead assay, used in this study, is a composite of 2 dyes: calcein AM and ethedium homodimer-1 (EthD-1). Fluorescent signal, obtained from calcein AM, is a product of calcein AM conversion by intracellular esterase activity into polyanionic dye calcein. Whereas EthD-1 can only penetrate cells with raptured cell membrane, and binding of the EthD-1 to nucleic acids results in 40-fold enhancement of fluorescence signal.

Ethanol-treated and non-treated hydrogel samples were exposed to calcein AM and EthD-1 treatments on day 1, 4 and 10 (Figure 28). Analysis of EthD-1 staining in both sample types, ethanol-treated and non-treated, revealed low specificity of this dye in the 3D hydrogel setting: samples, with methanol-treated cells, did not demonstrate a strong nucleus-specific EthD-1 signal on neither of the days.

At the same time, calcein AM has demonstrated consistently strong signal in both sample types, with non-treated “live” cells, as the culture time progressed. Whereas, samples with methanol-treated “dead” cells demonstrated only traces of intracellular esterase activity and complete absence of the signal on day 10 in both sample types. This observation validates the specificity of the calcein AM dye, and also verifies that the encapsulated cells are viable within the 3D PNIPAM+RRR setting on the basis of observed esterase activity. Importantly, ethanol-recovered PNIPAM+RRR polymer produced less autofluorescence, making the samples more suitable for microscopic analysis and future studies.

4.4.4 MSC differentiation in HB PNIPAM+RRR

The ability of MSCs to undergo differentiation is well known, where the capacity to form osteogenic, chondrogenic and adipogenic progenitor cells is considered to be a key characteristic feature (Roberts et al. 2011).

Recent work of our group has demonstrated that articular chondrocytes are viable and increase in number in graft and random PNIPAM-based hydrogels (Lapworth et al. 2011). In the current study, a highly functional and branched hydrogel was developed, allowing cell encapsulation. Assessment of the MSC phenotype within 3D environment of the hydrogel will help to prove or disprove the hypothesis that PNIPAM+RRR hydrogel can be used as a model environment to support and study MSC function in 3D milieu.

The ability of MSCs to undergo osteogenesis in the 3D environment of PNIPAM+RRR was tested first in order to establish the sensitivity of encapsulated cells to differentiation cocktails.

The encapsulated cells in the osteogenic and control conditions were found to be ALP positive, suggesting progression of osteogenic differentiation (Figure 29 and Figure 30). Further, these observations were confirmed on independent samples by ALP and von Kossa staining (Figure 32 and Figure 33). In order to cross-validate results of the von Kossa staining and eliminate possibility of non-specific staining of the phosphate groups, introduced by the washing solution, hydrogel sections were analysed under polarised light microscope (Figure 35 and Figure 36). Polarised light analysis method was used as it was previously found to provide birefringent signal from calcium phosphate structures (Clineff et al. 2005).

The osteogenesis study with FH496 donor sample has provided clear evidences of osteoinductive effect of PNIPAM+RRR polymers on MSCs in osteogenic and also basal conditions.

It is important to remember that MSCs used in this project were extracted from donors, who differed by age, sex, body mass index (BMI), tissue source and may also have had a history of degenerative disease (Table 11). Taking these facts in

account, together with inherent mutability in genetical make up between each individual and possibly non-homogeneous MSC population, may result in variability in cells' phenotypic characteristics (da Silva Meirelles et al. 2006; Sivasubramaniyan et al. 2012). In order to account for this potential variability, osteogenesis experiments were conducted on MSCs, which were obtained from 3 donor tissue samples.

MSCs, harvested from the second donor sample – K89, have demonstrated similar osteogenesis results to FH496 donor, however with a slight difference. Highest ALP activity in K89 3D samples was observed on day 15 in osteogenic and basal conditions, yet the number of ALP-positive cells was low, relatively to FH496 sample (Figure 30). Assessment of mineralisation in K89 revealed strong cellular response to the von Kossa stain in hydrogel samples on day 15, and particularly on day 21 in osteogenic environments (Figure 33). Whereas hydrogels under treatment with basal media did not demonstrate active mineral deposition on day 15, but von Kossa-positive cells were seen on day 21 (Figure 33). These observations support osteo-inductive nature of the hydrogel, first seen in FH496 donor sample.

In addition to osteogenesis, adipogenic capacity of K89 MSC within 3D hydrogel environment was also studied. MSCs in monolayer culture, treated with adipogenic media, have demonstrated lipid vesicle development on day 7 and further progressive lipid formation with time in culture (Figure 37). No lipid vesicles were observed in monolayer cultures, treated with basal media. Identical cell response was observed in 3D hydrogels, where encapsulated cells were exposed to adipo-inducing cocktail, no lipid forming cells were observed, suggesting adipogenesis-inhibiting properties of the PNIPAM+RRR gel.

K118 MSCs from the third donor sample demonstrated relatively weak ALP response in cell monolayers after osteogenic treatment (Figure 31). Contrary to monolayers in osteogenic media, no other sample has demonstrated ALP activity at any time point. Interestingly, mineralisation development was not observed in either of the tested samples, excluding 3D hydrogel samples under osteogenic conditions on day 14 and 21 (Figure 34). This observation was cross-confirmed by presence of

the birefringence in osteo-induced 3D hydrogel samples on day 14 and 21, and absence of the birefringence in hydrogels under basal conditions (Figure 36).

In addition, K118 MSC sample cells were not responsive to adipogenic media treatment: neither 2D monolayers nor 3D hydrogels showed lipid vesicle formation (Figure 38).

Summative assessment of MSC osteogenic differentiation potential within 3D PNIPAM+RRR samples indicates an osteo-conductive nature of the hydrogel environment in MSCs from all 3 donors; and osteo-inductive property of the same environment was seen in 2 donors. Adipogenic differentiation was induced in 2 donor samples, and collected results suggested adipo-inhibitive properties of the PNIPAM+RRR hydrogels.

Phenotype comparison between all 3 donor cells exemplifies variability in cell response. The link between age and gender effect on MSC mesodermal differentiation capacity would be initially assumed. However, a recent study on bone marrow MSCs from 20 male and 18 female (male, age 54.4 ± 11.3 years SD; 18 female, age 50.3 ± 16.9 years SD) donors identified no correlation between age, gender and mesodermal differentiation capacity of MSCs (Siegel et al. 2013). Concurrently, Prins and colleagues has demonstrated high discrepancy in tri-lineage differentiation capacity between sub-clones from the same donor (Prins et al. 2014). In addition, only 4 out of 7 donor MSC samples were able to form bone tissue *in vivo*, highlighting intrinsic variation in differentiation capacity of primary BM MSCs (Prins et al. 2014).

4.4.5 MSC osteogenic differentiation within PNIPAM-based hydrogels

Understanding of the fundamental stages in in osteogenic differentiation is essential for complete exposure of the beneficial effects that an engineered hydrogel environment has on differentiation in MSCs. An excellent example of this concept is a recent study by Dai and colleagues. BM MSCs of mice were cultured in monolayers until confluent, followed by coverage with thermos-sensitive PNIPAM-based hybrid gel, which forming a “sudo 3D” environment for the cells. This hybrid gel consisted of PNIPAM microgels with varied acrylic acid content (AA; AA

addition increased solution-gel transition temperature to 37˚C and provided pH sensitivity as an additional trigger for gelation). After 14 days of culture in control media (no differentiation stimulators added) a significant increase in mRNA expression of ALP, collagen 1 and Runx2 was observed in gel-covered samples with 20% AA content, what indicated progress in lineage specification. With onset of lineage specification, calcium deposition was expected. However, when cell-hydrogel samples were treated with Alizarin Red S on day 21 to assess mineralization, no staining was seen in all of the samples in control media, regardless of the AA content. Even the samples, which were kept in the osteogenic media (supplemented with conventional stimulating factors), did not demonstrate mineralisation, except for the sample with 10% AA content (lowest tested concentration; mineralisation was minimal). Hence, lack of mineralisation staining is suggesting induction of an early differentiation, followed by inhibition of the later stages of differentiation - maturation and mineralisation. However, when the MSCs in monolayers were first cultured for 7 days in osteogenic media (media was not replaced), followed by hydrogel with osteogenic or control media addition for the next 14 days (media was replaced every 3 days), all of the hydrogel-covered samples exhibited mineralization activity, especially in samples with osteogenic media. Therefore, by allowing MSCs first to deposit sufficient quantities of calcium in the first 7 days, followed by hydrogel addition, strong osteoconductive and mineralization-inductive properties of PNIPAM+AA microgels are observed. Dai et al. attributed absence of mineralization in hydrogel-cell composites, lacking initial cell pre-treatment with osteogenic stimulants, to sequestering of the cationic Ca^{2+} ions by the anionic carboxylic (COO^-) chain ends of the hydrogel polymers. Lineage specification was observed, but due to the absence of the Ca^{2+} ions, matrix maturation and mineralization processes were unable to progress. Considering Ca^{2+}/COO^- interaction, Dai and colleagues are proposing that the calcium, which was deposited in the first 7 days of osteogenic culture, is the chemo-attractant for PNIPAM+AA with COO^- functionalities. Such calcium-hydrogel interaction may model a mechanical stress transducer, which mediates mechanical forces, generated by ionic interaction between the microgels, to the cell. (Dai et al. 2014) In summary, this PNIPAM-based hydrogel demonstrates dual differentiation functionality. This hydrogel can act as an inhibitor, as well as the promoter, of osteogenic

differentiation in MSCs, depending on the stage at which it is added to the differentiation process.

Despite the diversity in PNIPAM architectures and functionalities, exemplified in Table 4 and Table 10 above, this material has been rarely used to study differentiation of MSCs. Specifically, evidences of osteoconductive and osteoinductive properties of PNIPAM are being published, but they are not common (section 4.1.3). Furthermore, no studies are published, demonstrating stimulation of osteogenesis in highly branched PNIPAM. Therefore, osteogenesis-stimulating nature, demonstrated by PNIPAM+RRR hydrogel, is extending applicability of the branched PNIPAM hydrogels in tissue engineering strategies and providing novel 3D model environment for MSC function examination.

4.4.6 Exploration of relationship between MSC morphology, proliferation and differentiation in 3D. RRR peptide – as a potential adhesion molecule

In the current project triple arginine sequence was used for hydrogel functionalisation, in order to improve solubility and stability of the highly branched PNIPAM hydrogel. Tri-arginine sequence is a novel peptide, which has not been researched previously. The only study on tri-arginine effect, currently available, is by Gilmore and colleagues, where she shows sequestering interaction of RRR with heparin (Gilmore et al. 2013). However, few studies on L-arginine show an important role it plays in cell adhesion. Work of Yeh et al. show that arginine treatment increases adhesion molecule (i.e. CD11b – an integrin family member that regulates leukocyte adhesion and migration) expression in bone marrow-sourced neutrophils (Yeh et al. 2007).

Furthermore, Rhoads and colleagues have found L-arginine to stimulate intestinal cell migration via an increase tyrosine phosphorylation of the focal adhesion kinase. Rhoads et al. further states that the arginine is digested by arginase, producing ornithine amino acid – the precursor of polyamines. (Rhoads et al. 2004)

Polyamines are involved in cell adhesion, as these polycations are required in a migrating cell during stress fibres and lamellipodia development (Rhoads et al.

2004). Interestingly, polyamines are also implicated in regulation of transcriptional and translational activity during bone development by stem cells (Borzì et al. 2014).

Upper mentioned studies that highlight involvement of arginine in cell migration, adhesion and differentiation via arginine metabolite are performed with non-bound form of arginine. Whereas in HB PNIPAM, RRR sequences were cross-linked to the carboxylic acid end of the parent branched structure via carbodiimide cross linker. Hence, availability of the interaction between the cells and the arginine is limited to surface receptor level in case of HB PNIPAM+RRR.

Even if the peptide-functionalised groups of PNPAM+RRR were not cross-linked, it is highly probable that permeation of tri-arginine through the cell membrane would be restricted. Work of Futaki et al. has vividly shown that peptide sequence, consisting out of 4 arginine repeats, will show very low translocation through the macrophage membrane. However, increase in arginine peptide length up to 8 members will improve translocation dramatically. 8 member sequence of arginine appears to be most optimal, as at 12 and 16 unit length translocation through membrane will be gradually reduced. (Futaki et al. 2001)

Hence, interaction of RRR with the MSC is most probable at the ligand-receptor level. It is an important hypothesis, as it may explain phenotypical changes in encapsulated MSCs.

Taking in account low stiffness of PNIPAM+RRR gel (G*=542.3 Pa), imposed spatial restrictions on MSCs by encapsulation in 3D environment and proliferation arrest, I hypothesise that combination of these 3 factors may provide osteoinductive environment for MSCs.

Equally, proliferation arrest closely describes a cell in a quiescent/G0 phase. Cell residence in G0 phase is common in terminally differentiated cells as well as in pre-differentiation cells (Filipak et al. 1989).

It is widely known that in differentiation of osteoblasts, a reciprocal process takes place: decrease in proliferation upregulates differentiation (Buttitta & Edgar 2007).

Therefore, MSC encapsulation in 3D hydrogel may mechanically restrict proliferation and prime cells for differentiation. Capacity for differentiation is an inherent and default property of non-differentiated cells. Stoppage of proliferation precedes differentiation and it is often described by withdrawal from the cell cycle (Walsh & Perlman 1997; Buttitta & Edgar 2007).

Along with stoppage in proliferation, MSCs were observed to take up rounded morphology. Winner and colleagues has demonstrated that MSCs with rounded morphology were non-proliferative when cultured on soft substrate (i.e. 250 Pa polyacrylamide gels, coated with collagen type 1 and fibronectin), but still responsive to chemical triggers of adipogenic differentiation (Winer et al. 2009). Osteogenesis and adipogenesis processes are closely interconnected – Jaiswal and colleagues more than a decade ago has provided evidences that inhibition of ERK signalling in MSCs results in blocking of osteogenic differentiation and promotion of adipogenesis (Jaiswal et al. 2000).

4.4.8 Rounded morphology of encapsulated MSCs

Multiple studies have found that osteogenic or adipogenic differentiation can be promoted by various substrate characteristics. As such, spreading inhibition on 2D substrate (McBeath et al. 2004), along with cell shape restriction to a circle-like shape (Kilian et al. 2010)(i.e. individual cell cultured on square-shaped substrate, opposed to elongated, rectangle – like shape) have shown promotion of adipogenesis and diminished osteogenic potential in MSCs. Whereas, appropriate stiffness of the substrate that facilities force translation (Discher et al. 2005; Pek et al. 2010), substrate functionalisation (Mauney et al. 2004; Polini et al. 2011) and hypoxic environment (Lennon et al. 2001) supported osteogenesis.

Furthermore, maintenance of a high differentiation potential, either osteogenic or adipogenic, requires suitable substrate. Mauney et al. demonstrated the importance of denatured collagen type I substrate in maintaining and supporting of the differential potential in both osteogenesis and adipogenesis (Mauney et al. 2005; Mauney et al. 2004). Whereas, inhibition of MSCs' integrin binding to fibronectin,

through treatment with heparin, resulted in upregulation of adipogenesis-related genes (Luo et al. 2008).

This collective insight into substrate effect and cell shape on differentiation suggests that MSCs with poor focal adhesion and rounded morphology should exhibit pre-adipogenic commitment.

Analysis of encapsulated MSCs in HB PNIPAM+RRR showed active osteogenesis and absence of adipogenesis. This finding contrasts with current view of the cell phenotype, as a predictor of differentiation fate, in a pliant culture environment. Research by Rodriguez *et al.*, McBeath *et al.* and Kilian *et al.* suggests, that MSCs with rounded morphology on a soft substrate are likely to demonstrate an opposite effect – strong adipogenesis and inhibition of osteogenesis (Rodríguez et al. 2004; McBeath et al. 2004; Kilian et al. 2010).

Differentiation capacity modulation of MSCs within HB PNIPAM+RRR may be explained by recent findings of Pek et al. who used polyethylene glycol-silica (PEG-silica) nanocomposite hydrogel, with the capacity to liquefy after exposure to a sheer stress (ranging from 7 Pa to 100 Pa) and presence or absence of the functional RGD domains as a 3D environment for MSC encapsulation (Pek et al. 2010). The analysis of cellular response, in terms of gene expression and proliferation, showed that increase in stiffness resulted in RUNX2 and osteocalcin expression increase, especially in the gel with stiffness of 75 Pa. At the same time, morphology of the cells in 100 Pa gels was strictly rounded, regardless of the RGD presence.

This observation made by Pek and colleagues, regarding the shape of the encapsulated MSCs, suggests that morphology of the MSCs is not a universal predictor of the lineage commitment and differentiation capacity of the cell. Further confirmation of this hypothesis can be drawn from analysis of the osteoblast morphology from bone marrow smears, where osteoblast cells are seen as large cells (25-50 μm in diameter) with rounded or oval shape (PathologyOutlines.com & Dragos 2012). Whereas myocytes, which are sharing the same germ layer origin with osteoblasts, are long and tubular cells (Evans et al. 2003).

Morphology of cells in 3D environment is a result of cell interaction with surrounding microenvironment, where focal adhesions play a pivotal role. Focal adhesions are instrumental for tensile or compressive force translation from the ECM. Balaban *et al.* calculated that typical fibroblast is capable of exerting 5500 Pa of stress on the surrounding matrix via focal adhesions (Balaban et al. 2001).

The focal adhesion complex is an intricate structure, which represents a dynamic interaction between three main components: cytoskeletal actin filaments, intramembranous integrins and ECM proteins (e.g. fibronectins). Each of these components plays a significant role in MSCs' fate determination. Furthermore, formation of focal adhesion complexes is essential for osteogenic differentiation (Salasznyk et al. 2007; Luo et al. 2008).

As one of the primary structures of focal adhesion complex, actin filaments are responsible for providing the basic shape to a cell by contracting and expanding cell's outer membrane. Furthermore, from all of the cytoskeletal filaments, actin's structural stability appears to have the highest impact on the differentiation fate of MSCs (Treiser et al. 2010). Where disruption of the actin cytoskeleton results in a rounded morphology of a cell (Rodríguez et al., 2004). In addition, a landmark study by McBeath and colleagues has demonstrated that actin disruption in MSCs leads to adipogenesis, what in turn links rounded morphology with actin disruption and adipogenesis (McBeath et al., 2004). This correlation was also confirmed by Kilian and colleagues (Kilian et al., 2010).

Integrins in particular are recognised as key drivers of osteogenesis (Salasznyk et al. 2007; Treiser et al. 2010). Work of Ingber enhanced understanding of the role of integrins as mechanoreceptors, which are capable of sensing and transmitting force between cytoskeleton and ECM instantaneously (Ingber 1997). This property of integrins may explain correlation between substrate stiffness and MSC differentiation fate, where soft substrate stimulates neurogenic differentiation and increase in substrate stiffness promotes osteogenic development in MSCs, both in 2D and 3D settings (Pek et al. 2010; Engler et al. 2006). Therefore, stiffness of the cells' microenvironment translates into tension within cytoskeleton and consequentially generates stimulus for MSCs' differentiation (McBeath et al. 2004).

ECM has been repeatedly shown to have a major effect on orchestrating cellular differentiation decisions (Martino et al. 2009; Daley et al. 2008). In order to produce osteogenesis-stimulating effect, ECM has to be in direct contact with integrins to allow force translation (Martino et al. 2009). Whereas in this project, the PNIPAM hydrogel was functionalised with a RRR peptide sequence, which may play a role of a ligand in MSCs' adhesion to the ECM.

This study set out with the aim of assessing the importance of MSC differentiation in 3D hydrogel structure does not propose that RRR peptide sequence is a proven adhesion molecule; however, only this chemical entity in theory is accessible for cell contact and may provide some degree of focal adhesion (Yeh et al. 2007). Prevailing opinion on MSC differentiation suggests that absence of focal adhesion results in abolition of osteogenic differentiation (Shih et al. 2011; Lu et al. 2011; Salasznyk et al. 2007; Luo et al. 2008; Trappmann et al. 2012; Higuchi et al. 2012). In contrast to earlier findings, however, MSCs in PNIPAM+RRR demonstrate clear signs of osteogenesis and inhibition of adipogenesis. This discrepancy could be attributed to a very weak adhesion which is probably present between the cell and the 3D environment, so that the actin cytoskeleton is in a collapsed or compacted state, but the ECM-integrin adhesion is sufficient to translate mechanical signals for osteogenic differentiation commencement. At the same time this degree of adhesion, formed by the MSCs, is not sufficient to promote remodelling of the external synthetic scaffold environment by the encapsulated cells and provide required space for cell cycle progression (i.e. growth and preparation for cell division). As a result, an active osteogenesis and a lack of proliferation is observed.

5 Study conclusion

The aim of this project was to develop a HB PNIPAM-based synthetic hydrogel scaffold, and employ this scaffold as a platform for assessment of MSC behaviour and guidance of differentiation in 3D environment.

To reach this aim, 5 objectives were set out for completion. The first objective was to synthesise a stable thermo-responsive PNIPAM hydrogel with highly branched architecture. The highly branched architecture of the polymer was achieved by employing RAFT polymerisation method, where structural stability of the polymer was attained after RRR peptide addition.

The second objective of this study was to characterise chemical and mechanical properties of the HB PNIPAM hydrogel. A thorough chemical characterisation of the non-functionalised HB PNIPAM and RRR-functionalised HB PNIPAM was done by numerous methods, including by UV-vis, zeta potential and μDSC. Whereas, mechanical properties of the peptide functionalised hydrogel was assessed on a cone-plate viscometer.

Thirdly, it was essential to optimise HB PNIPAM for encapsulation and long term culture of MSCs. As previously mentioned, RRR peptide functionalisation has improved stability of the polymer structure, as well water retention by the hydrogel network. As a result of peptide functionalisation it was possible to encapsulate the cells.

The central area of interest is this project were MSCs and their behaviour within 3D environment of the PNIPAM+RRR hydrogel. Key phenotypic parameters of MSCS, such as viability, proliferation and differentiation, were successfully assessed within 3D hydrogel environment. Hydrogel-encapsulated MSCs were found to be non-proliferating, but viable for up to 21 days. Finally, HB PNIPAM+RRR was found to have an osteo-conductive, osteo-inductive and adipo-supressing properties in majority of the donor samples.

6 Future work

Presented data and conclusions are demonstrating potential of the thermo-responsive HB PNIPAM+RRR hydrogel in providing a supportive 3D environment for MSCs functioning for up to 21 days. This hydrogel system was found to have an osteo-conductive and osteo-inductive effect on encapsulated MSCs. The results, presented in this study, have verified suitability of HB PNIPAM+RRR hydrogel as a MSC assessment platform. However, full potential of this material is yet to be explored.

Following experiments will allow to expand applicability of the highly branched PNIPAM hydrogels:

1. In the presented study only one architecture (i.e. 25 m.e. NIPAM : 1 m.e. RAFT) of HB PNIPAM was synthesised and characterised in detail. The dissolution mechanism in this architecture after a period of cell culture was found to be greatly retarded. Synthesis of architectures with different NIPAM:RAFT ratios will yield polymers with varying degrees of branching and molecular weight. These new architectures may undergo prompt dissolution with consequent release of the cells, making genotyping of the encapsulated cells possible.

2. Include degradation functionality, such as MMP-sensitive peptide sequences, into HB PNIPAM architecture to encourage cell migration and hydrogel remodelling.

3. Seed 500-1000 MSC spheroids into HB PNIPAM+RRR hydrogel to assess differentiation potential of multi-cellular organoids and observe spheroid fusion by means of time-lapse confocal microscopy.

4. Use HB PNIPAM+RRR in a high-throughput platform as an encapsulating environment for individual MSCs, to allow assessment of differentiation potential and trophic factor production at various temperature regimes.

5. Assess potential of minimally-invasive MSC delivery at the site of trauma in small animal model and consequent tissue regeneration.

7 Definitions

µDSC	Micro-scale differential scanning calorimetry
2-MBT	2-Mercaptobenzothiazole
a.u.	Arbitary unit
ACVA	4,4'-azobis(4-cyanopentanoic acid)
AIBN	4,4'-azobis(isobutyronitrile)
ALP	Alkaline phosphatase
ATR-FTIR	Attenuated total reflectance Fourier transform infrared spectroscopy
BM	Bone marrow
BMI	Body mass index
BSA	Bovine serum albumin
DIPEA	Diisopropylethylamine
Dkk-1	Dickkopf-1
DMF	N,N-Dimethylformamide
ECM	Extracellular matrix
FHxxx(e.g. FH123)	Femoral head
GAG	Glycosaminoglycan
GRGDS	Glycine-Arginine-Glycine-Aspartic acid-Serine peptide sequence
HB	Highly-branched
HBTU	(Benzotriazole-1-yl) tetramethyluronium hexafl uorophosphate
HPLC	High Performance Liquid Chromatography
Kxxx (e.g. K123)	Knee plate tissue
LCST	Lower critical solution temperature
LRP	Low-density lipoprotein receptor-related protein
MMP	Matrix metalloproteinase
M_n	Number average molecular weight
M_p	Peak molecular weight

MS	Mass Spectrometry
MSC	Mesenchymal stromal cells
M_w	Weight average molecular weight
OA	Osteoarthritis
pbf	2,2,4,6,7-Pentamethyldihydrobenzofurane-5-sulfonyl
PDI	Polydispersity index
PNIPAM	Poly(N-isopropylacrylamide)
pX (e.g. p3)	Cell passage number
ROI	Region of interest
ROS	Reactive oxygen species
rpm	Revolutions per minute
RRR	Tri-arginine peptide sequence
Runx-2	Runt-related transcription factor 2
SD	Standard deviation
sIPN	Semi interpenetrating polymer network
TCP	Tissue culture plate
TFA	Trifluoroacetic acid
TMTP	Transmitted light photomultiplier
UCST	Upper critical solution temperature
xxxg (e.g. 315g)	Gravitational force

8 List of references

Abbott, A., 2003. Biology ' s new dimension. *Nature*, 424, pp.870–872.

Aggarwal, S. & Pittenger, M.F., 2005. Human mesenchymal stem cells modulate allogeneic immune cell responses. *Blood*, 105(4), pp.1815–22.

Ahmed, E.M., 2013. Hydrogel: Preparation, characterization, and applications. *Journal of Advanced Research*.

Ahmed, T. a E., Dare, E. V & Hincke, M., 2008. Fibrin: A Versatile Scaffold for Tissue Engineering Applications. *Tissue engineering. Part B, Reviews*, 14(2).

Aizawa, Y. & Shoichet, M.S., 2012. The role of endothelial cells in the retinal stem and progenitor cell niche within a 3D engineered hydrogel matrix. *Biomaterials*, 33(21), pp.5198–205.

Akune, T. et al., 2004. PPARγ insufficiency enhances osteogenesis through osteoblast formation from bone marrow progenitors. *Journal of Clinical Investigation*, 113(6), pp.846–855.

Alarcon, C., Pennadam, S. & Alexander, C., 2005. Stimuli responsive polymers for biomedical applications. *Chemical Society reviews*, 34(3), pp.276–85.

Allı, S., Allı, A. & Hazer, B., 2012. Hyperbranched homo and thermoresponsive graft copolymers by using ATRP-macromonomer initiators. *Journal of Applied Polymer Science*, 124, pp.536–548.

Anselme, K., 2000. Osteoblast adhesion on biomaterials. *Biomaterials*, 21(7), pp.667–81.

Augello, A. & De Bari, C., 2010. The regulation of differentiation in mesenchymal stem cells. *Human gene therapy*, 21(10), pp.1226–38.

Baker, B.M. & Chen, C.S., 2012. Deconstructing the third dimension: how 3D culture microenvironments alter cellular cues. *Journal of cell science*, 125(Pt 13), pp.3015–24.

Balaban, N.Q. et al., 2001. Force and focal adhesion assembly: a close relationship studied using elastic micropatterned substrates. *Nature cell biology*, 3(5), pp.466–72.

Balducci, L. et al., 2010. Assessment and treatment of elderly patients with cancer. *Surgical oncology*, 19(3), pp.117–23.

Banfi, A. et al., 2000. Proliferation kinetics and differentiation potential of ex vivo expanded human bone marrow stromal cells: Implications for their use in cell therapy. *Experimental hematology*, 28(6), pp.707–15.

Bara, J.J. et al., 2014. Bone marrow-derived mesenchymal stem cells change phenotype following in vitro culture: Implications for basic research and the clinic. *Stem Cells*, 32(7), pp.1713–1723.

Barbero, A. et al., 2003. Plasticity of clonal populations of dedifferentiated adult human articular chondrocytes. *Arthritis and Rheumatism*, 48(5), pp.1315–1325.

Battula, V.L. et al., 2007. Human placenta and bone marrow derived MSC cultured in serum-free, b-FGF-containing medium express cell surface frizzled-9 and SSEA-4 and give rise to multilineage differentiation. *Differentiation*, 75(4), pp.279–291.

Battula, V.L. et al., 2009. Isolation of functionally distinct mesenchymal stem cell subsets using antibodies against CD56, CD271, and mesenchymal stem cell antigen-1. *Haematologica*, 94(2), pp.173–84.

Bayraktar, H.H. et al., 2004. Comparison of the elastic and yield properties of human femoral trabecular and cortical bone tissue. *Journal of Biomechanics*, 37(1), pp.27–35.

Beresford, J.N. et al., 1992. Evidence for an inverse relationship between the differentiation of adipocytic and osteogenic cells in rat marrow stromal cell cultures. *Journal of cell science*, 102 (Pt 2, pp.341–51.

Bergsma, E.J. et al., 1993. Foreign body reactions to resorbable poly(L-lactide) bone plates and screws used for the fixation of unstable zygomatic fractures. *J Oral Maxillofac Surg*, 51(6), pp.666–70.

Bhumiratana, S. et al., 2014. Large, stratified, and mechanically functional human cartilage grown in vitro by mesenchymal condensation. *Proceedings of the National Academy of Sciences of the United States of America*, 111(19), pp.6940–5.

Bianco, P. et al., 2001. Bone marrow stromal stem cells: nature, biology, and potential applications. *Stem cells*, 19(3), pp.180–192.

Bianco, P. et al., 2013. The meaning, the sense and the significance: translating the science of mesenchymal stem cells into medicine. *Nature medicine*, 19(1), pp.35–42.

Bissell, M.J. et al., 2002. The organizing principle: microenvironmental influences in the normal and malignant breast. *Differentiation; research in biological diversity*, 70(9-10), pp.537–46.

Bissell, M.J., Hall, H.G. & Parry, G., 1982. How does the extracellular matrix direct gene expression? *Journal of theoretical biology*, 99(1), pp.31–68.

Bisson, I. et al., 2002. Acrylic acid grafting and collagen immobilization on poly (ethylene terephthalate) surfaces for adherence and growth of human bladder smooth muscle cells. *Biomaterials*, 23, pp.3149–3158.

Black, I.B. & Woodbury, D., 2001. Adult rat and human bone marrow stromal stem cells differentiate into neurons. *Blood cells, molecules & diseases*, 27(3), pp.632–6.

Le Blanc, K., 2003. Immunomodulatory effects of fetal and adult mesenchymal stem cells. *Cytotherapy*, 5(6), pp.485–489.

Blanpain, C. et al., 2004. Self-renewal, multipotency, and the existence of two cell populations within an epithelial stem cell niche. *Cell*, 118(5), pp.635–648.

Borzì, R.M. et al., 2014. Polyamine delivery as a tool to modulate stem cell differentiation in skeletal tissue engineering. *Amino acids*, 46(3), pp.717–28.

Boxall, S. a. & Jones, E., 2012. Markers for characterization of bone marrow multipotential stromal cells. *Stem Cells International*, 2012.

Bühring, H.-J. et al., 2009. Phenotypic characterization of distinct human bone marrow-derived MSC subsets. *Annals of the New York Academy of Sciences*, 1176, pp.124–134.

Burdick, J. a & Anseth, K.S., 2002. Photoencapsulation of osteoblasts in injectable RGD-modified PEG hydrogels for bone tissue engineering. *Biomaterials*, 23(22), pp.4315–23.

Burdick, J. a & Prestwich, G.D., 2011. Hyaluronic acid hydrogels for biomedical applications. *Advanced materials (Deerfield Beach, Fla.)*, 23(12), pp.H41–H56.

Butcher, D.T., Alliston, T. & Weaver, V.M., 2009. A tense situation: forcing tumour progression. *Nature reviews. Cancer*, 9(2), pp.108–22.

Buttitta, L. a & Edgar, B. a, 2007. Mechanisms controlling cell cycle exit upon terminal differentiation. *Current opinion in cell biology*, 19(6), pp.697–704.

Caplan, A., 1991. Mesenchymal stem cells. *Journal of orthopaedic research : official publication of the Orthopaedic Research Society*, 9(5), pp.641–50.

Caplan, A.I. & Dennis, J.E., 2006. Mesenchymal stem cells as trophic mediators. *Journal of Cellular Biochemistry*, 98(5), pp.1076–1084.

Carrel, A., 1923. A METHOD FOR THE PHYSIOLOGICAL STUDY OF TISSUES IN VITRO. *J Exp Med*, 38, pp.407–418.

Carter, S., Rimmer, S., et al., 2005. Highly branched stimuli responsive poly[(N-isopropyl acrylamide)-co-(1,2-propandiol-3-methacrylate)]s with protein binding functionality. *Macromolecular bioscience*, 5(5), pp.373–8.

Carter, S., Hunt, B. & Rimmer, S., 2005. Highly Branched Poly (N - isopropylacrylamide) s with Imidazole End Groups Prepared by Radical Polymerization in the Presence of a Styryl Monomer Containing a Dithioester Group. *Macromolecules*, 38, pp.4595–4603.

Carter, S.R. et al., 2007. Functional graft poly(N-isopropyl acrylamide)s using reversible addition-fragmentation chain transfer (RAFT) polymerisation. *Macromolecular bioscience*, 7(8), pp.975–86.

Chan, N.L.M. et al., 2004. Umbilical vein and placental vessels from newborns with hereditary haemorrhagic telangiectasia type 1 genotype are normal despite reduced expression of endoglin. *Placenta*, 25(2-3), pp.208–217.

Charbord, P., 2010. Bone marrow mesenchymal stem cells: historical overview and concepts. *Human gene therapy*, 21(9), pp.1045–56.

Cheikh Al Ghanami, R. et al., 2010. Responsive particulate dispersions for reversible building and deconstruction of 3D cell environments. *Soft Matter*, 6(20), p.5037.

Chen, J. et al., 2012. Enhanced Osteogenesis of Human Mesenchymal Stem Cells by Periodic Heat Shock in Self-assembling Peptide Hydrogel. *Tissue Engineering Part A*, 19, p.121017044458000.

Chen, X.-D., 2010. Extracellular matrix provides an optimal niche for the maintenance and propagation of mesenchymal stem cells. *Birth defects research. Part C, Embryo today : reviews*, 90(1), pp.45–54.

Cheng, A. & Genever, P.G., 2010. SOX9 determines RUNX2 transactivity by directing intracellular degradation. *Journal of Bone and Mineral Research*, 25(12), pp.2404–2413.

Cheng, D. et al., 2012. Tuning properties of injectable hydrogel scaffold by PEG blending. *Polymer*, 53(22), pp.5124–5131.

Cheng, H., Shen, L. & Wu, C., 2006. LLS and FTIR Studies on the Hysteresis in Association and Dissociation of Poly(N- isopropylacrylamide) Chains in Water. *Macromolecules*, 39(6), pp.2325–2329.

Cheng, K., Lai, Y. & Kisaalita, W.S., 2008. Three-dimensional polymer scaffolds for high throughput cell-based assay systems. *Biomaterials*, 29(18), pp.2802–12.

Chiefari, J. et al., 1998. Living free-radical polymerization by reversible addition-fragmentation chain transfer: the RAFT process. *Macromolecules*, 31(16), pp.5559–5562.

Christman, K.L. et al., 2004. Injectable fibrin scaffold improves cell transplant survival, reduces infarct expansion, and induces neovasculature formation in ischemic myocardium. *Journal of the American College of Cardiology*, 44(3), pp.654–660.

Chueh, B.H. et al., 2010. Patterning alginate hydrogels using light-directed release of caged calcium in a microfluidic device. *Biomedical Microdevices*, 12(1), pp.145–151.

Chun, C. et al., 2009. The use of injectable, thermosensitive poly(organophosphazene)-RGD conjugates for the enhancement of mesenchymal stem cell osteogenic differentiation. *Biomaterials*, 30(31), pp.6295–6308.

Chung, E. et al., 2006. Biomimetic artificial ECMs stimulate bone regeneration. ... *Research Part A*, 79A(4), pp.815–826.

Chung, J.E. et al., 1998. Effect of molecular architecture of hydrophobically modified poly(N-isopropylacrylamide) on the formation of thermoresponsive core-shell micellar drug carriers. *Journal of controlled release : official journal of the Controlled Release Society*, 53(1-3), pp.119–30.

Clabaut, A. et al., 2010. Human osteoblasts derived from mesenchymal stem cells express adipogenic markers upon coculture with bone marrow adipocytes. *Differentiation*, 80(1), pp.40–45.

Clineff, T.D. et al., 2005. Analytical technique for quantification of selected resorbable calcium phosphate bone void fillers with the use of polarized-light microscopy. *Journal of biomedical materials research. Part B, Applied biomaterials*, 72(1), pp.125–30.

Clinicaltrials.gov, 2014. No Title. Available at: http://www.clinicaltrials.gov/ct2/results/details?term=embryonic+stem+cells.

Colombres, M. et al., 2008. Heparin activates Wnt signaling for neuronal morphogenesis. *Journal of cellular physiology*, 216(3), pp.805–15.

Colorado, P.C. et al., 2000. Anti-angiogenic Cues from Vascular Basement Membrane Collagen Anti-angiogenic Cues from Vascular Basement Membrane Collagen. *Cancer Res*, 60, pp.2520–2526.

Cooperstein, M. a & Canavan, H.E., 2013. Assessment of cytotoxicity of (N-isopropyl acrylamide) and Poly(N-isopropyl acrylamide)-coated surfaces. *Biointerphases*, 8(1), p.23.

Corning, 2013. Corning® Matrigel® Matrix Frequently Asked Questions. Available at: http://csmedia2.corning.com/LifeSciences//media/pdf/faq_DL_026_Corning_Matrigel_Matrix.pdf.

Covas, D.T. et al., 2008. Multipotent mesenchymal stromal cells obtained from diverse human tissues share functional properties and gene-expression profile with CD146 + perivascular cells and fibroblasts. *Experimental Hematology*, 36(5), pp.642–654.

Cracknell, R., 2010. The ageing population. *Key Issues for the New Parlament 2010*, pp.44–45.

Crisan, M. et al., 2008. A perivascular origin for mesenchymal stem cells in multiple human organs. *Cell stem cell*, 3(3), pp.301–13.

Crisostomo, P.R. et al., 2008. Human mesenchymal stem cells stimulated by TNF-alpha, LPS, or hypoxia produce growth factors by an NF kappa B- but not JNK-dependent mechanism. *American journal of physiology. Cell physiology*, 294(3), pp.C675–C682.

Cukierman, E. et al., 2001. Taking cell-matrix adhesions to the third dimension. *Science (New York, N.Y.)*, 294(5547), pp.1708–12.

Cushing, M.C. & Anseth, K.S., 2007. Hydrogel cell cultures. *Science (New York, N.Y.)*, 316(5828), pp.1133–4.

Cuthbert, R. et al., 2012. Single-platform quality control assay to quantify multipotential stromal cells in bone marrow aspirates prior to bulk manufacture or direct therapeutic use. *Cytotherapy*, 14(4), pp.431–440.

Cuthbert, R.J. et al., 2015. Examining the Feasibility of Clinical Grade CD271+ Enrichment of Mesenchymal Stromal Cells for Bone Regeneration. *Plos One*, 10(3), p.e0117855.

Dai, Z. et al., 2014. Effects of pH and thermally sensitive hybrid gels on osteogenic differentiation of mesenchymal stem cells. *Journal of Biomaterials Applications*, 29(9), pp.1272–1283.

Daley, W., Peters, S. & Larsen, M., 2008. Extracellular matrix dynamics in development and regenerative medicine. *Journal of cell science*, 121(3), pp.255–264.

Darling, E.M. & Athanasiou, K.A., 2006. Rapid phenotypic changes in passaged articular chondrocyte subpopulations. *Journal of Orthopaedic Research*, 23(2), pp.425–432.

Delair, T., 2012. In situ forming polysaccharide-based 3D-hydrogels for cell delivery in regenerative medicine. *Carbohydrate Polymers*, 87(2), pp.1013–1019.

Dickinson, M.E., 2006. Multimodal imaging of mouse development: tools for the postgenomic era. *Developmental dynamics : an official publication of the American Association of Anatomists*, 235(9), pp.2386–400.

Digirolamo, C.M. et al., 1999. Propagation and senescence of human marrow stromal cells in culture: A simple colony-forming assay identifies samples with the greatest potential to propagate and differentiate. *British Journal of Haematology*, 107(2), pp.275–281.

DiMarino, A.M., Caplan, A.I. & Bonfield, T.L., 2013. Mesenchymal stem cells in tissue repair. *Frontiers in Immunology*, 4(JUL), pp.1–9.

Ding, Y., Ye, X. & Zhang, G., 2005a. Microcalorimetric investigation on aggregation and dissolution of poly (N-isopropylacrylamide) chains in water. *Macromolecules*, 38, pp.904–908.

Ding, Y. & Zhang, G., 2006. Microcalorimetric investigation on association and dissolution of poly (N-isopropylacrylamide) chains in semidilute solutions. *Macromolecules*, 39, pp.9654–9657.

Discher, D.E., Janmey, P. & Wang, Y.-L., 2005. Tissue cells feel and respond to the stiffness of their substrate. *Science (New York, N.Y.)*, 310(5751), pp.1139–43.

Dojindo, Cell Counting Kit 8. Available at: http://www.dojindo.com/store/p/456-Cell-Counting-Kit-8.html.

Dolatshahi-Pirouz, A. et al., 2014. A combinatorial cell-laden gel microarray for inducing osteogenic differentiation of human mesenchymal stem cells. *Scientific reports*, 4, p.3896.

Dominici, M. et al., 2006. Minimal criteria for defining multipotent mesenchymal stromal cells. The International Society for Cellular Therapy position statement. *Cytotherapy*, 8(4), pp.315–317.

Domm, C. et al., 2002. Redifferentiation of dedifferentiated bovine articular chondrocytes in alginate culture under low oxygen tension. *Osteoarthritis and cartilage*, 10, pp.13–22.

Doycheva, M. et al., 2004. UV-Induced Cross-Linking of Poly(ethylene oxide) in Aqueous Solution. *Macromolecular Materials and Engineering*, 289(7), pp.676–680.

Duan, Q. et al., 2006. Thermoresponsive Property Controlled by End-Functionalization of Poly(N-isopropylacrylamide) with Phenyl, Biphenyl, and Triphenyl Groups. *Polymer Journal*, 38(3), pp.306–310.

Dugdale, D., 2013. Aging changes in organs - tissue - cells. Available at: http://www.nlm.nih.gov/medlineplus/ency/article/004012.htm.

Dvorak, H.F., 1986. Tumors: wounds that do not heal. Similarities between tumor stroma generation and wound healing. *The New England journal of medicine*, 315(26), pp.1650–1659.

Dyson, J. a et al., 2007. Development of custom-built bone scaffolds using mesenchymal stem cells and apatite-wollastonite glass-ceramics. *Tissue engineering*, 13(12), pp.2891–901.

Ebara, M. et al., 2014. Introductory Guide to Smart Biomaterials. In *Smart Biomaterials*. NIMS Monographs. Tokyo: Springer Japan, pp. 1–7.

Economist.com, 2010. The Silver tsunami. *The Economist*. Available at: http://www.economist.com/node/15450864.

Eldesoqi, K. et al., 2014. Safety evaluation of a bioglass-polylactic acid composite scaffold seeded with progenitor cells in a rat skull critical-size bone defect. *PLoS ONE*, 9(2), pp.1–13.

Elliott, J.E. et al., 2004. Structure and swelling of poly(acrylic acid) hydrogels: Effect of pH, ionic strength, and dilution on the crosslinked polymer structure. *Polymer*, 45(5), pp.1503–1510.

England, R. & Rimmer, S., 2010. Synthesis of chain end functionalized linear and branched polymers by radical polymerisation in the presence of a silyl enol. *Chemical communications (Cambridge, England)*, 46(31), pp.5767–9.

England & Rimmer, S., 2010. Hyper/highly-branched polymers by radical polymerisations. *Polymer Chemistry*, 1(10), p.1533.

Engler, A.J. et al., 2006. Matrix elasticity directs stem cell lineage specification. *Cell*, 126(4), pp.677–689.

Etheridge, S.L. et al., 2004. Expression profiling and functional analysis of wnt signaling mechanisms in mesenchymal stem cells. *Stem cells*, 22(5), pp.849–860.

Evans, H.J. et al., 2003. Novel 3D culture system for study of cardiac myocyte development. *American journal of physiology. Heart and circulatory physiology*, 285(2), pp.H570–8.

Filipak, M. et al., 1989. Integrated control of proliferation and differentiation of mesenchymal stem cells. *Environmental health perspectives*, 80, pp.117–25.

Findikli, N., Candan, N. & Kahraman, S., 2006. Human embryonic stem cell culture: current limitations and novel strategies. *Reproductive BioMedicine Online*, 13(4), pp.581–590.

Fischer, R.S. et al., 2012. Stiffness-controlled three-dimensional extracellular matrices for high-resolution imaging of cell behavior. *Nature protocols*, 7(11), pp.2056–66.

Fong, C.-Y., Gauthaman, K. & Bongso, A., 2010. Teratomas from pluripotent stem cells: A clinical hurdle. *Journal of cellular biochemistry*, 111(4), pp.769–81.

Fonseca, K.B. et al., 2011. Molecularly designed alginate hydrogels susceptible to local proteolysis as three-dimensional cellular microenvironments. *Acta biomaterialia*, 7(4), pp.1674–82.

Fraylich, M.R. et al., 2010. Thermally-triggered gelation of PLGA dispersions: Towards an injectable colloidal cell delivery system. *Journal of Colloid and Interface Science*, 344(1), pp.61–69.

Fridman, R. et al., 1990. Reconstituted basement membrane (matrigel) and laminin can enhance the tumorigenicity and the drug resistance of small cell lung cancer

cell lines. *Proceedings of the National Academy of Sciences of the United States of America*, 87(17), pp.6698–6702.

Friedenstein, A.J., 1976. Precursor cells of mechanocytes. *International review of cytology*, 47, pp.327–359.

Friedenstein, A.J., Chailakhyan, R.K. & Gerasimov, U. V, 1987. Bone marrow osteogenic stem cells: in vitro cultivation and transplantation in diffusion chambers. *Cell and tissue kinetics*, 20(3), pp.263–272.

Friedenstein, A.J., Piatetzky-Shapiro, I.I. & Petrakova, K. V, 1966. Osteogenesis in transplants of bone marrow cells. *Journal of embryology and experimental morphology*, 16(3), pp.381–390.

Friedl, P., 2004. Prespecification and plasticity: shifting mechanisms of cell migration. *Current opinion in cell biology*, 16(1), pp.14–23.

Frith, J.E., Thomson, B. & Genever, P.G., 2010. Dynamic Three-Dimensional Culture Methods and Increase Therapeutic Potential. *Tissue Engineering Part C*, 16(4), pp.735–749.

Frith, J.E., Thomson, B. & Genever, P.G., 2009. Dynamic three-dimensional culture methods enhance mesenchymal stem cell properties and increase therapeutic potential. *Tissue Engineering Part C: Methods*, Ahead of p, pp.1–44.

Fu, J. et al., 2010. Mechanical regulation of cell function with geometrically modulated elastomeric substrates. *Nature methods*, 7(9), pp.733–6.

Futaki, S. et al., 2001. Arginine-rich peptides. An abundant source of membrane-permeable peptides having potential as carriers for intracellular protein delivery. *The Journal of biological chemistry*, 276(8), pp.5836–40.

Galperin, A., Long, T.J. & Ratner, B.D., 2010. Degradable, Thermo-Sensitive Poly(N-isopropyl acrylamide)-Based Scaffolds with Controlled Porosity for Tissue Engineering Applications. *Biomacromolecules*, 11, pp.2583–2592.

Gan, T., Guan, Y. & Zhang, Y., 2010. Thermogelable PNIPAM microgel dispersion as 3D cell scaffold: effect of syneresis. *Journal of Materials Chemistry*, 20(28), p.5937.

Gan, T., Zhang, Y. & Guan, Y., 2009. In situ gelation of P(NIPAM-HEMA) microgel dispersion and its applications as injectable 3D cell scaffold. *Biomacromolecules*, 10(6), pp.1410–5.

Gil, E. & Hudson, S., 2004. Stimuli-reponsive polymers and their bioconjugates. *Progress in Polymer Science*, 29(12), pp.1173–1222.

Gilbert, S., 2000. The Neural Crest. In *Developmental Biology. 6th edition.* Sinauer Associates.

Gillette, B.M. et al., 2008. In situ collagen assembly for integrating microfabricated three-dimensional cell-seeded matrices. *Nature materials*, 7(8), pp.636–40.

Gilmore, L. et al., 2013. Arginine functionalization of hydrogels for heparin binding--a supramolecular approach to developing a pro-angiogenic biomaterial. *Biotechnology and bioengineering*, 110(1), pp.296–317.

Giobbe, G. et al., 2012. Confined 3D microenvironment regulates early differentiation in human pluripotent stem cells. *Biotechnology and ...*, 109(12), pp.3119–3132.

Glazer, P.J. et al., 2013. Multi-Stimuli Responsive Hydrogel Cilia. *Advanced Functional Materials*, 23(23), pp.2964–2970.

Gogolewski, S. et al., 1993. Tissue response and in vivo degradation of selected polyhydroxyacids: polylactides (PLA), poly(3-hydroxybutyrate) (PHB), and poly(3-hydroxybutyrate-co-3-hydroxyvalerate) (PHB/VA). *Journal of biomedical materials research*, 27(9), pp.1135–1148.

Granéli, C. et al., 2014. Novel markers of osteogenic and adipogenic differentiation of human bone marrow stromal cells identified using a quantitative proteomics approach. *Stem Cell Research*, 12(1), pp.153–165.

Grayson, W.L. et al., 2010. Engineering anatomically shaped human bone grafts. *Proceedings of the National Academy of Sciences of the United States of America*, 107(8), pp.3299–304.

Graziano, G., 2000. On the temperature-induced coil to globule transition of poly-N-isopropylacrylamide in dilute aqueous solutions. *International journal of biological macromolecules*, 27(1), pp.89–97.

Gronthos, S. et al., 2003. Molecular and cellular characterisation of highly purified stromal stem cells derived from human bone marrow. *Journal of cell science*, 116(Pt 9), pp.1827–1835.

Gronthos, S. et al., 2000. Postnatal human dental pulp stem cells (DPSCs) in vitro and in vivo. *Proceedings of the National Academy of Sciences of the United States of America*, 97(25), pp.13625–13630.

Gruber, H.E. et al., 2006. Three-dimensional culture of human disc cells within agarose or a collagen sponge: Assessment of proteoglycan production. *Biomaterials*, 27(3), pp.371–376.

Guan, Y. & Zhang, Y., 2011. PNIPAM microgels for biomedical applications: from dispersed particles to 3D assemblies. *Soft Matter*, 7(14), p.6375.

Guilherme, M.R. et al., 2006. Thermo-responsive sandwiched-like membranes of IPN-PNIPAAm/PAAm hydrogels. *Journal of Membrane Science*, 275(1-2), pp.187–194.

Gutowska, A. et al., 2008. Biomaterials for stem cell differentiation. *Advanced drug delivery reviews*, 60(2), pp.215–28.

Gutowska, A. et al., 1992. Heparin release from thermosensitive hydrogels. *Journal of Controlled Release*, 22(2), pp.95–104.

Gutowska, A. et al., 1995. Heparin release from thermosensitive polymer coatings: in vivo studies. *Journal of biomedical materials research*, 29(7), pp.811–21.

Gutowska, A. et al., 1994. Thermosensitive Interpenetratirig Polymer Networks: Synthesis, Characterization, and Macromolecular Release. , pp.4167–4175.

Halfon, S. et al., 2011. Markers distinguishing mesenchymal stem cells from fibroblasts are downregulated with passaging. *Stem cells and development*, 20(1), pp.53–66.

Härmä, V. et al., 2010. A comprehensive panel of three-dimensional models for studies of prostate cancer growth, invasion and drug responses. *PloS one*, 5(5), p.e10431.

Hartmann, C. & Tabin, C.J., 2000. Dual roles of Wnt signaling during chondrogenesis in the chicken limb. *Development (Cambridge, England)*, 127(14), pp.3141–3159.

Hass, R. et al., 2011. Different populations and sources of human mesenchymal stem cells (MSC): A comparison of adult and neonatal tissue-derived MSC. *Cell communication and signaling : CCS*, 9(1), p.12.

Hauser, S. et al., 2012. Isolation of Novel Multipotent Neural Crest-Derived Stem Cells from Adult Human Inferior Turbinate. *Stem Cells and Development*, 21(5), pp.742–756.

Hay, M. et al., 2014. Clinical development success rates for investigational drugs. *Nature biotechnology*, 32(1), pp.40–51.

Hayward, A.S. et al., 2013. Acrylic-acid-functionalized polyhipe scaffolds for use in 3d cell culture. *Macromolecular Rapid Communications*, 34(23-24), pp.1844–1849.

Hennink, W.E. & van Nostrum, C.F., 2012. Novel crosslinking methods to design hydrogels. *Advanced Drug Delivery Reviews*, 64, pp.223–236.

Heskins, M. & Guillet, J.E., 1968. Solution Properties of Poly(N-isopropylacrylamide). *Journal of Macromolecular Science: Part A - Chemistry*, 2(8), pp.1441–1455.

Higuchi, A. et al., 2012. Biomimetic Cell Culture Proteins as Extracellular Matrices for Stem Cell Di ff erentiation. *Chemical Reviews*, 112(8), pp.4507–4540.

Higuchi, A. et al., 2013. Physical cues of biomaterials guide stem cell differentiation fate. *Chemical reviews*, 113(5), pp.3297–328.

Hirschhaeuser, F. et al., 2010. Multicellular tumor spheroids: an underestimated tool is catching up again. *Journal of biotechnology*, 148(1), pp.3–15.

Hofstetter, C.P. et al., 2002. Marrow stromal cells form guiding strands in the injured spinal cord and promote recovery. *Proceedings of the National Academy of Sciences of the United States of America*, 99(4), pp.2199–204.

Holopainen, I.E., 2005. Organotypic hippocampal slice cultures: a model system to study basic cellular and molecular mechanisms of neuronal cell death, neuroprotection, and synaptic plasticity. *Neurochemical research*, 30(12), pp.1521–8.

Hölter, D., Burgath, A. & Frey, H., 1997. Degree of branching in hyperbranched polymers. *Acta Polymerica*, 35, pp.30–35.

Hong, Y. et al., 2007. Covalently crosslinked chitosan hydrogel: Properties of in vitro degradation and chondrocyte encapsulation. *ACTA BIOMATERIALIA*, 3(1), pp.23–31.

Hopkins, S. et al., 2009. Sub-micron poly(N-isopropylacrylamide) particles as temperature responsive vehicles for the detachment and delivery of human cells. *Soft Matter*, 5(24), pp.4928–4937.

Horwitz, E.M. et al., 2005. Clarification of the nomenclature for MSC: The International Society for Cellular Therapy position statement. *Cytotherapy*, 7(5), pp.393–395.

Huang, A.H. et al., 2008. High-throughput screening for modulators of mesenchymal stem cell chondrogenesis. *Annals of biomedical engineering*, 36(11), pp.1909–21.

Hunt, N.C. & Grover, L.M., 2010. Cell encapsulation using biopolymer gels for regenerative medicine. *Biotechnology letters*.

Hutmacher, D.W., 2000. Scaffolds in tissue engineering bone and cartilage. *Biomaterials*, 21(24), pp.2529–43.

Ibusuki, S. et al., 2003. Tissue-Engineered Cartilage Using an Injectable and in Situ Gelable Thermoresponsive Gelatin : Fabrication and in Vitro Performance. *Tissue Engineering*, 9(2).

Idziak, I. et al., 1999. Thermosensitivity of Aqueous Solutions of Poly (N , N - diethylacrylamide). *Macromolecules*, 32, pp.1260–1263.

Ilic-Stojanovic, S. et al., 2011. Stimuli-sensitive hydrogels for pharmaceutical and medical applications. *Facta universitatis - series: Physics, Chemistry and Technology*, 9(1), pp.37–56.

Ingber, D.E., 1997. Tensegrity: The Architectural Basis of Cellular Mechanotransduction. *Annu. Rev. Physiol.*, 59, pp.575–99.

Isern, J. et al., 2013. Self-renewing human bone marrow mesenspheres promote hematopoietic stem cell expansion. *Cell reports*, 3(5), pp.1714–24.

Isern, J. et al., 2014. The neural crest is a source of mesenchymal stem cells with specialized hematopoietic stem cell niche function. *eLife*, 3, pp.1–28.

Ishii, M. et al., 2005. Molecular markers distinguish bone marrow mesenchymal stem cells from fibroblasts. *Biochemical and Biophysical Research Communications*, 332(1), pp.297–303.

Jabs, A., Determination of Secondary Structure in Proteins by Fourier Transform Infrared Spectroscopy (FTIR).

Jaiswal, R.K. et al., 2000. Adult Human Mesenchymal Stem Cell Differentiation to the Osteogenic or Adipogenic Lineage Is Regulated by Mitogen-activated Protein Kinase. *Journal of Biological Chemistry*, 275(13), pp.9645–9652.

Jakob, M. et al., 2012. Perspective on the Evolution of Cell-Based Bone Tissue Engineering Strategies. *European Surgical ...*, 49, pp.1–7.

James, A.W., 2013. Review of Signaling Pathways Governing MSC Osteogenic and Adipogenic Differentiation. *Scientifica*, 2013, p.684736.

Janmey, P. a, Winer, J.P. & Weisel, J.W., 2009. Fibrin gels and their clinical and bioengineering applications. *Journal of the Royal Society, Interface / the Royal Society*, 6(30), pp.1–10.

Janmey, P., Amis, E. & Ferry, J., 1983. Rheology of Fibrin Clots. VI. Stress Relaxation, Creep, and Differential Dynamic Modulus of Fine Clots in Large Shearing Deformations. *Journal of Rheology*, 27(135).

Jha, A.K., Jackson, W.M. & Healy, K.E., 2014. Controlling Osteogenic Stem Cell Differentiation via Soft Bioinspired Hydrogels. *PloS one*, 9(6), pp.1–11.

Jikei, M. & Kakimoto, M., 2001. Hyperbranched polymers: a promising new class of materials. *Progress in Polymer Science*, 26(8), pp.1233–1285.

Jones, D.L. & Wagers, A.J., 2008. No place like home: anatomy and function of the stem cell niche. *Nature Reviews Molecular Cell Biology*, 9, pp.11–21.

Jones, E. et al., 2004. Enumeration and Phenotypic Characterization of Synovial Fluid Multipotential Mesenchymal Progenitor Cells in Inflammatory and Degenerative Arthritis. *Arthritis and Rheumatism*, 50(3), pp.817–827.

Jones, E. et al., 2010. Large-scale extraction and characterization of CD271+ multipotential stromal cells from trabecular bone in health and osteoarthritis: Implications for bone regeneration strategies based on uncultured or minimally

cultured multipotential stromal cells. *Arthritis and Rheumatism*, 62(7), pp.1944–1954.

Jones, E. & McGonagle, D., 2008. Human bone marrow mesenchymal stem cells in vivo. *Rheumatology (Oxford, England)*, 47(2), pp.126–31.

Jongpaiboonkit, L., King, W.J. & Murphy, W.L., 2009. Screening for 3D environments that support human mesenchymal stem cell viability using hydrogel arrays. *Tissue engineering. Part A*, 15(2), pp.343–53.

Jung, E.M. et al., 2011. Evidences for correlation between the reduced VCAM-1 expression and hyaluronan synthesis during cellular senescence of human mesenchymal stem cells. *Biochemical and Biophysical Research Communications*, 404(1), pp.463–469.

Kang, Q. et al., 2009. A comprehensive analysis of the dual roles of BMPs in regulating adipogenic and osteogenic differentiation of mesenchymal progenitor cells. *Stem cells and development*, 18(4), pp.545–59.

Karoubi, G. et al., 2009. Single-cell hydrogel encapsulation for enhanced survival of human marrow stromal cells. *Biomaterials*, 30(29), pp.5445–5455.

Kilian, K. a et al., 2010. Geometric cues for directing the differentiation of mesenchymal stem cells. *Proceedings of the National Academy of Sciences of the United States of America*, 107(11), pp.4872–7.

Kim, M. et al., 2012. Age-related alterations in mesenchymal stem cells related to shift in differentiation from osteogenic to adipogenic potential: implication to age-associated bone diseases and defects. *Mechanisms of ageing and development*, 133(5), pp.215–25.

Klaikherd, A., Nagamani, C. & Thayumanavan, S., 2009. Multi-stimuli sensitive amphiphilic block copolymer assemblies. *Journal of the American Chemical Society*, 131(13), pp.4830–8.

Kloxin, A.M. et al., 2009. Photodegradable hydrogels for dynamic tuning of physical and chemical properties. *Science (New York, N.Y.)*, 324(5923), pp.59–63.

Koehler, K.R. et al., 2013. Generation of inner ear sensory epithelia from pluripotent stem cells in 3D culture. *Nature*, 500(7461), pp.217–21.

Kogan, G. et al., 2007. Hyaluronic acid: A natural biopolymer with a broad range of biomedical and industrial applications. *Biotechnology Letters*, 29(1), pp.17–25.

Kolf, C.M., Cho, E. & Tuan, R.S., 2007. Mesenchymal stromal cells. Biology of adult mesenchymal stem cells: regulation of niche, self-renewal and differentiation. *Arthritis research & therapy*, 9(1).

Kraehenbuehl, T.P., Langer, R. & Ferreira, L.S., 2011. Three-dimensional biomaterials for the study of human pluripotent stem cells. *Nature Methods*, 8(9), pp.731–736.

Kubota, K., Fujishige, S. & Ando, I., 1990. Solution properties of poly(N-isopropylacrylamide) in water. *Polymer Journal*, 22(1), pp.15–20.

Kuhn, N. & Tuan, R., 2010. Regulation of stemness and stem cell niche of mesenchymal stem cells: implications in tumorigenesis and metastasis. *Journal of cellular physiology*, 222(2), pp.268–77.

Kulterer, B. et al., 2007. Gene expression profiling of human mesenchymal stem cells derived from bone marrow during expansion and osteoblast differentiation. *BMC genomics*, 8, p.70.

Kunz-Schughart, L. a et al., 2004. The use of 3-D cultures for high-throughput screening: the multicellular spheroid model. *Journal of biomolecular screening*, 9(4), pp.273–85.

Labusca, L., O'Brien, M. & Mashayekhi, K., 2013. A clinical perspective to mesenchymal stem cell-based musculoskeletal regeneration. *OA Musculoskeletal Medicine*, 1(1), pp.1–6.

Lai, J.Y., 2010. Biocompatibility of chemically cross-linked gelatin hydrogels for ophthalmic use. *Journal of Materials Science: Materials in Medicine*, 21(6), pp.1899–1911.

Lai, Y. et al., 2010. Reconstitution of marrow-derived extracellular matrix ex vivo: a robust culture system for expanding large-scale highly functional human mesenchymal stem cells. *Stem cells and development*, 19(7), pp.1095–107.

Langer, R. & Vacanti, J., 1993. Tissue Engineering. *Science*, 260(5110), pp.920–6.

Lapworth, J.W. et al., 2011. Thermally reversible colloidal gels for three-dimensional chondrocyte culture. *Interface*, 9(67), pp.362–75.

Lapworth, J.W., 2009. *Thermally-responsive Polymers for 3D Chondrocyte Culture*. Univeristy of Sheffield.

Laukkanen, A. et al., 2004. Formation of Colloidally Stable Phase Separated Poly (N -vinylcaprolactam) in Water : A Study by Dynamic Light Scattering , Microcalorimetry , and Pressure Perturbation Calorimetry. , pp.2268–2274.

Lawrence, B.J. & Madihally, S. V, 2008. Cell colonization in degradable 3D porous matrices. *Cell adhesion & migration*, 2(1), pp.9–16.

Leach, J.B. et al., 2003. Photocrosslinked hyaluronic acid hydrogels: Natural, biodegradable tissue engineering scaffolds. *Biotechnology and Bioengineering*, 82(5), pp.578–589.

Lee, K.Y. & Mooney, D.J., 2012. Alginate: Properties and biomedical applications. *Progress in Polymer Science (Oxford)*, 37(1), pp.106–126.

Lee, K.Y. & Mooney, D.J., 2001. Hydrogels for Tissue Engineering. *Chemical Reviews*, 101(7), pp.1869–1880.

Lee, Y., Kim, S. & Cho, C., 1996. Synthesis and swelling characteristics of pH and thermoresponsive interpenetrating polymer network hydrogel composed of poly (vinyl alcohol) and poly (acrylic acid). *Journal of applied polymer science*, 62, pp.301–311.

Legant, W.R. et al., 2010. Measurement of mechanical tractions exerted by cells in three-dimensional matrices. *Nature methods*, 7(12), pp.969–71.

Lei, Y. & Schaffer, D. V, 2013. A fully defined and scalable 3D culture system for human pluripotent stem cell expansion and differentiation. *Proceedings of the National Academy of Sciences of the United States of America*, 110(52), pp.E5039–48.

Lennon, D.P., Edmison, J.M. & Caplan, a I., 2001. Cultivation of rat marrow-derived mesenchymal stem cells in reduced oxygen tension: effects on in vitro and in vivo osteochondrogenesis. *Journal of cellular physiology*, 187(3), pp.345–55.

Leychkis, Y., Munzer, S.R. & Richardson, J.L., 2009. What is stemness? *Studies in History and Philosophy of Science Part C :Studies in History and Philosophy of Biological and Biomedical Sciences*, 40(4), pp.312–320.

Li, J. et al., 2003. Culture of primary rat hepatocytes within porous chitosan scaffolds. *Journal of biomedical materials research. Part A*, 67(3), pp.938–943.

Liao, Zhang, Y., et al., 2011. Gelation Kinetics of Thermosensitive PNIPAM Microgel Dispersions. *Macromolecular Chemistry and Physics*, 212(18), pp.2052–2060.

Liao, Chen & Chen, 2011. Osteogenic Differentiation and Ectopic Bone Formation of Canine Bone Marrow-Derived Mesenchymal Stem Cells in Injectable Thermo-Responsive Polymer Hydrogel. *Tissue Engineering Part C: Methods*, 17(11), pp.1139–1149.

Lin, C.S. et al., 2013. Commonly used mesenchymal stem cell markers and tracking labels: Limitations and challenges. *Histology and Histopathology*, 28(9), pp.1109–1116.

Lindner, U. et al., 2010. Mesenchymal Stem or Stromal Cells: Toward a Better Understanding of Their Biology? *Transfusion medicine and hemotherapy : offizielles Organ der Deutschen Gesellschaft fur Transfusionsmedizin und Immunhamatologie*, 37(2), pp.75–83.

Liu, F. et al., 2008. Changes in the expression of CD106, osteogenic genes, and transcription factors involved in the osteogenic differentiation of human bone

marrow mesenchymal stem cells. *Journal of Bone and Mineral Metabolism*, 26(4), pp.312–320.

Liu, Z. et al., 2002. Coordination of chondrogenesis and osteogenesis by fibroblast growth factor 18. *Genes and Development*, 16(7), pp.859–869.

Lodish, H. et al., 2000. Noncovalent Bonds. In *Molecular Cell Biology, 4th edition*.

Loebinger, M.R. et al., 2009. Mesenchymal stem cell delivery of TRAIL can eliminate metastatic cancer. *Cancer Research*, 69(10), pp.4134–4142.

Lu, D. et al., 2011. Salinomycin inhibits Wnt signaling and selectively induces apoptosis in chronic lymphocytic leukemia cells. *Proceedings of the National Academy of Sciences of the United States of America*, 2011, pp.2–7.

Lu, Y. et al., 2013. Solution behaviors and microstructures of PNIPAm-P123-PNIPAm pentablock terpolymers in dilute and concentrated aqueous solutions. *Physical chemistry chemical physics : PCCP*, 15(21), pp.8276–86.

Luo, W. et al., 2008. Disruption of cell-matrix interactions by heparin enhances mesenchymal progenitor adipocyte differentiation. *Experimental cell research*, 314(18), pp.3382–91.

Luscombe, N.M., Laskowski, R. a & Thornton, J.M., 2001. Amino acid-base interactions: a three-dimensional analysis of protein-DNA interactions at an atomic level. *Nucleic acids research*, 29(13), pp.2860–74.

Lutolf, Raeber, G., et al., 2003. Cell-responsive synthetic hydrogels. *Advanced Materials*, 15(11), pp.888–892.

Lutolf, Lauer-Fields, J.L., et al., 2003. Synthetic matrix metalloproteinase-sensitive hydrogels for the conduction of tissue regeneration: engineering cell-invasion characteristics. *Proceedings of the National Academy of Sciences of the United States of America*, 100(9), pp.5413–8.

Lutolf, M.P., 2009. Biomaterials: Spotlight on hydrogels. *Nature materials*, 8(6), pp.451–3.

Lv, F.-J. et al., 2014. Concise Review : The Surface Markers and Identity of Human Mesenchymal Stem Cells. *Stem Cells*, (32), pp.1408–1419.

Lynn, a. K., Yannas, I. V. & Bonfield, W., 2004. Antigenicity and immunogenicity of collagen. *Journal of Biomedical Materials Research - Part B Applied Biomaterials*, 71(2), pp.343–354.

Maeda, Y., Higuchi, T. & Ikeda, I., 2000. Change in hydration state during the coil-globule transition of aqueous solutions of poly (N-isopropylacrylamide) as evidenced by FTIR spectroscopy. *Langmuir*, 16, pp.7503–7509.

Mager, M.D., LaPointe, V. & Stevens, M.M., 2011. Exploring and exploiting chemistry at the cell surface. *Nature Chemistry*, 3(8), pp.582–589.

Majumdar, M.K. et al., 1998. Phenotypic and functional comparison of cultures of marrow-derived mesenchymal stem cells (MSCs) and stromal cells. *Journal of cellular physiology*, 176(1), pp.57–66.

Malvern Instruments Ltd, Zeta Potential An Introduction in 30 Minutes. *Zeta Potential An Introduction in 30 Minutes*. Available at: http://www.nbtc.cornell.edu/facilities/downloads/Zeta potential - An introduction in 30 minutes.pdf [Accessed January 5, 2012].

Mano, J.F. et al., 2004. Bioinert, biodegradable and injectable polymeric matrix composites for hard tissue replacement: State of the art and recent developments. *Composites Science and Technology*, 64(6), pp.789–817.

Marie, P.J., 2008. Transcription factors controlling osteoblastogenesis. *Archives of Biochemistry and Biophysics*, 473(2), pp.98–105.

Martin, K.J. et al., 2008. Prognostic breast cancer signature identified from 3D culture model accurately predicts clinical outcome across independent datasets. *PloS one*, 3(8), p.e2994.

Martino, M.M. et al., 2009. Controlling integrin specificity and stem cell differentiation in 2D and 3D environments through regulation of fibronectin domain stability. *Biomaterials*, 30(6), pp.1089–97.

Matsumoto, Y., Iwasaki, H. & Suda, T., 2011. Maintenance of Adult Stem Cells: Role of the Stem Cell Niche. In D. G. Phinney, ed. *Adult Stem Cells: Biology and Methods of Analysis*. Totowa, NJ: Humana Press, pp. 35–56.

Mauney, J.R., Kaplan, D.L. & Volloch, V., 2004. Matrix-mediated retention of osteogenic differentiation potential by human adult bone marrow stromal cells during ex vivo expansion. *Biomaterials*, 25(16), pp.3233–43.

Mauney, J.R., Volloch, V. & Kaplan, D.L., 2005. Matrix-mediated retention of adipogenic differentiation potential by human adult bone marrow-derived mesenchymal stem cells during ex vivo expansion. *Biomaterials*, 26(31), pp.6167–75.

Maximow, A., 1909. Der Lymphozyt als gemeinsame Stammzelle der verschiedenen Blutelemente in der embryonalen Entwicklung und im postfetalen Leben der Säugetiere. *Folia Haematologica*, 8, pp.125–134.

Maximow, A.A., 2009. The lymphocyte as a stem cell, common to different blood elements in embryonic development and during the post-fetal life of mammals. *Cellular Therapy and Transplantation*, 1(3), pp.14–24.

Mazumder, M. a J. et al., 2012. Cell-adhesive thermogelling PNIPAAm/hyaluronic acid cell delivery hydrogels for potential application as minimally invasive

retinal therapeutics. *Journal of biomedical materials research. Part A*, pp.1877–1887.

McBeath, R. et al., 2004. Cell shape, cytoskeletal tension, and RhoA regulate stem cell lineage commitment. *Developmental cell*, 6(4), pp.483–95.

McElroy, S.L. & Reijo Pera, R. a., 2008. Culturing Human Embryonic Stem Cells in feeder-free conditions. *Cold Spring Harbor Protocols*, 3(9), pp.1–4.

Meirelles, L.D.S. et al., 2009. Mechanisms involved in the therapeutic properties of mesenchymal stem cells. *Cytokine & growth factor reviews*, 20(5-6), pp.419–27.

Méndez-Ferrer, S. et al., 2010. Mesenchymal and haematopoietic stem cells form a unique bone marrow niche. *Nature*, 466(7308), pp.829–34.

Meng, X. et al., 2014. Stem cells in a three-dimensional scaffold environment. *SpringerPlus*, 3, p.80.

Metters, A.T., Anseth, K.S. & Bowman, C.N., 2000. Fundamental studies of a novel, biodegradable PEG-b-PLA hydrogel. *Polymer*, 41(11), pp.3993–4004.

Mironov, V. et al., 2009. Organ printing: tissue spheroids as building blocks. *Biomaterials*, 30(12), pp.2164–74.

Moad, G., Rizzardo, E. & Thang, S.H., 2005. Living Radical Polymerization by the RAFT Process. *Australian Journal of Chemistry*, 58(6), p.379.

Mobini, S. & Solati-Hashjin, M., 2013. Bioactivity and Biocompatibility Studies on Silk-Based Scaffold for Bone Tissue Engineering. *Journal of Medical and Biological Engineering*, 33(2), pp.207–214.

Mohammed, J.S. & Murphy, W.L., 2009. Bioinspired Design of Dynamic Materials. *Advanced Materials*, 21(23), pp.2361–2374.

Mori, S. et al., 2009. An Anchorage-Independent Cell Growth Signature Identifies Tumors with Metastatic Potential. *Oncogene*, 28(31), pp.2796–2805.

Mosby, 2009. *Mosby's Medical Dictionary* 8th Editio., Mosby.

Muraglia, a, Cancedda, R. & Quarto, R., 2000. Clonal mesenchymal progenitors from human bone marrow differentiate in vitro according to a hierarchical model. *Journal of cell science*, 113 (Pt 7, pp.1161–1166.

Muzzarelli, R. et al., 1988. Biological activity of chitosan: ultrastructural study. *Biomaterials*, 9(3), pp.247–52.

Na, K. et al., 2007. Osteogenic differentiation of rabbit mesenchymal stem cells in thermo-reversible hydrogel constructs containing hydroxyapatite and bone morphogenic protein-2 (BMP-2). *Biomaterials*, 28(16), pp.2631–7.

Nakatsu, M.N., Davis, J. & Hughes, C.C.W., 2007. Optimized fibrin gel bead assay for the study of angiogenesis. *Journal of visualized experiments : JoVE*, 3(3), p.186.

Nakayama, Y. et al., 2007. Heparin bioconjugate with a thermoresponsive cationic branched polymer: a novel aqueous antithrombogenic coating material. *Langmuir : the ACS journal of surfaces and colloids*, 23(15), pp.8206–11.

Narravula, S. et al., 2000. Regulation of endothelial CD73 by adenosine: paracrine pathway for enhanced endothelial barrier function. *Journal of immunology (Baltimore, Md. : 1950)*, 165(9), pp.5262–5268.

Navarro, F. a. et al., 2001. Perfusion of medium improves growth of human oral neomucosal tissue constructs. *Wound Repair and Regeneration*, 9(6), pp.507–512.

Nehls, V. & Drenckhahn, D., 1995. A novel, microcarrier-based in vitro assay for rapid and reliable quantification of three-dimensional cell migration and angiogenesis. *Microvascular research*, 50(3), pp.311–322.

Nuttelman, C.R., Tripodi, M.C. & Anseth, K.S., 2005. Synthetic hydrogel niches that promote hMSC viability. *Matrix biology : journal of the International Society for Matrix Biology*, 24(3), pp.208–18.

Oberpenning, F. et al., 1999. De novo reconstitution of a functional mammalian urinary bladder by tissue engineering. *Nature biotechnology*, 17(2), pp.149–55.

Oh, J.K., Lee, D.I. & Park, J.M., 2009. Biopolymer-based microgels/nanogels for drug delivery applications. *Progress in Polymer Science*, 34(12), pp.1261–1282.

Olsen, B.R., Reginato, a M. & Wang, W., 2000. Bone development. *Annual review of cell and developmental biology*, 16, pp.191–220.

Omidian, H. & Park, K., 2010. Introduction to Hydrogels. In *Biomedical Applications of Hydrogels Handbook*. pp. 1–16.

Organdonation.nhs.uk, 2014. Organ Donation and Transplantation - Activity figures for the UK as at 11 April 2014. Available at: http://www.organdonation.nhs.uk/statistics/downloads/annual_stats.pdf.

Ossipov, D.A. et al., 2007. Formation of the first injectable poly (vinyl alcohol) hydrogel by mixing of functional PVA precursors. *Journal of Applied Polymer Science*, 106(1), pp.60–70.

Otte, A. et al., 2013. Mesenchymal stem cells maintain long-term in vitro stemness during explant culture. *Tissue engineering. Part C, Methods*, 19(12), pp.937–48.

Otto, F. et al., 1997. Cbfa1, a candidate gene for cleidocranial dysplasia syndrome, is essential for osteoblast differentiation and bone development. *Cell*, 89(5), pp.765–771.

Ovsianikov, A. et al., 2011. Laser fabrication of three-dimensional CAD scaffolds from photosensitive gelatin for applications in tissue engineering. *Biomacromolecules*, 12(4), pp.851–858.

Palmer, M. a, 1993. A gelatin test to detect activity and stability of proteases produced by Dichelobacter (Bacteroides) nodosus. *Veterinary microbiology*, 36(1-2), pp.113–122.

Pampaloni, F., Reynaud, E.G. & Stelzer, E.H.K., 2007. The third dimension bridges the gap between cell culture and live tissue. *Nature reviews. Molecular cell biology*, 8(10), pp.839–45.

PathologyOutlines.com & Dragos, L., 2012. Bone marrow -nonneoplastic normal osteoblasts. *Bone marrow -nonneoplastic normal osteoblasts*. Available at: http://www.pathologyoutlines.com/topic/bonemarrowosteoblasts.html.

Pek, Y.S. et al., 2008. A thixotropic nanocomposite gel for three-dimensional cell culture. *Nature nanotechnology*, 3(11), pp.671–5.

Pek, Y.S., Wan, A.C. a & Ying, J.Y., 2010. The effect of matrix stiffness on mesenchymal stem cell differentiation in a 3D thixotropic gel. *Biomaterials*, 31(3), pp.385–91.

Peroglio, M. et al., 2013. Thermoreversible hyaluronan-based hydrogel supports in vitro and ex vivo disc-like differentiation of human mesenchymal stem cells. *The spine journal : official journal of the North American Spine Society*, 13(11), pp.1627–39.

Petrie, R.J. & Yamada, K.M., 2012. At the leading edge of three-dimensional cell migration. *Journal of cell science*, 125(Pt 24), pp.5917–26.

Pittenger, M.F. et al., 1999. Multilineage potential of adult human mesenchymal stem cells. *Science (New York, N.Y.)*, 284(5411), pp.143–7.

Place, E.S. et al., 2009. Synthetic polymer scaffolds for tissue engineering. *Chemical Society reviews*, 38(4), pp.1139–1151.

Planat-Benard, V. et al., 2004. Plasticity of human adipose lineage cells toward endothelial cells: physiological and therapeutic perspectives. *Circulation*, 109(5), pp.656–63.

Polini, A. et al., 2011. Osteoinduction of human mesenchymal stem cells by bioactive composite scaffolds without supplemental osteogenic growth factors. *PloS one*, 6(10), p.e26211.

Poloni, a et al., 2009. Selection of CD271(+) cells and human AB serum allows a large expansion of mesenchymal stromal cells from human bone marrow. *Cytotherapy*, 11(2), pp.153–162.

Portalska, K. et al., 2012. Endothelial Differentiation of Mesenchymal Stromal Cells. *PLoS ONE*, 7(10).

Pricola, K. et al., 2009. Interleukin-6 maintains bone marrow-derived mesenchymal stem cell stemness by an ERK1/2-dependent mechanism. *J Cell Biochem*, 108, pp.577–588.

Prins, H.-J. et al., 2014. In vitro induction of alkaline phosphatase levels predicts in vivo bone forming capacity of human bone marrow stromal cells. *Stem cell research*, 12(2), pp.428–40.

Pyle, A.D., Donovan, P.J. & Lock, L.F., 2004. Chipping away at "stemness". *Genome biology*, 5(8), p.235.

Quirici, N. et al., 2002. Isolation of bone marrow mesenchymal stem cells by anti-nerve growth factor receptor antibodies. *Experimental Hematology*, 30(7), pp.783–791.

Raeber, G.P., Lutolf, M.P. & Hubbell, J. a, 2005. Molecularly engineered PEG hydrogels: a novel model system for proteolytically mediated cell migration. *Biophysical journal*, 89(2), pp.1374–1388.

Ren, C. et al., 2008. Cancer gene therapy using mesenchymal stem cells expressing interferon-beta in a mouse prostate cancer lung metastasis model. *Gene therapy*, 15(21), pp.1446–1453.

Reubinoff, B.E. et al., 2000. Embryonic stem cell lines from human blastocysts: somatic differentiation in vitro. *Nature biotechnology*, 18(4), pp.399–404.

Rheologyschool.com, 2013. The A-Z of Rheology & Viscosity - from Angles to Zero Shear Viscosity. Available at: http://www.rheologyschool.com/advice/rheology-glossary.

Rhoads, J.M. et al., 2004. Arginine stimulates intestinal cell migration through a focal adhesion kinase dependent mechanism. *Gut*, 53(4), pp.514–522.

Rimmer, S. et al., 2007. Highly branched poly-(N-isopropylacrylamide)s with arginine–glycine– aspartic acid (RGD)- or COOH-chain ends that form sub-micron stimulus-responsive particles above the critical solution temperature. *Soft Matter*, 3(8), p.971.

Rimmer, S., Soutar, I. & Swanson, L., 2009. Switching the conformational behaviour of poly(N -isopropyl acrylamide). *Polymer International*, 58(3), pp.273–278.

Robel, S., Berninger, B. & Götz, M., 2011. The stem cell potential of glia: lessons from reactive gliosis. *Nature reviews. Neuroscience*, 12(2), pp.88–104.

Roberts, S. et al., 2011. Prospects of stem cell therapy in osteoarthritis. *Regenerative medicine*, 6(3), pp.351–66.

Rodriguez, J.P. et al., 2008. Involvement of Adipogenic Potential of Human Bone Marrow Mesenchymal Stem Cells (MSCs) in Osteoporosis. *Current Stem Cell Research & Therapy*, 3(3), pp.208–218.

Rodríguez, J.P. et al., 2004. Cytoskeletal organization of human mesenchymal stem cells (MSC) changes during their osteogenic differentiation. *Journal of cellular biochemistry*, 93(4), pp.721–31.

Roger, M. et al., 2010. Mesenchymal stem cells as cellular vehicles for delivery of nanoparticles to brain tumors. *Biomaterials*, 31(32), pp.8393–8401.

Rose, J.B. et al., 2014. Gelatin-based materials in ocular tissue engineering. *Materials*, 7(4), pp.3106–3135.

Røsland, G.V. et al., 2009. Long-term cultures of bone marrow-derived human mesenchymal stem cells frequently undergo spontaneous malignant transformation. *Cancer research*, 69(13), pp.5331–9.

Roux, R. & Ladavière, C., 2013. Particle assemblies: Toward new tools for regenerative medicine. *Materials Science and …*, 33(3), pp.997–1007.

Rowley, J. a., Madlambayan, G. & Mooney, D.J., 1999. Alginate hydrogels as synthetic extracellular matrix materials. *Biomaterials*, 20(1), pp.45–53.

Ruoslahti, E., 1996. RGD and other recognition sequences for integrins. *Annual review of cell and developmental biology*, 12, pp.697–715.

Ryan, J., 2008. Evolution of Cell Culture Surfaces. *BioFiles*, 3.8(21).

Salasznyk, R.M. et al., 2007. Focal adhesion kinase signaling pathways regulate the osteogenic differentiation of human mesenchymal stem cells. *Experimental cell research*, 313(1), pp.22–37.

Saleh, F. a, Whyte, M. & Genever, P.G., 2011. Effects of endothelial cells on human mesenchymal stem cell activity in a three-dimensional in vitro model. *European cells & materials*, 22(Area 9), pp.242–57; discussion 257.

Saleh, F.A. et al., 2012. Three-dimensional in vitro culture techniques for mesenchymal stem cells K. A. Mace & K. M. Braun, eds. *Methods Mol Biol*, 916, pp.31–45.

Salinas, C.N. & Anseth, K.S., 2008. The influence of the RGD peptide motif and its contextual presentation in PEG gels on human mesenchymal stem cell viability. *Journal of tissue engineering and regenerative medicine*, 2(5), pp.296–304.

Sammon, C. et al., 2006. ATR–FTIR studies of a thermo-responsive ABA triblock copolymer gelator in aqueous solution. *Polymer*, 47(17), pp.6123–6130.

Scadden, D.T., 2006. The stem-cell niche as an entity of action. *Nature*, 441(7097), pp.1075–9.

Scales, C.W., Convertine, A.J. & McCormick, C.L., 2006. Fluorescent labeling of RAFT-generated poly(N-isopropylacrylamide) via a facile maleimide-thiol coupling reaction. *Biomacromolecules*, 7(5), pp.1389–92.

Scarpa, J.S., Mueller, D.D. & Klotz, I.M., 1967. Slow Hydrogen-Deuterium Exchange in a Non-a-helical Polyamide. *Journal of the American Chemical Society*, 89(24), pp.6024–6030.

Schild, H.G., 1992. POLY (N-ISOPROPYLACRYLAMIDE): EXPERIMENT , THEORY AND APPLICATION. *Progress in Polymer Science*, 17, pp.163–249.

Schmaljohann, D., 2006. Thermo- and pH-responsive polymers in drug delivery. *Advanced drug delivery reviews*, 58(15), pp.1655–70.

Schmedlen, K.H., Masters, K.S. & West, J.L., 2002. Photocrosslinkable polyvinyl alcohol hydrogels that can be modified with cell adhesion peptides for use in tissue engineering. *Biomaterials*, 23(11), pp.4325–4332.

Seol, Y.-J. et al., 2004. Chitosan sponges as tissue engineering scaffolds for bone formation. *Biotechnology letters*, 26(13), pp.1037–1041.

Serra, M. et al., 2011. Microencapsulation technology: a powerful tool for integrating expansion and cryopreservation of human embryonic stem cells. *PloS one*, 6(8), p.e23212.

Shay, M.-E., 2001. Transplantation Without a Donor. *Science*. Available at: http://sciencecareers.sciencemag.org/career_magazine/previous_issues/articles/2001_11_02/nodoi.6458489939025632936.

Shih, Y.-R. V et al., 2011. Matrix stiffness regulation of integrin-mediated mechanotransduction during osteogenic differentiation of human mesenchymal stem cells. *Journal of bone and mineral research : the official journal of the American Society for Bone and Mineral Research*, 26(4), pp.730–8.

Siegel, G. et al., 2013. Phenotype, donor age and gender affect function of human bone marrow-derived mesenchymal stromal cells. *BMC medicine*, 11, p.146.

Siersbæk, R., Nielsen, R. & Mandrup, S., 2010. PPARγ in adipocyte differentiation and metabolism - Novel insights from genome-wide studies. *FEBS Letters*, 584(15), pp.3242–3249.

Da Silva Meirelles, L. et al., 2009. MSC frequency correlates with blood vessel density in equine adipose tissue. *Tissue engineering. Part A*, 15(2), pp.221–229.

Da Silva Meirelles, L., Caplan, A.I. & Nardi, N.B., 2008. In search of the in vivo identity of mesenchymal stem cells. *Stem cells (Dayton, Ohio)*, 26(9), pp.2287–99.

Da Silva Meirelles, L., Chagastelles, P.C. & Nardi, N.B., 2006. Mesenchymal stem cells reside in virtually all post-natal organs and tissues. *Journal of cell science*, 119(Pt 11), pp.2204–13.

Sivasubramaniyan, K. et al., 2012. Phenotypic and functional heterogeneity of human bone marrow- and amnion-derived MSC subsets. *Annals of the New York Academy of Sciences*, 1266, pp.94–106.

Song, G. et al., 2013. Facile Fabrication of Tough Hydrogels Physically Cross-Linked by Strong Cooperative Hydrogen Bonding. *Macromolecules*, 46(18), pp.7423–7435.

Song, L. et al., 2006. Identification and functional analysis of candidate genes regulating mesenchymal stem cell self-renewal and multipotency. *Stem cells*, 24(7), pp.1707–1718.

Spaeth, E. et al., 2008. Inflammation and tumor microenvironments: defining the migratory itinerary of mesenchymal stem cells. *Gene therapy*, 15(10), pp.730–738.

Stile, R. a & Healy, K.E., 2001. Thermo-responsive peptide-modified hydrogels for tissue regeneration. *Biomacromolecules*, 2(1), pp.185–94.

Stile, R.A., Burghardt, W.R. & Healy, K.E., 1999. Synthesis and Characterization of Injectable Poly (N -isopropylacrylamide) -Based Hydrogels That Support Tissue Formation in Vitro. *Macromolecules*, 32, pp.7370–7379.

Stolzing, A. et al., 2008. Age-related changes in human bone marrow-derived mesenchymal stem cells: consequences for cell therapies. *Mechanisms of ageing and development*, 129(3), pp.163–73.

Sun, B., Lin, Y. & Wu, P., 2007. Structure analysis of poly(N-isopropylacrylamide) using near-infrared spectroscopy and generalized two-dimensional correlation infrared spectroscopy. *Applied spectroscopy*, 61(7), pp.765–71.

Sung, H.J. et al., 2010. Stemness evaluation of mesenchymal stem cells from placentas according to developmental stage: Comparison to those from adult bone marrow. *Journal of Korean Medical Science*, 25(10), pp.1418–1426.

Tan, H. et al., 2009. Thermosensitive injectable hyaluronic acid hydrogel for adipose tissue engineering. *Biomaterials*, 30(36), pp.6844–53.

Tanaka, F. et al., 2011. Hydration, phase separation and nonlinear rheology of temperature-sensitive water-soluble polymers. *Journal of physics. Condensed matter : an Institute of Physics journal*, 23.

Tao, W. & Yan, L., 2010. Thermogelling of highly branched poly (N-isopropylacrylamide). *Journal of Applied Polymer Science*, 118, pp.3391–3399.

Thiele, J. et al., 2014. Designer hydrogels for cell cultures: a materials selection guide. *Advanced materials (Deerfield Beach, Fla.)*, 26(1), pp.125–47.

Thomson, J., Itskovitz-Eldor, J. & Jones, J., 1998. Embryonic Stem Cell lines derived from Human Blastocysts. *Science*, 282(5391), pp.1145–1147.

Tibbitt, M.W. & Anseth, K.S., 2009. Hydrogels as extracellular matrix mimics for 3D cell culture. *Biotechnology and Bioengineering*, 103(4), pp.655–663.

Toda, S. et al., 2002. A new organotypic culture of thyroid tissue maintains three-dimensional follicles with C cells for a long term. *Biochemical and biophysical research communications*, 294(4), pp.906–11.

Toh, W.S. et al., 2012. Modulation of mesenchymal stem cell chondrogenesis in a tunable hyaluronic acid hydrogel microenvironment. *Biomaterials*, 33(15), pp.3835–3845.

Tormin, A. et al., 2011. CD146 expression on primary non-hematopoietic bone marrow stem cells correlates to in situ localization CD146 Expression on Primary Non-Hematopoietic Bone Marrow Stem Cells Correlates to In situ Localization. , 117(19), pp.5067–5078.

Trappmann, B. et al., 2012. Extracellular-matrix tethering regulates stem-cell fate. *Nature materials*, 11(7), pp.642–9.

Treiser, M.D. et al., 2010. Cytoskeleton-based forecasting of stem cell lineage fates. *Proceedings of the National Academy of Sciences of the United States of America*, 107(2), pp.610–5.

Tzameli, I. et al., 2004. Regulated production of a peroxisome proliferator-activated receptor-gamma ligand during an early phase of adipocyte differentiation in 3T3-L1 adipocytes. *The Journal of biological chemistry*, 279(34), pp.36093–36102.

Uccelli, A., Moretta, L. & Pistoia, V., 2006. Immunoregulatory function of mesenchymal stem cells. *European Journal of Immunology*, 36(10), pp.2566–2573.

Vo, T.N. et al., 2014. In vitro and in vivo evaluation of self-mineralization and biocompatibility of injectable, dual-gelling hydrogels for bone tissue engineering. *Journal of controlled release : official journal of the Controlled Release Society*.

Wagers, a J. & Weissman, I.L., 2004. Plasticity of adult stem cells. *Cell*, 116(5), pp.639–648.

Wagner, W. et al., 2005. Comparative characteristics of mesenchymal stem cells from human bone marrow, adipose tissue, and umbilical cord blood. *Experimental Hematology*, 33(11), pp.1402–1416.

Wagner, W. et al., 2008. Replicative senescence of mesenchymal stem cells: A continuous and organized process. *PLoS ONE*, 3(5).

Wagner, W. et al., 2006. The heterogeneity of human mesenchymal stem cell preparations--evidence from simultaneous analysis of proteomes and transcriptomes. *Experimental hematology*, 34(4), pp.536–548.

Wakitani, S., Saito, T. & Caplan, A., 1995. MYOGENIC CELLS DERIVED FROM STEM CELLS EXPOSED TO 5-AZACYTIDINE. *Muscle & Nerve*, 18, pp.1417–1426.

Walsh, K. & Perlman, H., 1997. Cell cycle exit upon myogenic differentiation. *Current Opinion in Genetics & Development*, 7, pp.597–602.

Wang, C. et al., 2010. An enzyme-responsive polymeric superamphiphile. *Angewandte Chemie (International ed. in English)*, 49(46), pp.8612–5.

Wang, D. et al., 2011. Thermoreversible hydrogel for in situ generation and release of HepG2 spheroids. *Biomacromolecules*, 12(3), pp.578–84.

Wang, X. & Wu, C., 1999. Light-Scattering Study of Coil-to-Globule Transition of a Poly(N-isopropylacrylamide) Chain in Deuterated Water. *Society*, pp.4299–4301.

Weaver, V.M. et al., 1997. Reversion of the malignant phenotype of human breast cells in three-dimensional culture and in vivo by integrin blocking antibodies. *The Journal of cell biology*, 137(1), pp.231–45.

Wei, H. et al., 2006. Self-assembled thermoresponsive micelles of poly(N-isopropylacrylamide-b-methyl methacrylate). *Biomaterials*, 27(9), pp.2028–34.

Wei, X. et al., 2013. Mesenchymal stem cells: a new trend for cell therapy. *Acta pharmacologica Sinica*, 34(6), pp.747–54.

Whyte, M.P., 1994. Hypophosphatasia and the role of alkaline phosphatase in skeletal mineralization. *Endocrine reviews*, 15(4), pp.439–61.

Widera, D. et al., 2009. Adult palatum as a novel source of neural crest-related stem cells. *Stem Cells*, 27(8), pp.1899–1910.

Willerth, S. & Sakiyama-Elbert, S., 2008. Combining stem cells and biomaterial scaffolds for constructing tissues and cell delivery. Available at: http://www.stembook.org/node/450.

Williams, C.G. et al., 2003. In vitro chondrogenesis of bone marrow-derived mesenchymal stem cells in a photopolymerizing hydrogel. *Tissue engineering*, 9(4), pp.679–688.

Winer, J.P. et al., 2009. Bone marrow-derived human mesenchymal stem cells become quiescent on soft substrates but remain responsive to chemical or mechanical stimuli. *Tissue engineering. Part A*, 15(1), pp.147–54.

Wislet-Gendebien, S. et al., 2005. Plasticity of cultured mesenchymal stem cells: switch from nestin-positive to excitable neuron-like phenotype. *Stem cells*, 23(3), pp.392–402.

Wognum, A.W., Eaves, A.C. & Thomas, T.E., 2004. Identification and isolation of hematopoietic stem cells. *Archives of medical research*, 34(6), pp.461–75.

Woolf, A.D. & Pfleger, B., 2003. Burden of major musculoskeletal conditions. *Bulletin of the World Health Organization*, 81(9), pp.646–56.

Wu, C. & Zhou, S., 1996. Effects of Surfactants on the Phase Transition of Poly(N-isopropylacrylamide) in Water. *Journal of Polymer Science: Part B: Polymer Physics*, 34, pp.1597–1604.

Wu, J., Zhou, B. & Hu, Z., 2003. Phase Behavior of Thermally Responsive Microgel Colloids. *Physical Review Letters*, 90(4), p.048304.

Wu, Y. et al., 2014. Galactosylated reversible hydrogels as scaffold for HepG2 spheroid generation. *Acta biomaterialia*, 10(5), pp.1965–74.

Yang, C. et al., 2014. Mechanical memory and dosing influence stem cell fate. *Nature materials*, 13(June), pp.645–652.

Yang, F. et al., 2005. The effect of incorporating RGD adhesive peptide in polyethylene glycol diacrylate hydrogel on osteogenesis of bone marrow stromal cells. *Biomaterials*, 26(30), pp.5991–5998.

Yazdani, M. et al., 2012. Disease modeling using embryonic stem cells: MeCP2 regulates nuclear size and RNA synthesis in neurons. *Stem Cells*, 30, pp.2128–2139.

Yeh, C.-L. et al., 2007. Effect of arginine on cellular adhesion molecule expression and leukocyte transmigration in endothelial cells stimulated by biological fluid from surgical patients. *Shock (Augusta, Ga.)*, 28(1), pp.39–44.

Yokoi, H., Kinoshita, T. & Zhang, S., 2005. Dynamic reassembly of peptide RADA16 nanofiber scaffold. *Proceedings of the National Academy of Sciences of the United States of America*, 102(24), pp.8414–9.

Yoon, D. & Fisher, J., 2009. Biomedical materials. In R. Narayan, ed. *Biomedical Materials*. Springer US, p. 419.

Young, R.G. et al., 1998. Use of mesenchymal stem cells in a collagen matrix for Achilles tendon repair. *Journal of orthopaedic research : official publication of the Orthopaedic Research Society*, 16(4), pp.406–413.

Yow, S.Z. et al., 2009. Collagen-based fibrous scaffold for spatial organization of encapsulated and seeded human mesenchymal stem cells. *Biomaterials*, 30(6), pp.1133–42.

Zeng, F., Zheng, X. & Tong, Z., 1998. Network formation in poly (N-isopropyl acrylamide)/water solutions during phase separation. *Polymer*, 39(5), pp.1249–1251.

Zhang, J., Qian, Z. & Gu, Y., 2009. In vivo anti-tumor efficacy of docetaxel-loaded thermally responsive nanohydrogel. *Nanotechnology*, 20(32), p.325102.

Zhang, J., Skardal, A. & Prestwich, G.D., 2008. Engineered extracellular matrices with cleavable crosslinkers for cell expansion and easy cell recovery. *Biomaterials*, 29(34), pp.4521–4531.

Zhang, L. et al., 2010. Melatonin inhibits adipogenesis and enhances osteogenesis of human mesenchymal stem cells by suppressing PPARγ expression and enhancing Runx2 expression. *Journal of Pineal Research*, 49(4), pp.364–372.

Zhao, L.-R. et al., 2002. Human bone marrow stem cells exhibit neural phenotypes and ameliorate neurological deficits after grafting into the ischemic brain of rats. *Experimental neurology*, 174(1), pp.11–20.

Zhou, B.O. et al., 2014. Leptin-receptor-expressing mesenchymal stromal cells represent the main source of bone formed by adult bone marrow. *Cell Stem Cell*, 15(2), pp.154–168.

Zhu, J. & Marchant, R.E., 2011. Design properties of hydrogel tissue-engineering scaffolds. *Expert Review of Medical Devices*, 8(5), pp.607–626.

Zimmermann, U. et al., 1992. Production of mitogen-contamination free alginates with variable ratios of mannuronic acid to guluronic acid by free flow electrophoresis. *Electrophoresis*, 13(5), pp.269–274.